TURBINE-COMPOUND FREE-PISTON
LINEAR ALTERNATOR ENGINE

by

Chang-ping Lee

A dissertation submitted in partial fulfillment
of the requirements for the degree of
Doctor of Philosophy
(Mechanical Engineering)
in the University of Michigan
2014

Doctoral Committee:

      Associate Professor Claus Borgnakke, Co-Chair
      Professor Dionissios N. Assanis, Co-Chair, Stony Brook University
      Professor Andre Boehman
      Professor Jin Sun
      Russell Durrett, General Motor Co.

Table of Contents

LIST OF TABLES

LIST OF FIGURES

ABSTRACT

The free-piston engine (FPE) was being used on stationary power plants and automobile test back in 1950's. However, due to the maturity of the conventional cranked engine, the FPE was finally abandoned due to low controllability. The advantages of the FPE are obtained mainly from the freely moving piston, with which a variable compression ratio can be easily achieved. This gives the possibility of high compression ratio with high efficiency and the flexibility of burning different fuels. With many alternative fuels, such as biofuels under development to replace the traditional gasoline or diesel fuel, the potential of the FPE is again becoming valuable and therefore many groups around the world have re-launched the research on the FPE concept.

The primary aim of the present research is to develop a numerical model of the FPE that can be used to understand the conceptual design and operation. Until now, a model for the FPE was not available, so a model is built in Matlab/Simulink with many user-defined functions and algorithms. The model was then validated by comparison with the historical data. The validated results provided the confidence in the model, so it can be used for future design and control studies.

The second goal was to integrate the FPE with a linear alternator. Historically, the FPE extracted power solely through a power turbine. Many research groups have used the linear alternator with the FPE and have claimed high efficiency. This study focused on using both power extraction devices together, namely turbine-compound free-piston linear alternator (TCFPLA). The portion of power extracted by alternator can be adjusted for different loads. It is believed that the linear alternator as the secondary power output has the potential to increase the efficiency when combined with the turbine.

The major contribution of this study was to quantify the benefit of this novel device based on thermodynamic laws. The First Law is commonly used in the engine analysis, but the Second Law is not usually applied. The Second Law, however, provides

a different view of available energy that can be truly used. In addition, the losses due to the irreversible process can only be analyzed based on Second Law. This study also gives a clear guideline on how the Second Law analysis can be done for any device other than the traditional engine.

The most special characteristic of the TCFPLA engine is its energy-recovering configuration. With the air box fully surrounding the combustion chamber, it absorbs most of the heat from the combustion chamber. This heat recovery process was proven in the study to be a great advantage on efficiency. Two important control parameters were defined, namely the bounce chamber mass and the injection position. These two parameters have to change with load for the best performance output. A 2D engine map is generated for various linear alternator output at each given fueling rate. The brake efficiency reached 50% at the mid to high load conditions with high alternator output. This makes the TCFPLA engine very competitive with the diesel engine.

A special study was performed for the comparison between the TCFPLA engine and the cranked opposed-piston engine. Different piston motions between these two change the timing of the processes in the closed cycle even though the overall engine speed is the same. The cranked engine experiences more heat losses during the closed cycle with the combustion chamber at high temperature resulting in a smaller efficiency. However, a heat recovery can reduce the significant loss of heat in the cranked engine, and make these two devices more comparable.

CHAPTER 1

Introduction

Hybrid electric vehicle are becoming the mainstream in the automotive industry. They not only provide better fuel efficiency than conventional vehicles, but the emissions reduction has encouraged the development of the more environmental friendly technology. While pure electric vehicles still face barriers related to battery capacity, the self-charging system in the hybrid powertrain could deliver a driving range equivalent to or larger than conventional vehicles. Current hybrid powertrains use an engine coupled to an electrical generator in various possible configurations, where most researches typically focus on the control logic for most efficient power delivery. However, these vehicles still use the conventional crank-driven internal combustion (IC) engine, fueled by either gasoline or diesel. It is desirable to seek a different type of IC engine, which may be better suited to utilize the hybrid power concept and would have the potential to run on alternative fuels, such as methane or biofuels, that can further reduce the environmental impact.

1.1 Free-Piston Engine

The free-piston term is commonly used to distinguish a "free" moving piston engine from a rotating crankshaft engine. The word "free" is used because in this type of engine, the piston movement is totally determined by the forces acting upon the piston, but not the position of the crankshaft as in conventional engines.

The free-piston engine (FPE) has some distinct characteristics due to the special piston motion. First, the length of stroke and compression ratio is variable. This can be achieved by varying combustion timing. The later the start of combustion (SOC), the higher the compression ratio, because the pressure rise due to combustion is the main

force driving the piston to change direction. The variable compression ratio implies the potential to use alternative fuels with various self-igniting temperatures. This makes the FPE more suitable for the currently popular HCCI combustion mode, as it can infinitely increase the compression ratio for very lean burn, if necessary. A second special characteristic of this engine is, that the piston has higher accelerations around top and bottom center positions. The interaction between pressure forces on both sides of piston determines the turnaround point, and the higher-pressure side pushes the piston away from the zero velocity locations. Therefore, the heat losses are reduced because pistons spend less time where the heat transfer rate is high. Finally, the friction is reduced in the free-piston configuration due to the elimination of the crankshaft mechanism.

Several FPE concepts have been developed. One configuration uses a single piston with combustion on both sides, while others may have allowed combustion only on one side with a gas spring on the other side. Dual pistons and combustion chambers are also used in some designs. This work mainly focuses on opposed piston configuration, which consists of two single piston assemblies with a common combustion chamber. Therefore, each piston requires a bounce chamber as a gas spring to push piston backward. The following sections review some noteworthy devices in the history of FPEs.

1.1.1 Pescara Free-Piston Compressor
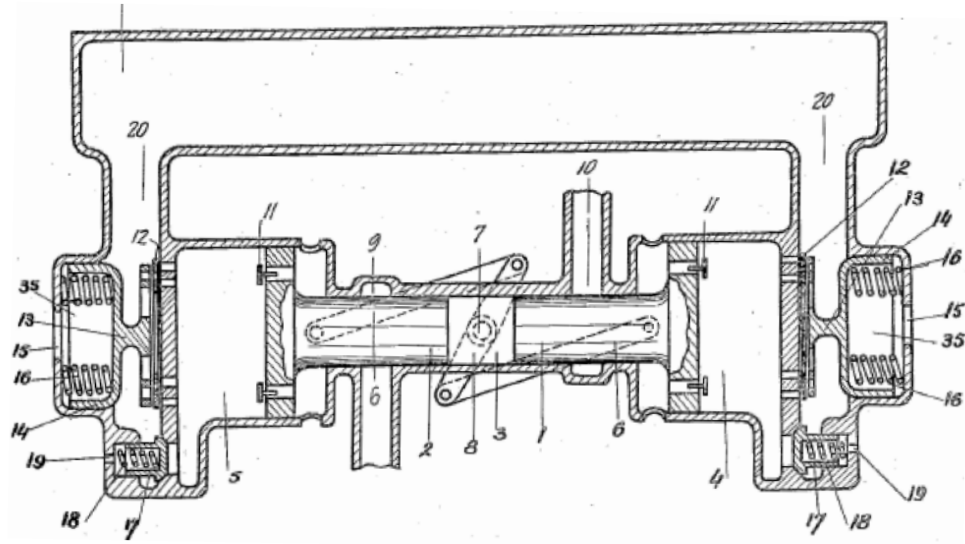
Figure 1-1 Pescara Air Compressor, 1931 [1]

In 1925, the Argentinian engineer Rual Pateras Pescara came up with the idea of a single free-piston compressor to help propel his helicopter. Even though this first idea was never realized, a new concept for the internal combustion engine had been born. Later in the 1930's, the Swiss engineer, Robert Huber, designed a prototype for a direct injection diesel free-piston compressor named after Pescara [1]. This early version of the free-piston machine used a connecting rod to synchronize the opposed pistons, and the air was compressed on the outward stroke. This outward compression design makes sense in terms of efficiency because the air is delivered into air box during the engine scavenging process, reducing the pumping losses. However, an external pipe is required to direct the air into the air box. Figure 1-1 shows a sketch of the Pescara Air Compressor concept.

1.1.2 Pescara Gas Turbine & SIGMA GS-34
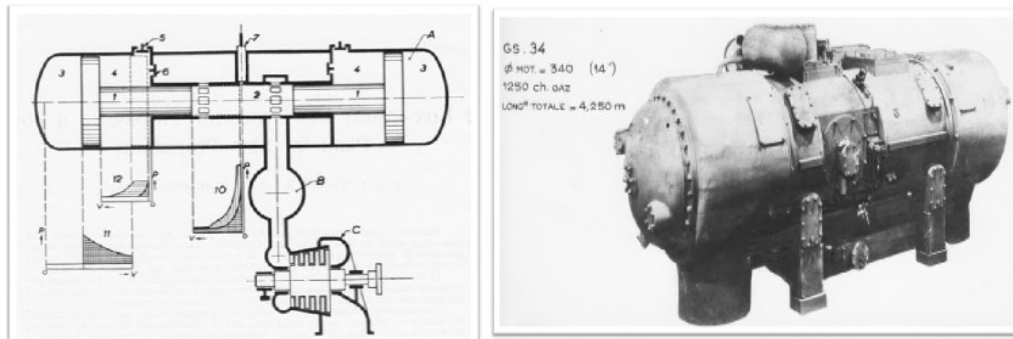
Figure 1-2 GS-34 concept and the actual device [2]

In 1941, Pescara achieved a breakthrough in the design of free-piston devices with the invention of an inward compression machine. This configuration had the benefit of reducing the overall size and complexity of the engine by eliminating the external pipe. In 1945, the Pescara GS-34, or SIGMA GS-34, was built. It was a disel-fueled, opposed piston compressor and combustor with the inward compression configuration, which then fed a power gas turbine. This has been the most successful free-piston machine, with over 300 units sold in Europe. Due to its size, it was mainly used as a stationary engine with more than 1000 HP (745.7 kW). It has been reported that 15 of them were used in series as the power supply for Imperial Chemical Industries, Ltd [3]. A conceptual drawing and a real device are shown in Figure 1-2. This device has become a popular prototype for followers due to its key advantages. For example, General Motor (GM) researcher Gregorgy Flynn reported 25,000 hours of operation for the GS-34 [4] in an effort to understand the physics behind this device. As a result, GM later introduced their own version of the free-piston engine.

1.1.3   Free-Piston Engine for Automotive Use

In the 1950's, American automotive companies, General Motors and Ford, became interested in the free-piston concept, and developed their own prototypes based on the GS-34. In order to use it in automotive application, the size of the engine had to

4

be dramatically reduced to fit into the engine bay. Ford's single-cylinder engine had an output of 150 HP (112kW) and GM "Hyprex", a two-cylinder unit, outputs 250 HP (186 kW) with an overall thermal efficiency of 35%.

According to Underwood [5], other than the general benefits of free-piston engines, the GM Hyprex has the following advantages for vehicle use. First, the efficiency was competitive to any gasoline or diesel engine at that time, and a cheaper fuel could be used with same efficiency. Second, the engine operation was very smooth. The vibration was minor, which had been demonstrated by showing that a nickel could be easily balanced on the machine while operation. Additionally, no crankshaft meant the motor could be mounted without considering the torsional movement, making the design of engine bay much simpler. Third, the turbine inlet temperature was low, because the combustion products were mixed with a large amount of scavenging air from the air box where the temperature is around 400K. Low temperature, 500 to 800 K as reported, is ideal for the durability of turbine blades. Therefore, a cheaper material could be used for lowering costs.

Frey et al. [6] described some early problems in Ford's machine. They included the starting system, breakage of piston ring, injection pump failures, and poor combustion efficiency. Although those problems were properly improved by more in-depth research and newer designs, free-piston engines were finally abandoned due to increasing maturity of the conventional engines and gas turbines.

1.2 Free-Piston Linear Alternator (FPLA)

A linear alternator is a type of electrical generator, which generates alternating current (AC). It works by the principle of electromagnetic induction discovered by Michael Faraday. Inducted current is generated in any closed electrical circuit when magnetic flux through the circuit changes. This current also produces an electromotive force, given by Faraday's law below:

$$EMF = -\frac{d\Phi_B}{dt}$$

EMF stands for electromagnetic force, and Φ_B [Wb] is the magnetic flux passing throughout the coil. The negative sign shows that the induced force always acts in the direction opposite to the change in magnetic flux. After the conventional engines took a tremendous share of market, the free-piston engines were struggling to find a different approach to survive, and the linear alternators were most investigated and that made the linear alternators more pimportant.

In 1962, Stirling [7] Colgate proposed an opposed piston linear alternator design, as shown in Figure 1-3. The design was based on Pescara's free-piston engine with the alternator coils on the cooler side of the piston. He asserted that the magnets should be thermally decoupled, that is, away from the combustion chamber, because high temperature would reduce the magnetic field of permanent magnets. For example, modern NdFeB magnets can be used up to 100 °C, and the more expensive SmCo magnets up to about 200 °C.
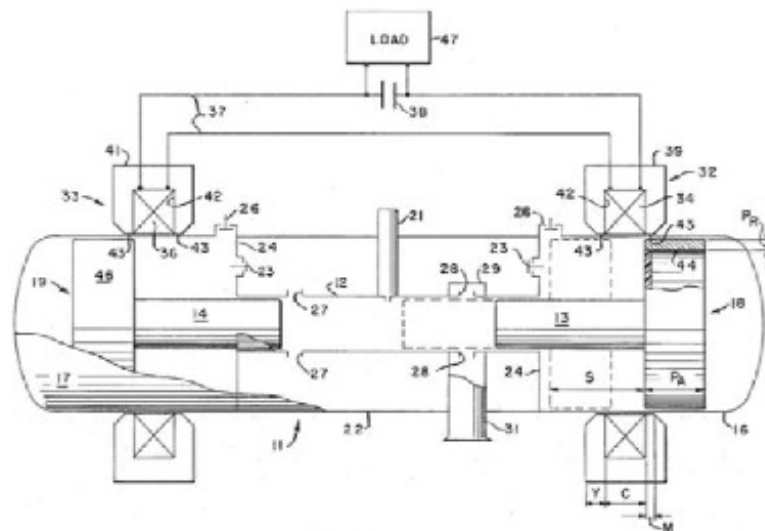
Figure 1-3 Stirling free-piston linear alternator

In addition to Stirling's alternator, other designs were proposed between the 1960's and 1970's. Most of the designs were never successfully built, mainly because high flux density rare-earth magnets were not available then. In 1997, a private company, Galileo Research [8], developed its own version of FPLA but had to abandon it due to lack of funds. West Virginia University [9] later started working on a similar concept, showing in Figure 1-4 below. This design was also thermally decoupled, with the combustion chamber on both sides and alternator in the middle.
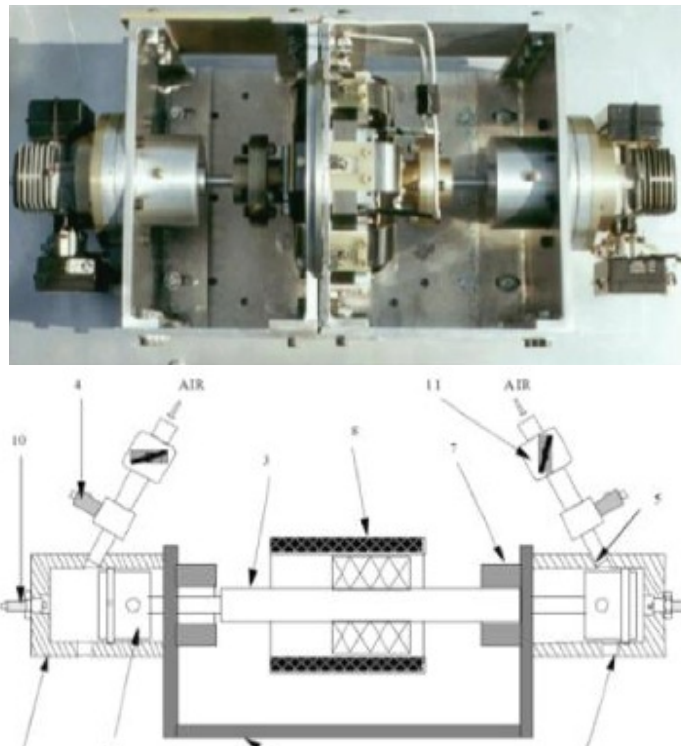
Figure 1-4 Galileo and West Varginia University FPLA design

Recently, Sandia National Laboratories developed a prototype design of an FPLA [10], which uses an opposed piston configuration with the combustion chamber located in the center. However, the bounce chamber is not a simple closed volume as Sterling's FPLA. Instead, the bounce chamber contains an injection valve to introduce high-pressure gas, and a release vent to discharge the extra gas into ambient. The purpose behind this design was to get better control of piston frequency by changing the pressure

7

in the bounce chamber. However, this requires pressurized gas as an outside source to supply the gas injection during operation. Therefore, the precise pressure monitoring and control is necessary to achieve a steady condition. Figure 1-5 shows the configuration of Sandia FPLA.
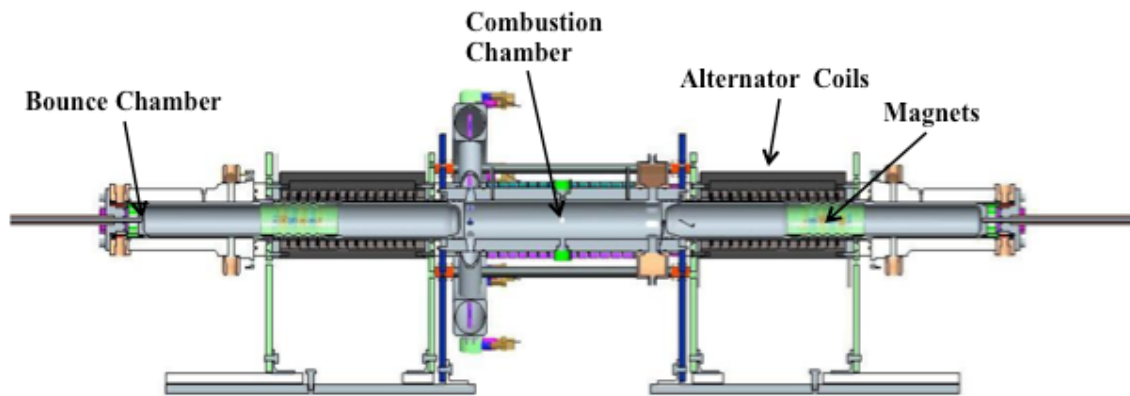
Figure 1-5 Sandia free-piston linear alternator

Li et al. [11] developed a free-piston engine linear generator, which contains two combustion chambers one in each end. The design replaced the crankshaft case in a two-stroke motorcycle engine with the linear alternator. This study focused on the computer modeling work as the initial stage for the developing experimental test. The free-piston engine model contained combustion, thermodynamics and dynamics. Combustion is modeled by the Wiebe function, and the ignition is triggered by a spark plug at given position. Conservation of energy is calculated to satisfy the First Law of thermodynamics. The key design parameters were studied, such as piston mass, compression ratio, ignition timing, to understand the influences on system performance. Figure 1-6 shows the architecture of this design below.
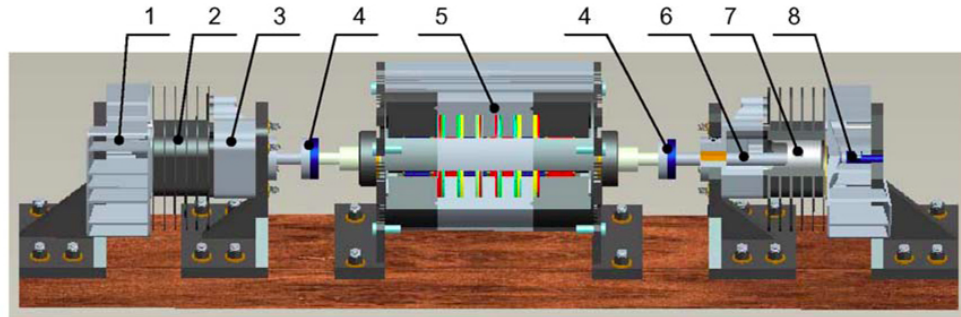
1-cylinder head, 2-cylinder block, 3-scavenging box, 4-adapting flange, 5-linear generator,
6-connecting rod, 7-piston, 8-spark plug

Figure 1-6 Architecture of the free-piston engine-alternator by Li et al. [11]

Huang [12] designed an opposed-piston FPLA. It is a two-stroke, spark ignition engine, which generates 15 kW of electric output at 42% thermal efficiency. Previous free-piston engines generally use either a gas spring or combustion chamber for maintaining reciprocating movement of the free-piston. However, a very special design component of Huang's device is the mechanical springs, which connect with the movers in the linear alternators for storing the compression energy. The Weibe function is applied for given shape of heat release rate, and conservation of energy for obtaining the in-cylinder pressure. Several parameters are investigated, including ignition position, piston mass and top center, to observe the system responses. A sketch of Huang's device is shown below in Figure 1-7.
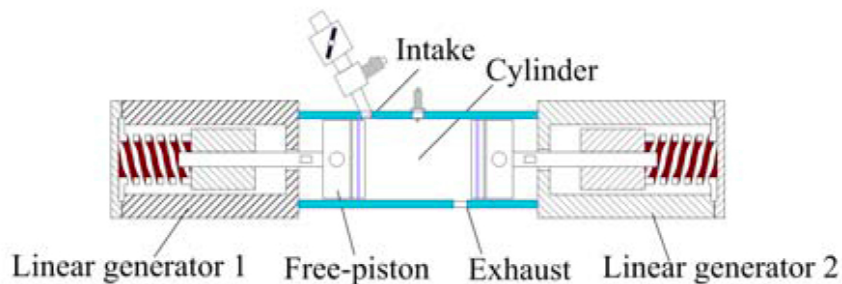
Figure 1-7 Opposed-piston free-piston linear alternator with mechanical springs

German Aerospace Center (DLR) introduced another version of free-piston linear generator for an automotive application [13]. The DLR free-piston linear generator

9

configures a two-stroke gasoline combustion chamber on one end, and the gas spring on the other. The linear alternator is set in the middle, as can be seen in Figure 1-8. The research consists of both numerical and experimental studies with a smaller demonstration system, which will be expanded into an actual system for vehicle use. It developed a controller to regulate the operating parameters, including linear generator, valve timing, ignition timing, injection, etc. Furthermore, the "engine" is not actually fired but a virtual combustion is generated by the linear alternator for energy balance study. A computational fluid mechanics (CFD) study was also performed in the previous work [14]. The latest work focused on the combustion mode as the homogeneous charge compression ignition (HCCI) is highly desired for emission control [15].

Combustion chamber   Linear generator   Gas spring
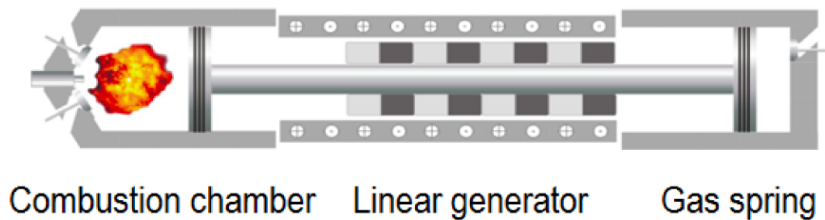
Figure 1-8 Scheme of the DLR free-piston linear generator

1.3 Motivation: Turbine-Compound Free Piston Linear Alternator (TCFPLA) Engine

The lack of a crankshaft in free-piston engines requires the power to be output through either a gas turbine or a linear alternator. Gas turbines have the disadvantages of low speed and load efficiency due to reduced gas flow rate, and the slow response time to changes in power demand. The alternator, on the other hand, cannot be operated at high spped conditions due to the limitation imposed by Faraday's Law, which dictates that the coil cannot generate the electromagnetic force (EMF) when the rate of change of magnetic field is too high. Moreover, the opposed free-piston engine requires "recirculation" of hot air from the air box into the compressor to heat up the intake air to maintain combustion at low loads [5]. This can be achieved by connecting the air box

10

and intake manifold with a valve, and opening the valve whenever it is necessary. More likely, it was done manually since no precise electrical control system was available at that time to adjust the valve with load.

The TCFPLA engine itself is a hybrid machine, generating both mechanical work for propulsion and electrical work for battery charging. By adjusting the power extraction ratio from the two devices, high thermal efficiencies can be expected within a broad range of speed and load. An extra generator may also be connected to the turbine at very low loads, so the turbine can maintain at certain level of speed without sacrificing the efficiency. However, this is beyond the scope of this work, which mainly focuses on the core TCFPLA engine design.

Several modeling works were done in the reported references [11] [12]. Most of them focus on the initially conceptual study to understand the system response and performance by simplified combustion and thermodynamic sub-models. With the lack of heat transfer, friction and flow sub-models, the losses cannot be fully determined. More importantly, since the free-piston movement is highly based on the energy balance of the piston itself, the change in piston dynamics due to the losses may be overlooked in the previous works. As a result, a detailed free-piston engine model is desired to fully determine the energy flows throughout the system. Furthermore, the linear alternator, which effects as the secondary power device are a key in terms of control and performance, so it will also be integrated into the free-piston engine.

1.4 Fundamentals of TCFPLA Engine
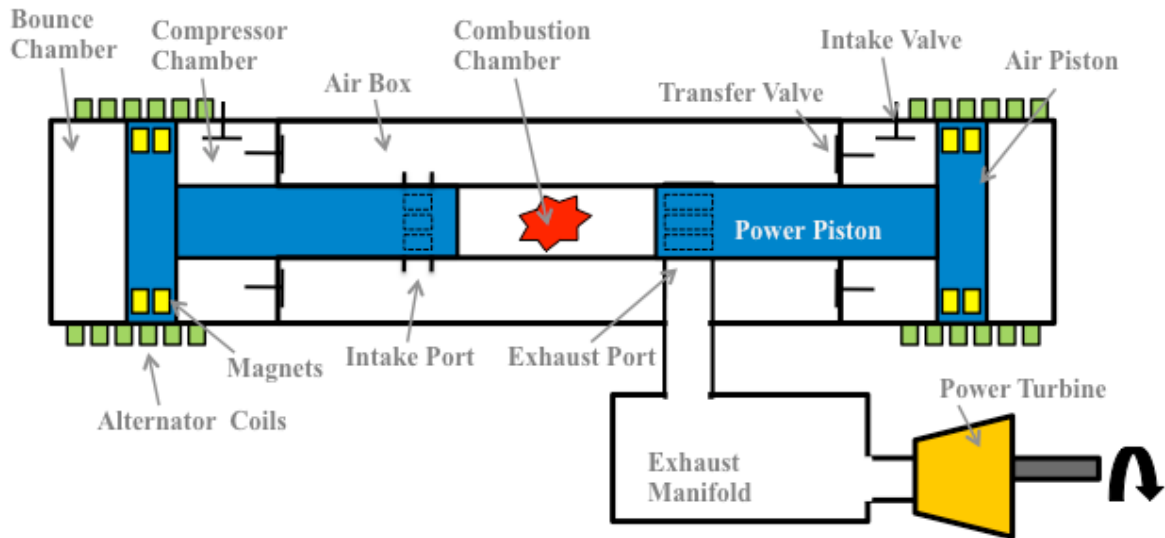
Figure 1-9 Configuration of TCFPLA

The detailed configuration of the TCFPLA engine is shown in Figure 1-9. The design is based on the GM Hyprex engine as described in Underwoord [5], and is very similar to the SIGMA GS-34 [2]. This is an inward compression, opposed free-piston engine with the linear alternators decoupled from the common combustion chamber in the center. The pistons are in the shape of "T" and separated into two parts: power piston and air piston. Power piston is named after its role of compressing the fuel-air mixture for combustion, and the air piston only works with air in bounce and compressor chamber. The valves in the TCFPLA engine are actually reed type, and the poppet valves shown in Figure 1-9 are for the ease of drawing. Reed valves are a type of check valve, which restrict the flow of fluids to a single direction, opening and closing based on the pressure on each side. The air box is a reservoir for storing the compressed air from the compressor. The bounce chambers on both ends are closed volumes, filled with air to supply the bouncing forces while being compressed.

The engine works as a two-stroke engine with scavenging ports for breathing. The operating process is sketched below.
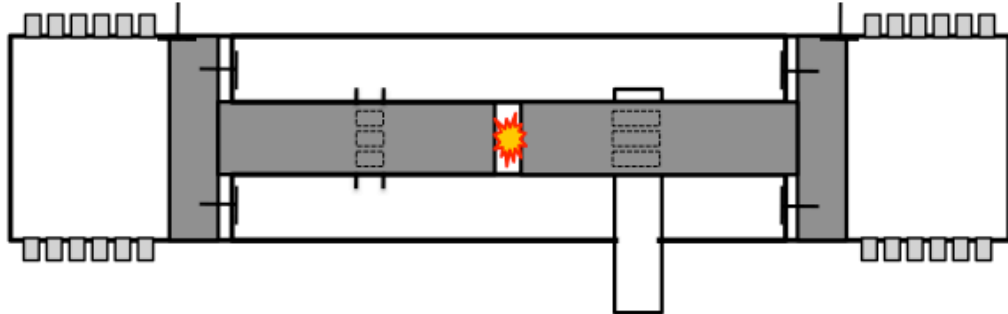
12
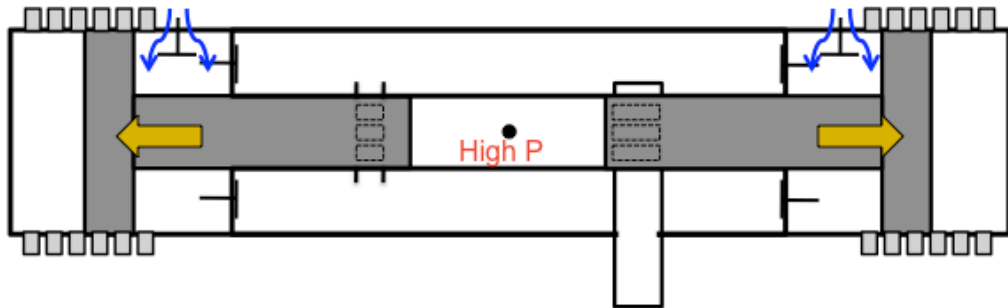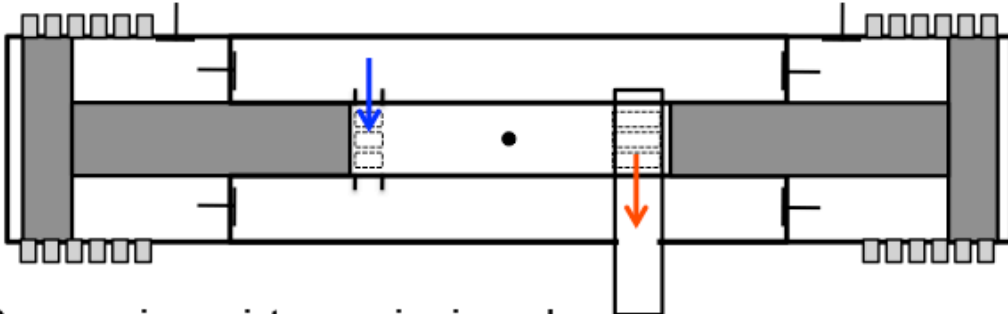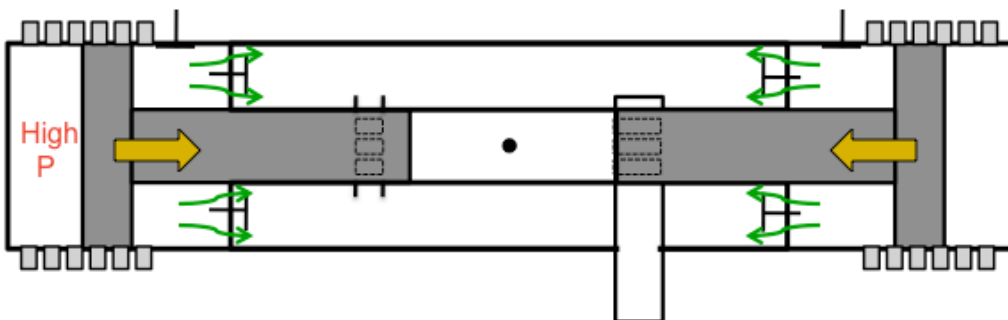
Figure 1-10 Operating procedures of the TCFPLA engine

In Figure 1-10, starting with the combustion process as the combustion chamber is compressed for the auto-ignition. The high pressure produced by combustion pushes the pistons away while generating vacuum in the compressor chamber for the intake process. The pistons keep moving outwardly to open the scavenging ports at some point. The high-pressure air stored in the air box pushes the combustion products out of the combustion chamber. The outflow then enters the turbine for power generation. Meanwhile, the bounce chambers store the energy, pushing the pistons back in the next cycle as the compression process. The fresh air inside the compressor chambers is compressed and delivered into the air box. The pistons move inwardly and close the scavenging ports for combustion, finishing as a cycle. During the cycle, the linear alternator is generating electricity at any moments when the magnetic fields pass through the coils. The TCFPLA engine operation can also be sketch as a flow chart in Figure 1-11, showing the mass transfer from upstream to downstream and energy transfer internally. More detailed will be discussed in the following chapters.
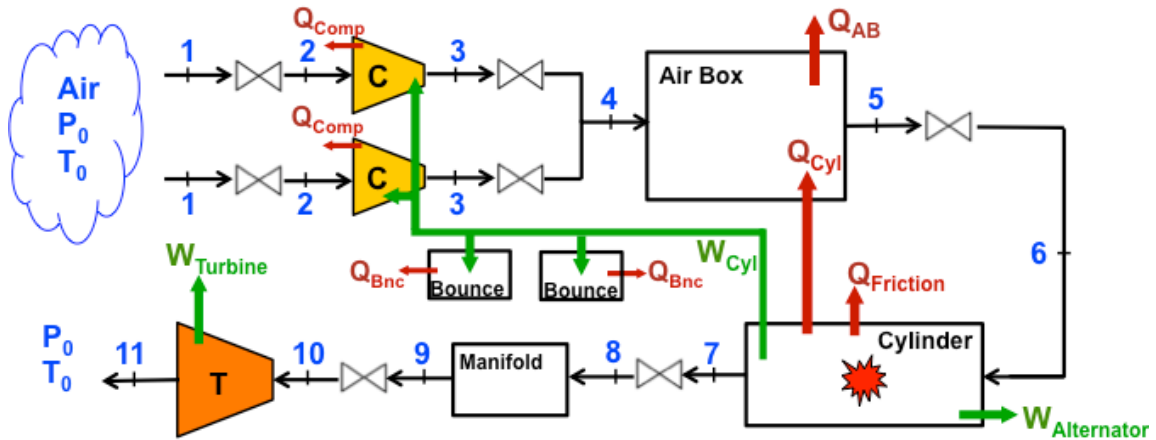
Figure 1-11 TCFPLA operation principles and relations between volumes

Regardless of the linear alternator, the free-piston gas turbine has one significant advantage over the conventional gas turbine. The conventional one consists of separate compressor and combustor, and the gas turbine has to supply the energy for compressor. On the other hand, the current free-piston gas turbine combines the compressor and

combustor into piston-cylinder architecture, and consequently makes the turbine power as net output. In order to produce the same amount of power in the conventional gas turbine, the combustor size has to be increased and more fuel burned. This requires more room for engine installation and stronger turbine blades for tolerating higher temperature.

Bibliography

[1]   US Patent 1,950,063, United State Patent Office, March 6th, 1934

[2]   http://www.freikolben.ch

[3]   F. A. I. Muntz, "Free-Piston Progress", Jounal of the American Society for Naval Engineers, vol. 70, Issue 4, 1958

[4]   Gregory Flynn, Jr., "Observation on 25,000 Hours of Free-Piston-Engine Operation", SAE National West Coast Meeting, San Francisco, 1956

[5]   F. Underwood, "The GMR 4-4 'HYPREX' Engine, A Concept of The Free-Piston Engine for Automotive Use", SAE 570032, 1957

[6]   D. N. Frey, P. Klotsch, A. Egli, "The Automotive Free-Piston-Turbine Engine", SAE 570051, 1957

[7]   US Patent 3,234,395, Feb 8 1966

[8]   http://gallileo-fpe.com

[9]   C. Toth-Nagy, "Linear Engine Development for Series Hybrid Electric Vehicles", Dissertation, Department of Mechanical and Aerospace Engineering, West Virginia University, 2004

[10]   S. S. Goldsborough, P. Van Blarigan, "A Numerical Study of a Free Piston IC Engine Operating on Homogeneous Charge Compression Ignition Combustion", SAE 1999-01-0619, 1999

[11]   L. Li, Y. Luan, Z. Wang, J. Deng and Z. Wu, "Simulations of Key Design Parameters and Performance Optimization for a Free-piston Engine", SAE 2010-01-1105, 2010

[12]   L. Huang, "An Opposed-Piston Free-Piston Linear Generator Development for HEV", SAE 2012-01-1021, 2012

[13]   F. Kock, J. Haag, H. E. Friedrich, "The Free Piston Linear Generator - Development of an Innovative, Compact, Highly Efficient Range- Extender Module", SAE 2013-01-1727, 2013

[14]   J. Haag, C. Ferrari, J. H. Starcke, M. Stöhr, U. Riedel, "Numerical and Experimental Investigation of In -Cylinder Flow in a Loop-Scavenged Two-Stroke Free Piston Engine", SAE 2012-32-0114

[15]   J. Haag, F. Kock, M. Chiodi, O. Mack, M. Bargende, C. Naumann, N. Slavinskaya, A. Heron, U. Riedel, C. Ferrari ," Development Approach for the Investigation of Homogeneous Charge Compression Ignition in a Free-Piston Engine", SAE 2013-24-0047

CHAPTER 2

Modeling Approach

Because of the significantly higher cost related to experimental work, this work employed a research methodology based mainly on computer model and simulation. Several free-piston engine models were built recently, but most of them were highly simplified for a simple conceptual study. A detailed model which includes most of the important physical processes in a realistic manner is more desired to fully explore the system behavior. Additionally, linear alternators associated with the free-piston engine increase the complexity of modeling work. None of the existing engine simulation software platforms can configure the unique design of the TCFPLA engine. Therefore, a customized Matlab®/Simulink® model was developed and built.

2.1 Model Overview
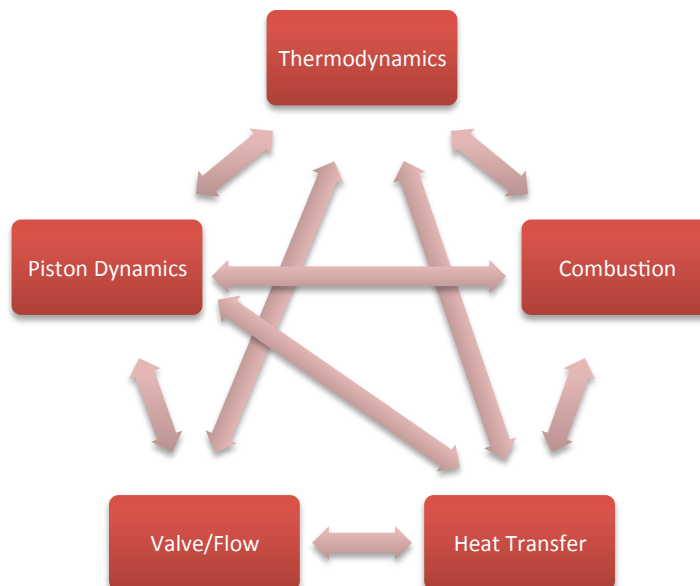
Figure 2-1 TCFPLA engine model structure

The model structure can be seen in Figure 2-1. In order to fully describe the systematic behavior of the TCFPLA engine, several interconnected sub-models are needed. For example, the combustion model provides the thermodynamic model with the instantaneous burn rate for calculation of mixture properties. Communication between sub-models is achieved by connected Simulink® blocks, each of which contains an embedded Matlab® function. Each function receives necessary inputs and calculates outputs based on general physical equations. Therefore, these functions are not limited for use in Simulink®, but can be shifted to other software. Because Simulink® has the flexibility to change the numbers of inputs and outputs with easy connection, it is chosen as the platform for the TCFPLA engine model.

The Simulink® model uses rate equations conforming to the time-based simulation approach. It numerically integrates the ordinary differential equations at given time steps, and uses the rate to estimate the value for next moment. A variable time step integrator was chosen to reduce the computational cost, where the time step is decreased when high rates are encountered. For example, the flow rate changes fast during the valve opening and closing, so the time step has to be small enough to capture the change with a reasonable accuracy. A build-in algorithm in Simulink® is used to define the step size.

2.2 Thermodynamic Model

The thermodynamic sub-model is used for all the system control volumes (CV). Each CV receives the information on temperature, specific volume, and species to calculate all necessary thermodynamics properties, such as specific heat, gas constant, and enthalpy, etc. In addition, the temperature and pressure are assumed to be uniform throughout the control volume. With the information of mass inflow and outflow, the conservation laws can then be fully defined.

Conservation of Mass: $\dfrac{dm}{dt} = \dot{m}_{in} - \dot{m}_{ex}$ (Eq 2.1)

Conservation of Energy:
$$\frac{dU}{dt} = \dot{H}_{in} - \dot{H}_{out} + \dot{Q}_{in} - \dot{U}_{comb} - P\frac{dV}{dt} \qquad \text{(Eq 2.2)}$$

where
$$\frac{dU}{dt} = \frac{d(mu)}{dt} = \dot{m}u + m_{CV}C_v\frac{dT}{dt} \qquad \text{(Eq 2.3)}$$

Conservation of Species:
$$\frac{dy_i}{dt} = \frac{dy_i}{dt}\bigg|_{in} - \frac{dy_i}{dt}\bigg|_{ex} + \frac{dy_i}{dt}\bigg|_{comb} \qquad \text{(Eq 2.4)}$$

where
$$\frac{dy_i}{dt}\bigg|_{CV} = \frac{\dot{m}_{in}(y_{i,in} - y_{i,CV}) - \dot{m}_{ex}(y_{i,ex} - y_{i,CV})}{m_{CV}} \qquad \text{(Eq 2.5)}$$

Eq. 2.1 describes the mass change in the control volume, where the mass flow rates on the right hand side are calculated from the flow sub-model. In Eq. 2.2, $\dot{U}_{comb}$ is the internal enthalpy change due to combustion process and is calculated from the combustion sub-model. Since the right hand side of Eq. 2.2 is known, Eq. 2.3 can be used to compute the temperature change, dT/dt. Eq. 2.4 is used to calculate the change of species resulting from flows and combustion. The subscription of "CV,in" refers to the change of species in the control volume due to inflow, calculated by Eq. 2.5. Based on Eq. 2.5, if the inflow and outflow has the same compositions as the control volume, the numerator on the right hand side will be zero, and there will be no change in composition in the control volume.

By integrating these equations, the mass, temperature, species can be obtained for the next time step, where the volumes are also known from the piston dynamics sub-model. Consequently, all thermodynamic properties, such as specific heat, enthalpy, internal energy and gas constant can be estimated, and the pressure then follows from the ideal gas law when the volume constraint is used.

2.3 Flow Model

Based on the fundamental fluid dynamics, flow happens whenever two points have a pressure difference. Since the control volumes have uniform pressures, the flow model only works between two or more connected control volumes. The model assumes

compressible flow through a restriction. There are two kinds of flow restrictions in this system: orifices and reed valves.

Orifices are used for scavenging ports and the turbine inlet. The turbine inlet port is always open with a given flow area. On the other hand, the opening area of the scavenging ports is determined by the piston position. The ports are physically covered and uncovered by the piston, and it is possible to encounter choked flow situations when the area is small and the pressure difference large. This usually occur for a short periods of time during the initial opening period. If the flow remains choked when the ports are fully opened, it means the port dimensions are not well designed, and the area needs to be increased. For the orifices in this model, the discharge coefficient is set as 0.8.

Reed valves are commonly used in the motorcycle engines or other 2-stroke engines. It contains several thin metal blades, which are lifted if the upstream pressure is higher than the downstream one. It is a type of one-way valve, so the blades do not lift if the downstream pressure is higher. The lifted blades uncover the flow area and allow the flows to go through. Larger pressure difference lifts the valves more unless they are stopped by stop plates preventing the blades from over bending. It is designed to open at a specific pressure difference across both sides based on the stiffness of the valve blades. Reed valves are typically modeled as a cantilever beam [1]. The lift of the tip is determined by the pressure force loading on the beam and the material characteristics. Krieger [2] provides an empirical correlation for flow area as a function of reed lift at the tip for a specific reed design (see Appendix A). This correlation also provides the discharge coefficients in the forward directions. The reed valve structure is shown in Figure 2-2 below.
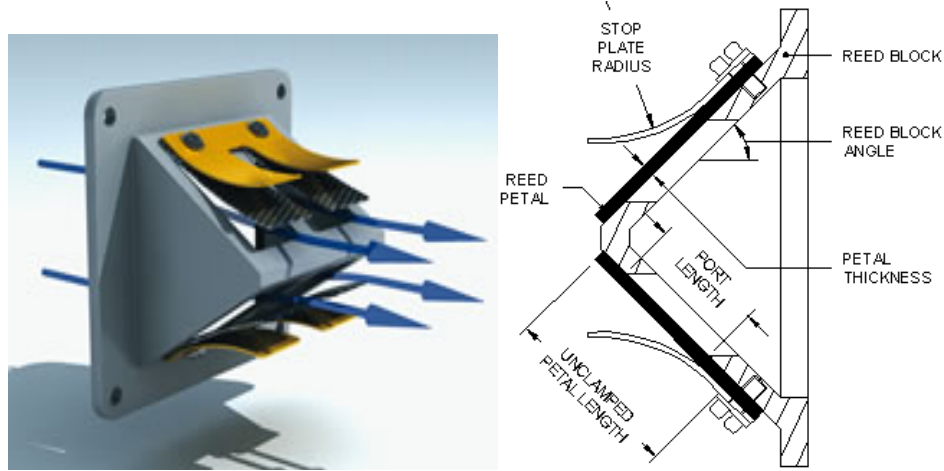
Figure 2-2 Reed valve structure and flow direction

With knowledge of the valve flow area and discharge coefficient, the mass flow rate can be estimated according to the compressible flow equations in Heywood [3].

Non-choked Flow:

$$\dot{m} = \frac{C_D A_R p_0}{(RT_0)^{1/2}} \left(\frac{p_T}{p_0}\right)^{1/2} \left\{\frac{2\gamma}{\gamma-1}\left[1-\left(\frac{p_T}{p_0}\right)^{(\gamma-1)/\gamma}\right]\right\}^{1/2}$$ (Eq 2.6)

Choked Flow:

$$\dot{m} = \frac{C_D A_R p_0}{(RT_0)^{1/2}} \gamma^{1/2} \left(\frac{2}{\gamma+1}\right)^{(\gamma+1)/2(\gamma-1)}$$ (Eq 2.7)

In Eq. 2.6 and 2.7, C_D is the discharge coefficient, A_R is the flow area (m^2), p_0 and T_0 are the pressure (Pa) and temperature (K) at upstream, p_T is the pressure (Pa) at downstream, and γ is the ratio of specific heats. The calculated mass flow rates are used as boundary conditions for the control volumes, closing the conservation laws described in previous section.

2.4 Combustion and Ignition Model

Combustion is currently modeled as heat addition into system, where the burn rate is described by a Wiebe function, formulated in Eq. 2.8:

$$x_b = 1 - e^{-a\left(\frac{t-t0}{\Delta t}\right)^n}$$ (Eq 2.8)

Parameters *a* and *n* control the peak burn rate and smoothness, which give the shape of the burn curve. t is a the time (sec) after combustion starts, t_0 (sec) is the ignition timing, and Δt_b (sec) is the burn duration. Based on the burn rate, the heat addition rate can be calculated with a known amount of injected fuel and the lower heating value is used for the energy release by combustion.

The ignition in the free-piston engine is predicted using the auto-ignition integral approach, with an ignition delay correlation relevant to HCCI conditions [4], based on experiments in a rapid compression machine with iso-octane, N_2, and O_2 mixture.

Ignition Delay: $\qquad\qquad \tau = 1.3 \times 10^{-7} \cdot P^{-1.05} \cdot \phi_{FO}^{-0.77} \cdot x_{O_2}^{-1.41} \cdot e^{\frac{E}{R \cdot T}}$ (Eq 2.9)

Ignition Integral: $\qquad\qquad \int_0^{t_{IGN}} \frac{1}{\tau} \, dt = 1$ $\qquad\qquad$ (Eq 2.10)

In Eq. 2.9, *P* is pressure (atm), *T* is temperature (K), ϕ_{FO} is the molar fuel/oxygen equivalence ratio, x_{O_2} is the oxygen mole fraction (%), *R* is the universal gas constant (J/mol-K), E is the activation energy (33.7 kcal for iso-octane), and τ is the ignition delay time (sec). Ignition is assumed to start once integral reaches a value of 1.

2.5 Heat Transfer Model

Much research has been done on heat transfer for conventional cranked engines. However, there is little or no research on heat transfer in the free-piston engine configuration, whose pistons have higher acceleration around the top and bottom centers. In the absence of heat transfer measurement, existing heat transfer correlations developed for cranked engines are generally used [5] for free-piston studies.

2.5.1 Heat Transfer for Compressing Volumes

Considering that the piston movement and compression process are similar to the cranked engine, the Woschni correlation [6] is currently used in the model to estimate the convictive heat transfer coefficient.

23

Woschni:
$$w = C_1 \times SP_{mean} + C_2 (\frac{V_d T_{ref}}{P_{ref} V_{ref}})(P - P_{motor})$$

where
$$
\begin{aligned}
&C_1 = 6.18, \ C_2 = 0 && \textit{Gas Exchange} \\
&C_1 = 2.28, \ C_2 = 0 && \textit{Compression} && \text{(Eq 2.11)} \\
&C_1 = 2.28, \ C_2 = 3.24e^{-3} && \textit{Combustion \& Expansion}
\end{aligned}
$$

C_1 and C_2 are constants given for the various processes, as described in Eq. 2.11. SP_{mean} is the mean piston speed (m/s) obtained from previous cycle; V_d is the displaced volume (m^3); T_{ref}, P_{ref} and V_{ref} are temperature (K), pressure (Pa) and volume (m^3) at reference point, assumed to be the scavenging port closing point in this case; P is the instantaneous pressure (Pa) and P_{motor} is respective motoring pressure (Pa). Once the value of w is obtained, the heat transfer coefficient and heat transfer rate can be estimated as below.

H.T. Coefficient:
$$h_{coef} = 3.26 \times Bore^{-0.2} \times P^{0.8} \times T^{-0.53} \times w^{0.8} \qquad \text{(Eq 2.12)}$$

H.T Rate:
$$\dot{q} = h_{coef} \times A_{HT} \times (T_{wall} - T) \qquad \text{(Eq 2.13)}$$

In Eq. 2.12 the *Bore* refers to the bore size (m) of corresponding control volume. In Eq. 2.13, A_{HT} is the effective heat transfer area (m^2) and T_{wall} is the cylinder wall temperature (K) where the direction of heat transfer is defined by the sign of the temperature difference. This heat transfer model applies to the engine (combustion chamber), compressor and bounce chamber with their respective areas and wall temperature.

2.5.2 Heat Transfer for Air Box

The air box is an annulus volume with the combustion cylinder at the core. Even though the flow is delivered from the compressor chamber, the gas in the air box is not directly compressed. Therefore, heat transfer models for chambers undergoing compression and expansion processes, such as Woschni described in previous section, are not appropriate. On the other hand, the heat transfer model for an annulus can be found in any heat transfer handbook. According to Incropera [7], the Nusselt number for

laminar flow can be determined by a look-up table as a function of ratio of inner to outer diameter ratio. For turbulent condition, the Nusselt number is based on the Dittus-Boelter equation.

Dittus-Boelter: $$Nu_D = 0.023 \cdot Re_D^{0.8} \cdot Pr^{0.3} \qquad \text{(Eq 2.14)}$$

where $$Re_D = \frac{\rho u_m D_h}{\mu} \qquad \text{(Eq 2.15)}$$

Prandtl number "Pr" in Eq. 2.14 does not fluctuate with the changes in temperature and pressure, so a value of 0.7 for air is assumed. In Eq. 2.15, ρ (kg/m^3) is the density of fluid; u_m (m/s) is the mean flow speed, which can be defined as the instantaneous mass flow rates for both inflow and outflow divided by fluid density and flow cross-section area; μ (N·s/m^2) is the dynamic viscosity of air, and D_h (m) is the hydraulic diameter defined as the difference between the outer and inner diameters. The heat transfer coefficient, h, is then obtained by the definition of Nusselt number:

Nusselt Number: $$Nu_D = \frac{hD_h}{k} \qquad \text{(Eq 2.16)}$$

Thermal conductivity k can be determined by a look-up table as a function of temperature.

2.6 Piston Dynamics and Friction
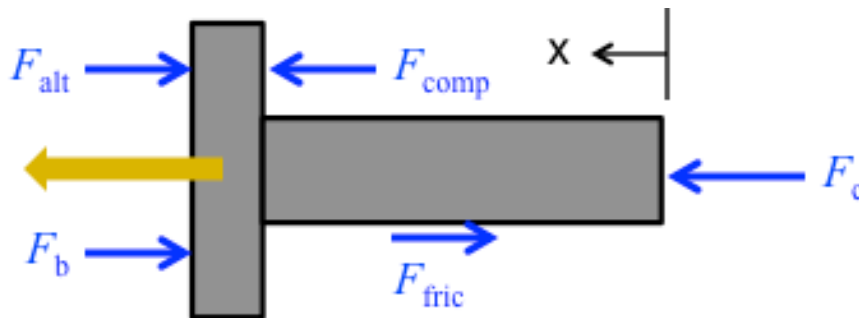
Figure 2-3 Force balance on the piston

Piston movement is determined by Newton's Second Law and the forces applied on the piston, as shown above in Figure 2-3.

Newton's Law:
$$m \cdot \frac{d^2 x}{dt^2} = F_c + F_{comp} - F_b - F_{alt} - F_{fric}$$
(Eq 2.17)

F_c, F_{comp}, and F_b in Eq. 2.17 represents pressure forces in combustion chamber, compressor chamber, and bounce chamber, respectively. F_{fric} is the friction force estimated as a linear combination of piston velocity plus a constant C_s, as shown in Eq. 2.18 below.

$$F_{fric} = C_k \cdot V_{pis} + C_s$$
(Eq 2.18)

C_k is the kinetic friction coefficient related to the instantaneous velocity, and the C_s is the static friction coefficient as a constant part of the friction force.

The alternator force, F_{alt} is generated by the alternator coils and resists the change of magnetic field. With given piston mass, the acceleration can be computed. The alternator model is introduced in the next section.

2.7 Linear Alternator Model

The induced voltage, or electromagnetic field (EMF), is determined by the rate of change of magnetic flux Φ through the coil.

Induced Voltage:
$$V_{ind} = -\frac{d\Phi}{dt}$$
(Eq 2.19)

The negative sign represents the physical nature of the induced voltage against the change in magnetic flux. Applying the chain rule and basic electronic circuit relation on Eq. 2.19:

$$V_{ind} = -\frac{d\Phi}{dt} = -\frac{d\Phi}{dx}\frac{dx}{dt} = iR_{coil}$$
(Eq 2.20)

The coil resistance R_{coil} can be easily measured once the alternator is built. The chain rule transforms the flux rate of change into two terms: flux as a function of piston

position and piston velocity. Considering the power of the alternator with Eq. 2.19 substituted

Induced Power:
$$P_{ind} = iV_{ind} = -i\frac{d\Phi}{dx}\frac{dx}{dt}$$
(Eq 2.21)

This power is equivalent to the power extracted from the piston by the electromagnetic force.

$$P_{mech} = F_{alt}\frac{dx}{dt}$$
(Eq 2.22)

Substituting Eq. 2.22 into Eq. 2.21,

$$F_{alt} = -i\frac{d\Phi}{dx}$$
(Eq 2.23)

The alternator force is then obtained as a function of $d\Phi/dx$, which is the design parameter of the alternator, and is based on magnetic strength, coil turns, and gaps between magnets, among others. In Sandia's FPLA modeling work [5], this parameter is determined through an electromagnetic simulation. $d\Phi/dx$ as a function of piston position is known for every single coil in the alternator. With measured position and velocity, all values in Eq. 2.18 through 2.23 can be obtained.

In the TCFPLA engine, the alternator model was developed in parallel at Stony Brook University. For most part of this work, a simplified alternator model is used. Based on Eq. 2.20 and 2.23, the electromagnetic characteristics in the alternator can be lumped into a single parameter A, with the alternator force proportional to the piston velocity.

$$F_{alt} = -A\frac{dx}{dt}$$
(Eq 2.24)

Substituting into Eq.2.22,

$$P_{alt} = -A\cdot(\frac{dx}{dt})^2$$
(Eq 2.25)

Therefore, the power and force generated by the alternator can be varied by changing the power extraction coefficient *A*, representing different designs of alternators that extract different power levels. It is a holistic parameter for the alternator performance, as opposed to the individual parameters for each physical component.

2.8 Turbine Model

The turbine is modeled as an orifice with a prescribed isentropic efficiency. Knowing the inlet pressure, inlet temperature and outlet pressure at ambient, the isentropic outlet temperature can be estimated from thermodynamic relations. The gas composition is also known from the thermodynamic sub-model, so the inlet enthalpy h_{in}, inlet entropy s_{in} and isentropic outlet enthalpy $h_{ex,i}$ can be calculated.

$$(h_{in}, s_{in}) = f(P_{in}, T_{in}, Y_{in}) \qquad \text{(Eq 2.26)}$$

If isentropic, the entropy for inlet and outlet are the same. The species does not change before and after turbine. Based on the isentropic efficiency $\eta_{turbine}$, the turbine work can be obtained with known mass flow rate.

$$h_{ex,i} = f(P_{ex}, s_{ex}, Y_{ex}) \qquad \text{(Eq 2.27)}$$

$$W_{turbine} = \dot{m} \cdot \eta_{turbine}(h_{in} - h_{ex,i}) \qquad \text{(Eq 2.28)}$$

The turbine efficiency is then used to calculate the actual outlet enthalpy, which is in turn used to calculate the actual exhaust temperature.

$$h_{in} - \eta_{turbine}(h_{in} - h_{ex,i}) = h_{ex,a} \qquad \text{(Eq 2.29)}$$

$$T_{ex} = f(h_{ex,a}, P_{ex}, Y_{ex}) \qquad \text{(Eq 2.30)}$$

The function *f* in Eq. 2.26, 2.27 and 2.30 represents the thermodynamic relations.

2.9 Free-Piston Engine System

All the sub-models were discussed in the previous sections. Some assumptions have been made for the completeness of simulation. The assumptions for each of the

control volume are listed below. One general rule for all volumes are the thermodynamic state is uniform and homogeneous, meaning no temperature or pressure distribution, boundary layer, or fuel stratification at any given time.

Bounce Chamber

The working fluid is pure air. It is assumed as a perfect closed volume with no leakage between the piston and cylinder. It has heat transfer through the wall at the wall temperature of 330 K. The heat transfer is modeled by Woschni correlation with no flow in or out.

Intake Manifold

The intake manifold is a large volume connecting the fixed ambient condition (1atm, 298K) and the compressor chamber. Therefore, when the intake valves of compressor chamber open, the pressure drops slightly at an instant, but the intake manifold is refilled by the ambient at the same time. As a result, very minor pressure oscillations occur during the intake process. The low load strategy, known as the "recirculation", changes the temperature and compositions of the intake accordingly, as discussed in Section 4.5.

Compressor Chamber

The compressor chamber has an intake flow from the intake manifold. With no recirculation, the intake is pure air at the ambient condition. The heat transfer is modeled by Woschni correlation and the wall temperature is fixed at 360 K. There is some backflow from the air box that may change the composition inside the compressor chamber as well. The amount of intake mass is determined by the operating stroke, speed, and intake manifold condition.

Air Box

The air box composition consists of N2, O2, CO2, and H2O, as the beginning of the scavenging process bring some backflow from the combustion chamber. The working fluid in the air box is hotter, since the inlet air has been compressed in the compressor chamber. The heat transfer is estimated by the Dittus-Boelter equation as

described in Section 2.5.2. The wall temperature is at 500 K if the heat recovery process is considered, and 360 K if not. This reflects the heating effects of the heat recovery from the engine which will be discussed with further details in Section 5.2 and 6.4.

Combustion Chamber

Combustion chamber has wall temperature of 700 K if the heat recovery is involved, and 500 K if not. Woschni correlation is applied for heat transfer. Combustion efficiency is assumed to be 100%, meaning all fuel is burned and the combustion products are only CO_2 and H_2O. The combustion process is prescribed by the Wiebe function with parameters a = 2 and n = 5 in Eq. 2.8. The parameters are related to the shape of the burned mass fraction, as studied and described in Section 3.5.1. Injection timing is a variable parameter but the injection period is assumed as a constant 1 msec, regardless how much fuel is injected and duration of the combustion is constant 2.8 msec, similar to a modern diesel engine operation. The scavenging process is a "perfect-mixing" process, which will be explained later in this section.

Exhaust Manifold

Exhaust manifold is a fixed volume and assumed adiabatic. It receives the flow from the combustion chamber and delivers it to the turbine. The inlet flow comes from the scavenging process, so the state changes by time as the scavenging air continuously mixes with the combustion products. The outlet flow is much smaller than the inlet flow due to the small orifice connecting to the turbine, causing the mass to accumulate in the exhaust manifold. Therefore, the pressure increases during the scavenging process and decreases when the scavenging ports close. The temperature and composition changes with the inlet flow, according to the conservations of energy and species. As a result, a mixing process occurs during the scavenging event creating an irreversible process.

Turbine

The turbine is assumed to operate in pseudo steady state mode so the dynamic effect is assumed zero. That is, the mass flow through the turbine is a constant flow with its enthalpy extracted based on the thermodynamic relations. The turbine is assumed

30

adiabatic with 85% isentropic expansion efficiency with the outlet condition at 1 atm and 298 K as the ambient.

Flow

Regarding to the mass transfer, the flow through a restricted area is an adiabatic process. The flow compositions are the same as the upstream condition, and mix with the downstream instantaneously to form the uniform state in the downstream volume. This is also the "perfect-mixing" scavenging process, namely the mixture in the combustion chamber is homogeneous at any moment.

Linear Alternator

Linear alternator, as described in Section 2.7, is a simplified model, which estimates the electromagnetic force based on the piston velocity. The model assumes that the magnets are fully engaged with the coils at any moment, except two turnaround points. Therefore, the simplified model does not have the oscillations and only follows the piston velocity, as can be seen in Figure 4-14. Moreover, it contains no estimation of the electric voltage and current. As mentioned in Section 2.7, the power extraction coefficient *A* can be varied based on different load conditions. This is based on the assumption that the coils in the alternator can be disconnected by active electric control unit. Considering the alternator current is used to charge a battery, an AC-to-DC conversion efficiency of 85% is used. A more realistic linear alternator model with actual electric components will be introduced in Chapter 4 and compared with this simplified model.

Sample Results

By integrating the sub-models, the whole free-piston engine can be studied. It is a complicated system, as each sub-model has to communicate with other sub-models. To obtain the thermodynamic states of the air box, for example, requires the flow and heat transfer sub-models for calculating the laws of conservation. In addition to the complexity of each volume, free-piston engines have unique characteristics. Therefore,

some sample results are presented here to illustrate the operation fundamentals of the free-piston engine.
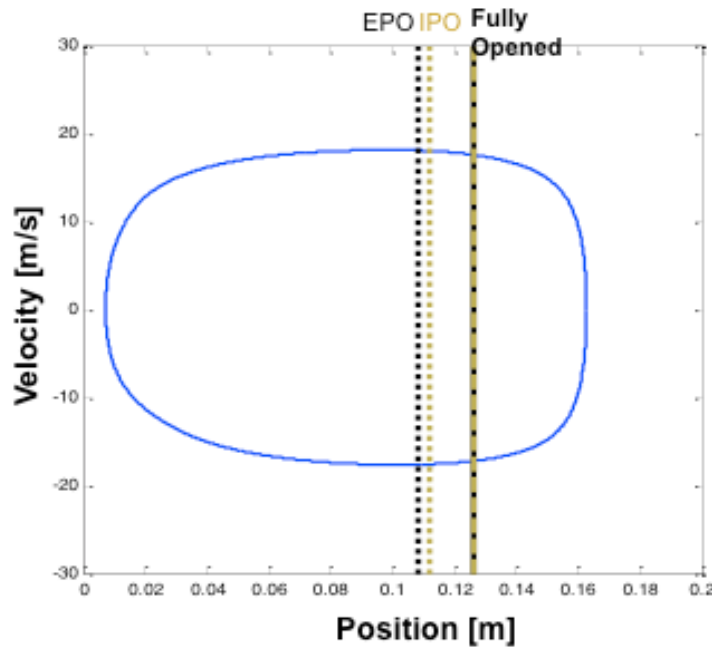
Figure 2-4 Free-piston position vs. velocity

Figure 2-4 shows the piston motion, and the position of exhaust port opening (EPO), intake port opening (IPO) are both marked. The velocities are zero at the dead centers or the turnaround points where the value of velocity changes sign.   This rectangular shaped profile indicates the free-piston has high acceleration near the dead centers. Recalling that the cranked-driven piston has highest velocity at mid-stroke, free-piston shows a different scheme.

32
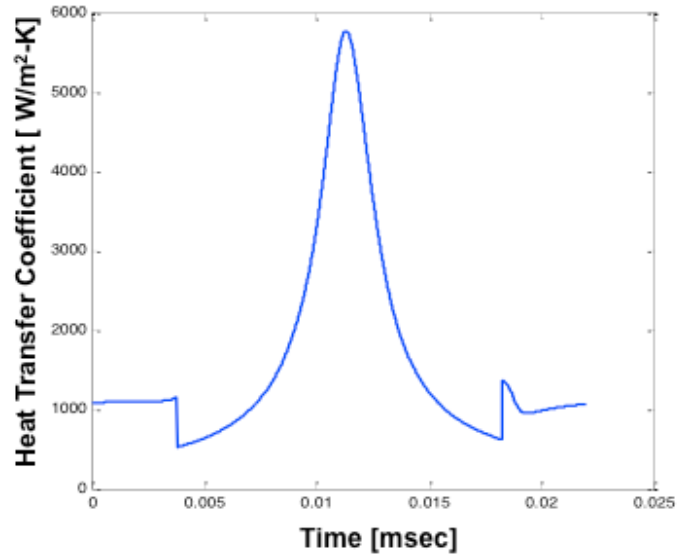
Figure 2-5 Combustion chamber heat transfer coefficient in a cycle

Figure 2-5 shows the heat transfer coefficient based on the modified Woschni correlation for the opposed-piston scheme, as described in Section 2.5. The Woschni correlation has different equations for open and closed cycle, and this explains the instant raise and drop at two points, where the scavenging ports open.
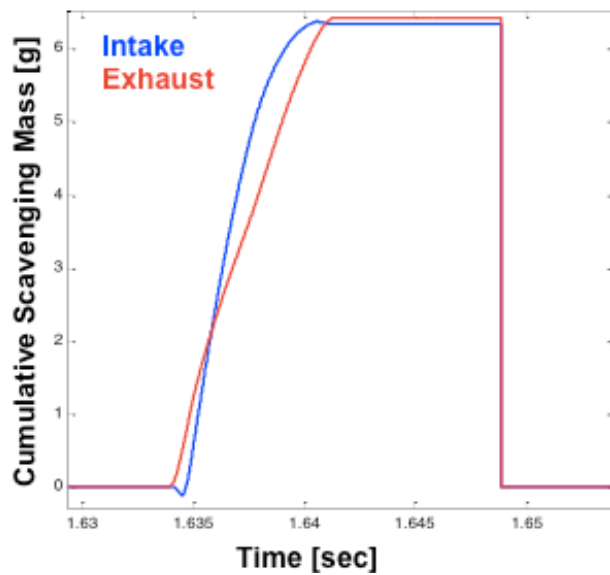
Figure 2-6 Cumulative mass during one scavenging process

33

Figure 2-6 shows the scavenging flow process. The exhaust port (red) opens slightly earlier for the blow down to prevent too much backflow through the intake port (blue). The intake flow has small backflow as seen the value goes to negative at first.
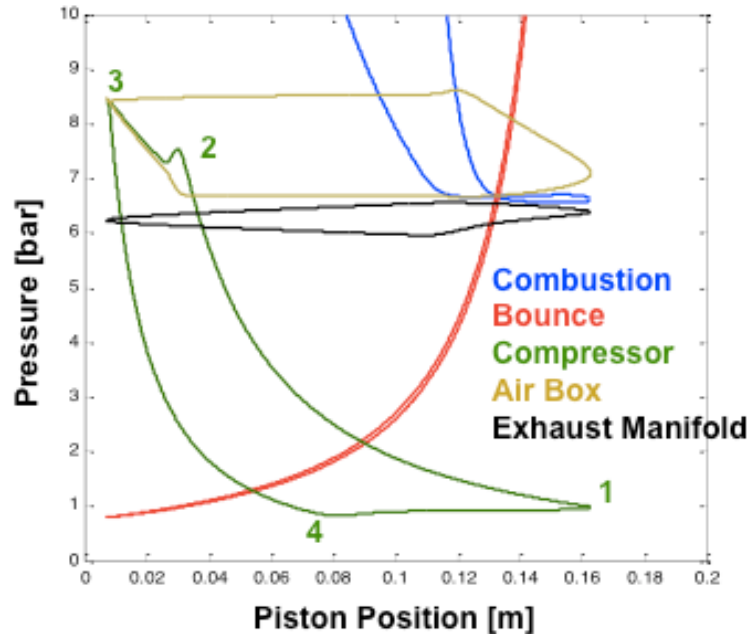
Figure 2-7 Pressure vs. piston position for all control volumes

The pressure profiles for all control volumes are shown in Figure 2-7. In order to show most profiles clearly, large portion of the combustion chamber pressure curve is out of sight. The bounce chamber works as gas springs, compressing and expanding through similar curves. Note that the bounce chamber curves have opposite directions with the compressor and combustion chamber, because the bounce chamber goes reverse stroke. The compressor starts the compression stroke at "1". "2" is the point where the delivery reed valves open, and the air starts being transferred into the air box. The small drop is due to the compressor filling the large air box at lower pressure. The curve then climbs up again as these two connected volumes are compressed together by the piston until point "3". While the piston reaches the dead center and returns, the delivery valves close and the compressor chamber expands to "4". The air box stores the air for scavenging, so the pressure reduces during the breathing process. The exhaust manifold is an adiabatic

34

reservoir, allowing the exhaust flow transfer throughout the turbine with small pressure variation followed by the scavenging flow.

Bibliography

[1]   M. Costagliola, "Dynamics of A Reed Valve", Dissertation thesis, Massachusetts Institute of Technology, 1949

[2]   R. B. Krieger, "The Simulaion of a Two Cycle, Crankcase Scavenged, Spark Ignition Engine on a Digital Computer and Comparison of Results with Experimental Data", Dissertation thesis, University of Wisconsin, 1968

[3]   J. B. Heywood, "Internal Combustion Engine Fundamentals", ISBN-10:007028637X, 1988

[4]   X. He, M. T. Donovan, B. T. Zigler, T. R. Palmer, S. M. Walton, M. S. Wooldridge, A. Atreya, "An Experimental and Modeling Study of Iso-octane Ignition Delay Times Under Homogeneous Charge Compression Ignition Conditions", Journal of Combustion and Flame 142, 2005

[5]   S. S. Goldsborough, P. Van Blarigan, "A Numerical Study of a Free Piston IC Engine Operating on Homogeneous Charge Compression Ignition Combustion", SAE 1999-01-0619, 1999

[6]   G. Woschni, "A Universally Applicable Equation for the Instantaneous Heat Transfer Coefficient in the I.C. Engine", SAE paper 670931, 1967

[7]   F. P. Incropera, "Fundamental of Heat and Mass Transfer", ISBN-10:0471457280, 6th Edition, 2006

CHAPTER 3

TCFPLA Engine Model Demonstration

In the previous chapter, the model was described in full. Most parts of the model are built based on physics or empirical correlations. In the present chapter, the simulation results are demonstrated against available historical data of GS-34, an opposed free-piston gas turbine manufactured by a French company named Société industrielle générale de mécanique appliquée (SIGMA) and discussed in Chapter 1. This engine was chosen for demonstration due to its commercial success and the lack of modern free-piston engine data. Because of the data insufficiency, several sensitivity tests were done for eliminating the possible error in the data measurement and determining the range of variations.

3.1 Configuration of SIGMA GS-34

The 1000 HP output of the GS-34, as a stationary engine, is not comparable in terms of size with an automotive application. However, the GM Hyprex used the successful GS-34 design as a guide; hence, the engine architecture is very similar. In addition, understanding the system reaction with different parameter setups is helpful before studying the downsized version. This is a highly stable free-piston engine, and Flynn tested this engine for 25,000 hours without breaking a part [1]. Power output of the GS-34 relies on a power gas turbine, utilizing the high-pressure exhaust gas to push turbine blades for mechanical torque.

The detailed configuration of the GS-34 can be seen in Figure 3-1 below.

1	Casing	6	Intake valves	11	Stuffing box
2	Compressor cylinder	7	Discharge valves	12	Starting mechanism
3	Bounce-cylinder head	8	Pressure-equalizing pipe	13	Stabilizer
4	Engine cylinder	9	Cooling-water inlet	14	Synchronizing mechanism
5	Scavenge chamber	10	Cooling-water outlet		
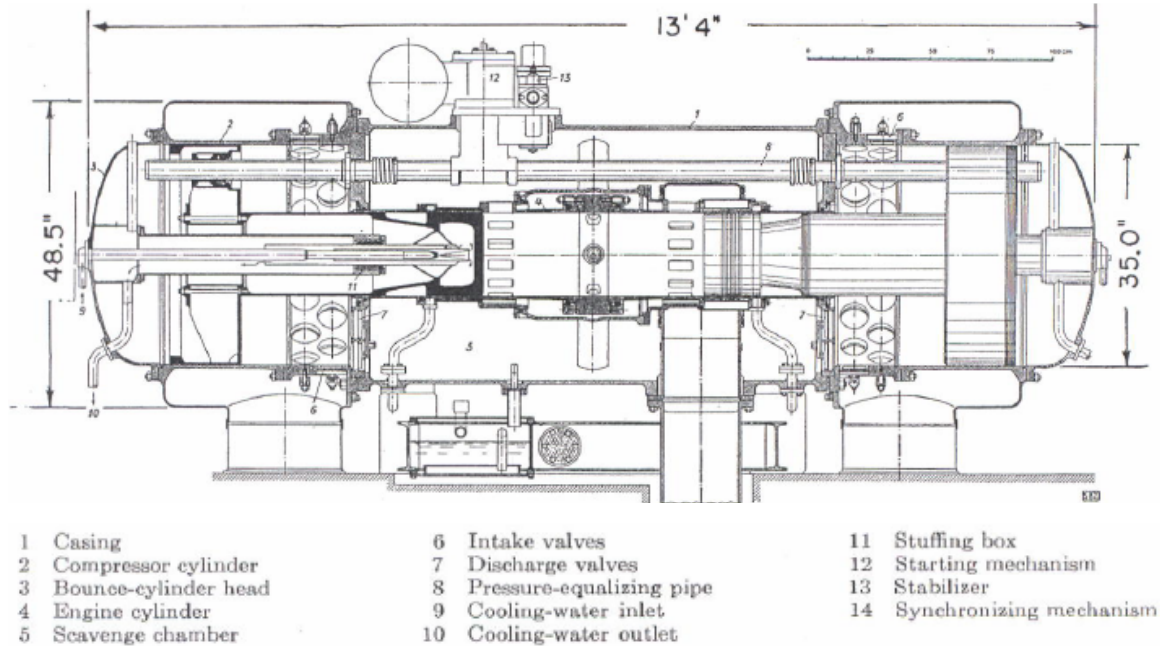
Figure 3-1 Configuration of SIGMA GS-34 with transparent view on the left piston [2]

It is worth noting that part 8, the pressure-equalizing pipe, plays an important role to synchronize the two pistons. This pipe connects both bounce chambers with a controlling device, called stabilizer as part 13. This stabilizer regulates the average pressure in the bounce chambers that correspond to different loads. It conducts the air from bounce chamber to air box (scavenge chamber) when the bounce pressure is higher, and vise versa. The stabilizer is a 2-way valve with a spring loading on one side, which builds a linear adjustment between bounce chamber and air box pressures. The effects of the stabilizer are beyond the scope of this work and will be proposed for future work.

Table 3-1 Geometric information of GS-34

Engine Bore (m)	0.340
Bounce Bore (m)	0.895
Compressor Effective Bore (m)	0.823

Engine Piston Length (m)	0.975
Compression Piston Length (m)	0.279
Compressor Offset (m)	0.03
Bounce Offset (m)	0.68
Turbine Orifice (m)	0.093
Piston Solidity (%)	24.1
Piston Mass (kg)	508

The geometric information for the GS-34 is listed in Table 3-1 above. Notice that the "compressor effective bore", is not an actual bore dimension, but effective bore based on the actual compressor area, which is partially occupied by the engine piston and pressure-equalizing pipe as seen in Figure 3-1. The compressor and bounce offsets are defined as the clearance from their piston tops to their cylinder ends when the engine piston head is at the centerline. The piston solidity, or solidness, is how much the metal actually fills the piston's outlined volume, so 100% means the piston is fully solid. As seen in Figure 3-1, the piston has the water pipe enclosed for cooling purpose and therefore the solidity is only a fraction of one.

3.2 GS-34 Experimental Results

The only available experimental study was conducted by Professor Eichelberg in 1948, and the data was collected in the technical report by Oppenheim and London [3]. The reported data for GS-34 at full load is listed below in Table 3-2.

Table 3-2 Experimental results of GS-34 reported by Eichelberg

Power Output (hp)	1338

Frequency (cycle/min)	613
Effective Stroke (m)	0.443
Average Piston Velocity (m/s)	9.05
Turbine Inlet Temperature (K)	780
Turbine Inlet Pressure (bar)	4.4
Gas Delivery Rate (kg/s)	3.65
Compression Pressure (bar)	73.5
Heat Transfer (%)	19.4
Thermal Efficiency (%)	41.2

The experimental test lasted for 17 hours, and the engine remained in good condition after the test. Longer duration of test runs were also performed totaling 3000 hours, showcasing the successful design and good reliability of the GS-34 at the time.

3.3 Numerical Analysis of the GS-34 Engine

In the same report mentioned in previous section [3], London and Oppenheim presented a thermodynamic-dynamic model as part of the design procedure for this type of free-piston gas turbine. Due to the lack of actual information from the real engine, they made some assumptions that allowed them to achieve 1000 HP shaft output. Therefore, the mathematical model did not match the results from the experimental work from Professor Eichelberg, but it provided insights to the free-piston engine system design parameters.

In 1952, Welge [4] followed this calculation procedure but was able to match Eichelberg's results, validating the model and supplying more details on thermodynamics and dynamic behavior to enable better design analysis. Later that year, London and

Oppenheim presented the experimental results [2], combined with the numerical calculations based on their thermodynamic-dynamic model. These provide the most complete set of information in the literature for a free-piston engine.

Table 3-3 below is copied directly from London [2], showing some thermodynamic and performance data from the GS-34. The units are also converted into SI units for convenience. Note that the frequency is 613 rpm, which is the same as in Eichelberg's experiments. This is because London's numerical model employs some real experimental results as known conditions in the calculation.

Table 3-3 Summary of SIGMA GS-34 Design and Performance

Combustion Chamber	Bore (m)	0.340
	Area (m^2)	0.091
	Length (m)	0.965
	Effective Stroke (m)	0.246
	Compression Ratio	8.5
	IMEP (bar)	15.9
Compressor Chamber	Effective Bore (m)	0.823
	Effective Area (m^2)	0.533
	Stroke (m)	0.445
	Pressure Ratio	5.42
Bounce Chamber	Effective Bore (m)	0.895
	Effective Area (m^2)	0.629
	Stroke (m)	0.445

	Pressure Level (bar)	1.8
	Temperature Level (K)	533
Turbine	Power (kW)	850
	Flow Rate (kg/sec)	3.62
	Pressure Inlet (bar)	4.45
	Temperature Inlet (K)	1033
	Orifice (m)	0.093
Operating Condition	Frequency (rpm)	613
	Fueling Rate (mg/cycle)	5673
	Piston Mass	503
Thermodynamic Data	Heat Losses (% of fuel LHV)	19.4
	Friction (% of compressor work)	12.0
	Brake Efficiency (%)	34.6

In addition to the data in the Table 3-3, the pressure-volume (P-V) diagrams in control volumes are key to understanding the system design. For example, since the peak pressure in the compressor is the delivery pressure, this implies that there is back-pressure in the air box. Also, the blow down process observed in the engine cylinder pressure indicates the position of exhaust port opening, which is a very important parameter for the system performance. Figure 3-2, 3-3 and 3-4 below show the P-V curves in different control volumes.
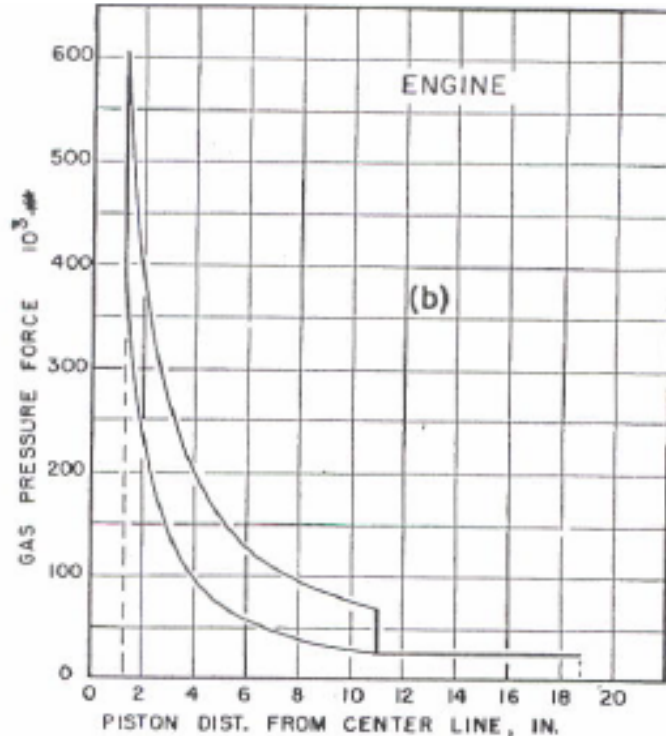
Figure 3-2 P-V diagram of combustion chamber
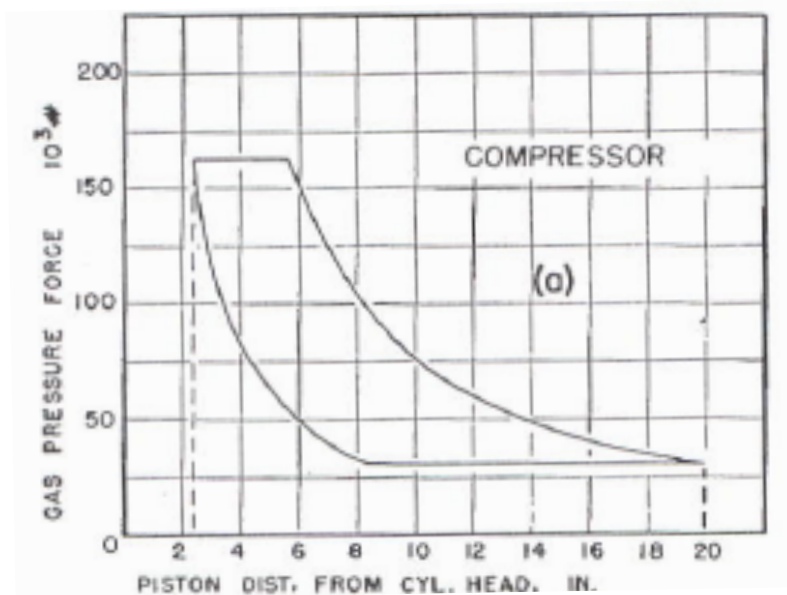
Figure 3-3 P-V diagram of compressor chamber

43
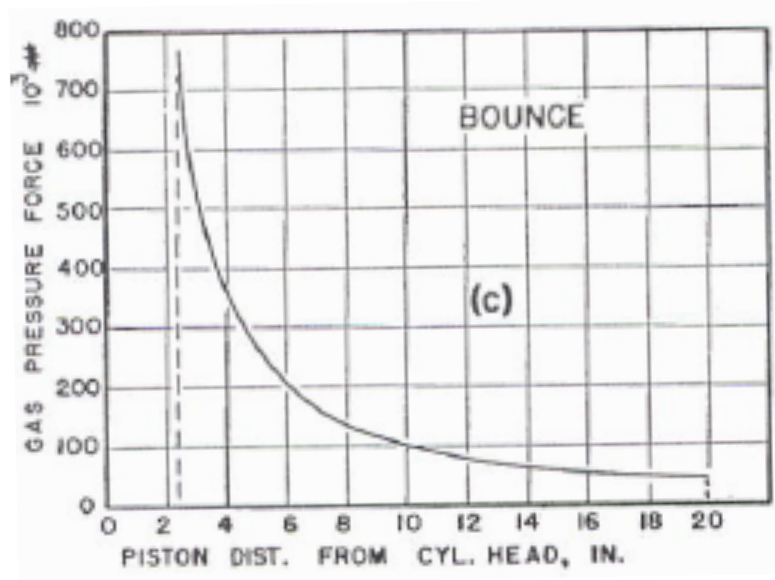
Figure 3-4 P-V diagram of bounce chamber

Note that the Y-axis is a "gas pressure force" in units of "#", which is pound-force [2]. The pressure force, by definition, is the force caused by the gas pressure acting on the piston surface area. In compressor chamber, for example, the lowest gas pressure force is around 30,000 lbf. Assuming an area of 5.73 ft2 based on Table 3-3, this translates to a minimum pressure of 36.4 psi, or 2.5 bar, which is the inlet condition of compressor. Since the GS-34 does not have a boosting device, a pressure higher than the ambient was confusing at the early stage of this work. Until the detailed calculation reference by Weige [4] was found, it became clear that the unit in those figures is pound-force per pound of air delivered. Therefore, the actual air delivered per pound per cycle per compressor chamber is 0.388 lb mentioned in table 3-3, which reflect the pressure inlet for the compressor chamber is 2.5 multiply by 0.388, equaling to 0.97 bar. This slightly lower-than-ambient pressure is due to the pressure drop while passing the intake reed valve.

3.4 Demonstration of New Matlab/Simulink Model

The model described in Chapter 2 was calibrated and validated using the available geometric information and pressure data for the GS-34. The input parameters were specified based on Table 3-1 and Table 3-3. For example, the fuel injection rate was 5600 mg/cycle at 613 cycles per minute.

The friction coefficients Eq. 2.18 were initially set to be as $C_k = 500$, $C_s = 3000$ to match the data of friction work as 12% of compressor work. Heat transfer from the Woschni model had to be enhanced by 150% to match the 19% total heat losses as given. The coefficients for the Wiebe function in Eq. 2.8 giving the heat release rate were a = 4.4 and n = 1.5, with 28 msec burn duration. The heat release rate adjustment ensures that both the peak pressure and expansion curve matched the reference figure. Sensitivity analysis on the model parameters was carried out to understand the effects of these factors on the system performance.

Table 3-4 list some important results for comparison between London's simple thermodynamic model and the new Matlab/Simulink model, referred to as the UM model.

Table 3-4 Results comparison for London's and UM model

Model	London	UM model
Brake Efficiency (%)	34.6	36.1
Compression Ratio	8.5	8.45
Frequency (Hz)	10.2	11.5
Mass Flow Rate (kg/compressor/cycle)	0.176	0.174
Pcomp, delivery(bar)	5.1	5.0

Pin,turbine, avg (bar)	4.4	4.3
Pbounce, max (bar)	9	10.3
ηvol (%)	60.8	59.9
ODP (mm)	475	492
IDP (mm)	33	33
Turbine Work (kJ/cycle)	83.3	85.5
Turbine Inlet T (K)	780	805
Mengine Trapped Ratio	0.47	0.44
Net IMEP (bar)	8.7	9.6
Heat Losses (% of fuel)	19.7	18.7
Friction (% of comp. work)	12.0	12.1

The results from UM model show good agreement with London's calculations. It is important to note while London's model operated based on some known values obtained directly from the experimental results, the simulation with the UM model is initialized with the assumption that the engine was fully at rest and with ambient conditions in all volumes. That means the model is able to match the experiments quite well without requiring significant tunings. The models for friction, heat transfer, and combustion were tuned, but the calibrated parameters were all within the expected range,

and gas properties were calculated instantaneously based on the current thermodynamic states. The only assumption that was kept the same was the adiabatic bounce chamber.

The data from Figure 3-2, 3-3, and 3-4 were extracted and converted into SI units for comparison with the UM model. The results are shown in Figure 3-5 to 3-7.
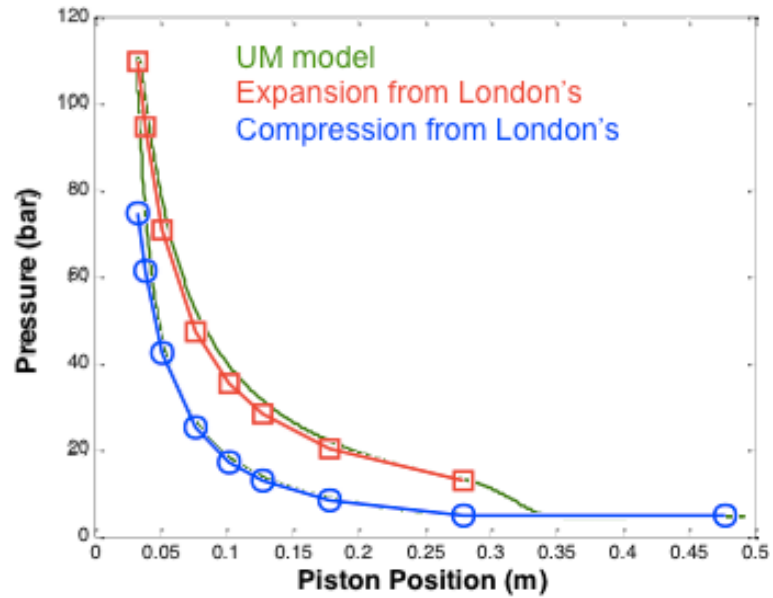
Figure 3-5 Pressure-volume diagram of combustion chamber
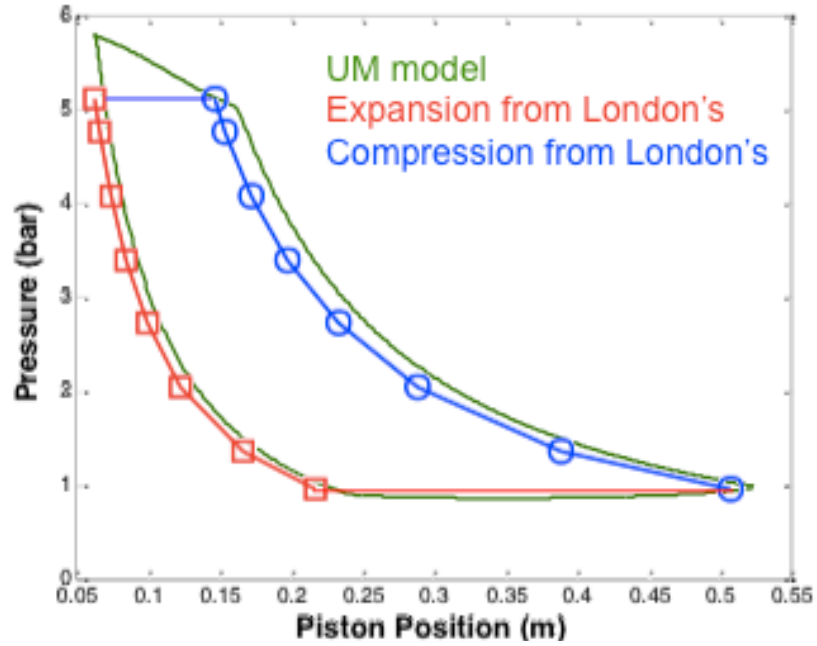
Figure 3-6 Pressure-volume diagram of compression chamber
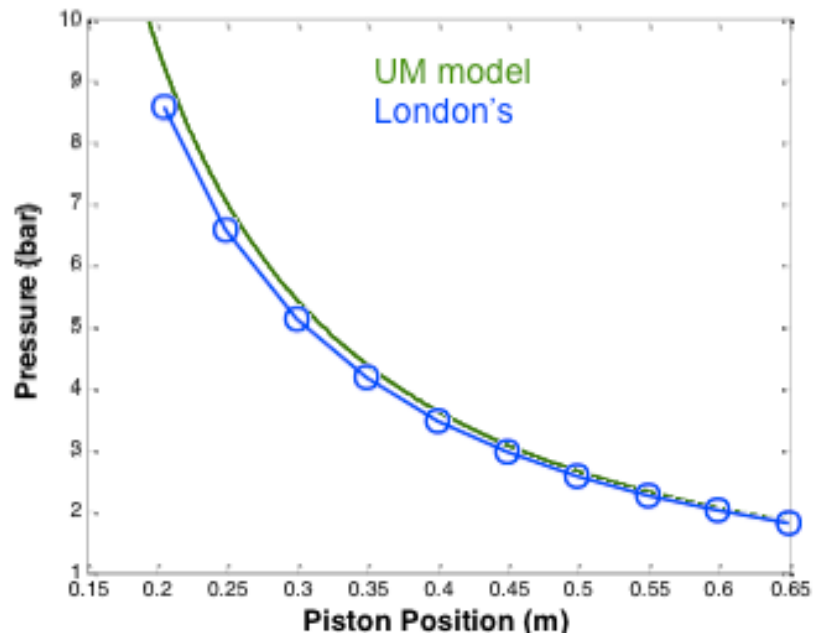
Figure 3-7 Pressure-volume diagram of bounce chamber

London's model calculates the compression and expansion processes separately. This is why the figures were plotted in two distinct curves for the combustion and compression chambers. In the bounce chamber, since the processes are assumed to be isentropic, there is a single overlapping curve.

Figure 3-5 shows the difference between the idealized exhaust blow down process in London's model as a vertical line, compared to a more realistic blow down curve predicted by the UM model. Also, Figure 3-6 shows the gas delivery process occurring at the end of the compression process of the compressor chamber as a flat line instead of the sloped line from the UM model. These differences arise because London's model does not contain any valves or ports. Furthermore, as shown in Figure 3-5, London assumes the combustion process is at constant volume, while this is not the case in the UM model, where a more realistic finite burning curve is used.

In general, the pressures predicted by the UM model in the combustion chamber and compressor chamber are slightly higher than those from London's model during the outward movement process. This is mainly due to the dependence of specific heats on temperature and pressure in the UM model. The higher pressures acting on the piston would make the piston move faster, and reach further into the outward dead point (ODP). This is the reason why in the frequency, ODP and net IMEP are larger in the UM model, as seen in Table 3-4. However, the majority of results show very good agreement, so the model can be considered properly demonstrated.

3.5 Discussion on the Model Demonstration

It is generally not a good idea to compare a model with another model, as was done here. Nevertheless, resources and experimental data were quite limited for this type of engine. London's modeling approach was to take all available experimental results and apply basic thermodynamic principles to obtain the best possible estimates. The combustion and expansion processes in the combustion chamber wee highly modified to match the experimental results [3]. The fuel chemical energy release was modeled as

heat addition at constant volume. However, in Welge's calculation [4], even though the added heat increases the actual temperature to 2260 K, the peak temperature was limited to 1300 K for all the other calculations. Furthermore, the expansion work was also adjusted to 77% of the isentropic expansion work based on the Otto cycle. It is not clear where these adjustments came from, but it is reasonable to assume that these try to reflect at least two events that are not accounted in London's model; the first is the high heat losses, as no heat transfer model was used; and second, the long burn duration also prevents the expansion pressure from dropping rapidly. These adjustments to London's model resulted the modified calculations shown as below:
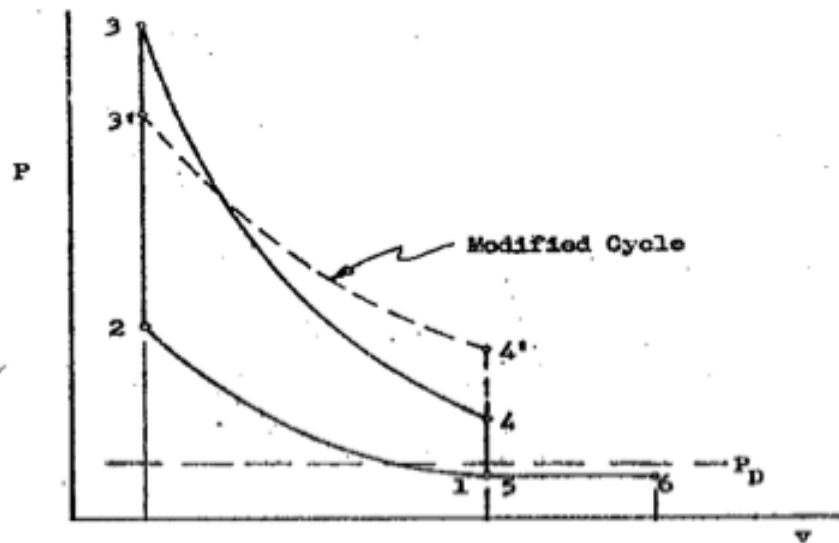
Figure 3-8 London's modified expansion process

In Figure 3-8, the constant-volume heat addition brings the pressure to point 3, but the limited temperature at 1300K also limits the pressure at point 3'. The expansion work under curve 3-4 is reduced to 77% and presented under curve 3'-4'. The polytropic exponent is based on the modified expansion work, limited temperature and known compression ratio. Therefore, this information can only be obtained by a posteriori and cannot be computed based on simple thermodynamic relations.

On the other hand, the UM model is able to predict the thermodynamic-dynamic relation using physical input parameters, such as sizing, piston mass and fuel injection. The Wiebe combustion model can also be tuned to change instantaneous burn rate and burn duration, including the timing of peak burn rate, all of which directly affect the pressure change in the cylinder during combustion. Hence, the question lies on how to adjust the Wiebe function to match the pressure curve. London's compression and expansion curve in the combustion cylinder is shown as below.
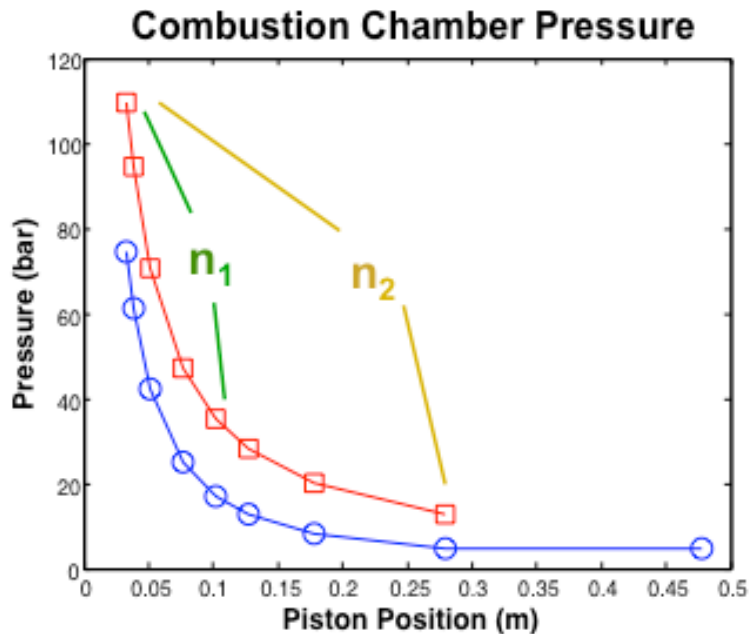
Figure 3-9 P-V diagram of combustion chamber from London's result

n_1 and n_2 here in Figure 3-9 are London's polytropic exponents between two given points as indicated. n_1 and n_2 are 0.95 and 0.99, respectively. The values are much lower than the expected isentropic exponent (k~1.3), which implies that the expansion process is far from isentropic as it usually is in modern engine cycles. Modern engines have larger polytropic exponents because the heat is losses during expansion process and expansion rates. Conversely, the low polytropic exponents in the GS-34 indicate that heat is being added during the expansion stroke, which is only possible if fuel is still burning. Considering the large size of the GS-34 and the large amount of fuel required to

51

run the engine, it is possible for the burn duration to be fairly long. Olson [5] presented simulation work in 1958 on a free-piston device not explicitly mentioned, but according to the general structure and stroke, it is believed to be the GS-34 or a very similar engine. In his work, a very long burn duration was implemented as can be seen below in Figure 3-10.
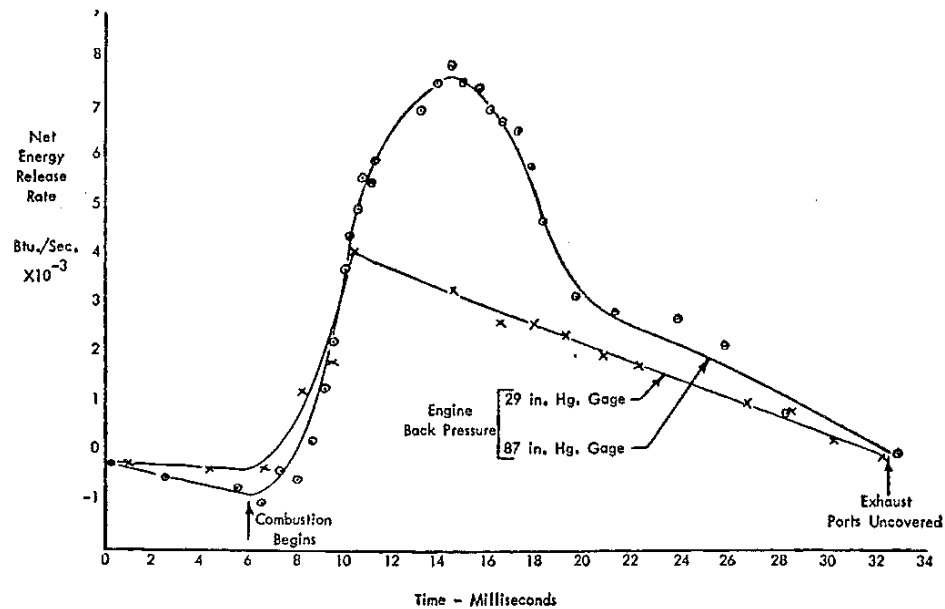
Figure 3-10 Energy release rate for free-piston engine combustion

Two curves in Figure 3-10 represent the heat release rates at different loads. Both of them have more than 25 milliseconds of heat releasing duration. It is extremely long, compared with modern diesel engines whose burn duration is about 4 milliseconds. Considering the GS-34 as a huge stationary engine with more than 5600 mg/cycle of fuel injected, the long burn duration seems to be reasonable. This again explains why the uncommon adjustments are needed in London's model, because the long burn time in reality is far from his assumption of constant volume combustion.

3.5.1 Sensitivity to Burn Rate

From Figure 3-10, it is clear that the duration of combustion heat release is at least 25 milliseconds. Even though the GS-34 runs at a low rpm, the combustion duration is

52

still very long. After adjusting the combustion model with an appropriately long burn duration, the expansion pressure curve was matched, as shown in Figure 3-5, and as long as the burn duration lasts most of the expansion process, the polytropic exponent should be close to 1 as in London's result. However, the shape of heat release rate will also affect the pressure profile in other ways. For example, by varying the coefficients of the Wiebe function, the burn rates vary as shown below:
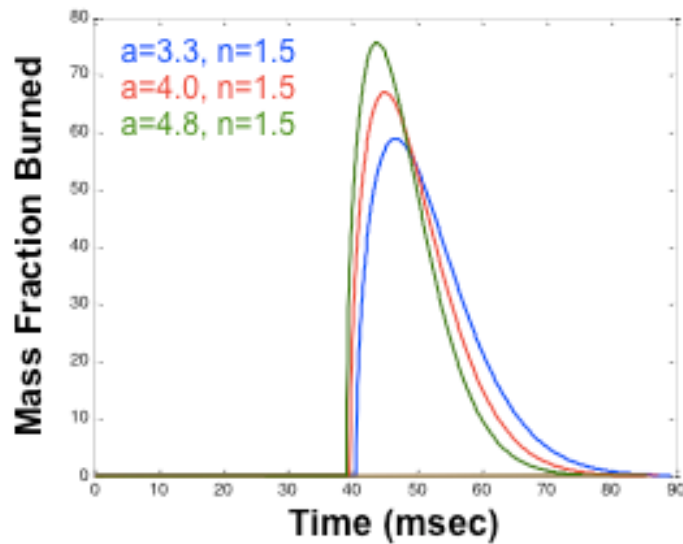
Figure 3-11 Mass fraction burn rate with different Weibe coefficient "a"

The fueling rate is kept constant for all the cases, and combustion is triggered when the piston achieves the same compression ratio as that reported by London. This isolates the burn rate effects. The coefficient "a" in Wiebe function (Eq. 2-8) primarily affects the peak burn rate value, and the faster burn in the early stages leads to a slower burn later. The pressure profile is especially important in the free-piston engine because it changes not only the produced work but also the frequency or speed. This is the reason why the start-of-combustion points are different in the time domain in Figure 3-11.
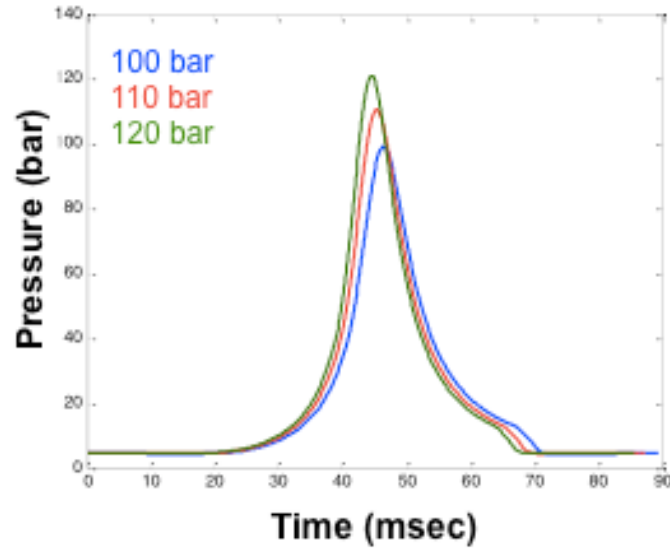
Figure 3-12 Pressure profiles with corresponding Wiebe functions in Figure 3-11

The pressure time histories in Figure 3-12 reflect the change in burned rate where the peak pressures are 100, 110, and 120 bar for "a" equals to 3.3, 4.0, and 4.8, respectively.   The peak pressure in London's simulation was 110 bar, but it was calculated based on idealized thermodynamics not accounting for real combustion behavior.   This study attempted to capture the sensitivity and the possible errors associated to London's assumptions of fixed compression polytropic exponent and constant volume combustion.

Table 3-5 Sensitivity study of burn rate/peak pressure effect

Model	London	UM model 100 bar	UM model 110 bar	UM model 120 bar
Brake Efficiency (%)	34.6	35.1	36.1	36.9
Compression Ratio	8.5	8.2	8.4	8.6
Frequency (Hz)	10.2	11.2	11.5	11.7
Mass flow rate	0.176	0.169	0.174	0.179

(kg/compressor/cycle)				
$P_{comp,delivery}$(bar)	5.1	4.8	5.0	5.2
$P_{in,turbine,avg}$ (bar)	4.4	4.1	4.3	4.5
$P_{bounce, max}$ (bar)	9	9.6	10.3	10.9
ηvol (%)	60.8	59.8	59.9	59.9
ODP (mm)	475	482	492	500
IDP (mm)	33	34	33	32
Turbine Work (kJ/cycle)	83.3	83.2	85.5	87.3
Turbine Inlet T (K)	780	825	805	790
Mengine Trapped Ratio	0.47	0.43	0.44	0.44
IMEP (bar)	8.7	9.3	9.6	9.9
Heat Losses (% of fuel)	19.7	19.6	18.7	17.6
Friction (% of comp. work)	12.0	11.9	12.1	12.3

As shown in Table 3-5, a higher peak pressure leads to a higher frequency, compression ratio, mass flow rate, stroke, and efficiency. The inward dead point (IDP) remains close throughout because the combustion events are triggered at the same point. The greater outward dead point (ODP) plays a more important role in improving engine breathing, which increases the mass flow rate through the turbine. In addition, more fresh air reduces the exhaust temperature through scavenging, which benefits the turbine durability.

Comparing the results between London's model and UM's model for the 110 bar case, it can be seen that the thermodynamic properties and performance numbers show

good agreement. The burn rate does have some effects on the pressure profile, which affects the system dynamic and performance. However, recalling that London had to significantly modify the combustion and expansion processes, it is assumed the predicted pressure is within a reasonable range, as compared to experimental data. Therefore, small variations of pressure due to the shape of burn rate do not affect system performance considerably. For example, a 10 bar increase in peak pressure increases efficiency by 1%, compression ratio by 0.2 points, frequency by 0.2 ~ 0.3 Hz, stroke by 10mm, and turbine inlet temperature by 20K. The results indicate that 10 bar difference in peak pressure caused by Wiebe function variations are not significant.

3.5.2 Sensitivity to Heat Transfer

Section 2.5.1 has described the heat transfer model in the new free-piston engine simulation. As mentioned in Section 3.4, the heat transfer was enhanced by 150% to match the reference data. Calibration of the heat transfer coefficient in common in modeling work because of the engine structural variation and many other factors that affect heat transfer rates. In general, this change is in the range of 80% ~ 130% for automotive engine. However, considering that the GS-34 is a stationary engine, it has a much larger surface area than the mobile ones due to its size and special configuration, so 150% is still considered acceptable. Heat transfer is further varied by 125% and 100% in this study to understand its effect.

Table 3-6 Sensitivity study of heat transfer effect

Model	London	UM model 100% H.T.	UM model 125% H.T.	UM model 150% H.T.
Brake Efficiency (%)	34.6	38.2	37.1	36.1
CR	8.5	8.42	8.44	8.45
Freq (Hz)	10.2	11.6	11.5	11.5

Mass flow rate (kg/compressor/cycle)	0.176	0.175	0.175	0.174
$P_{comp,delivery}$(bar)	5.1	5.2	5.1	5.0
$P_{in,turbine,avg}$ (bar)	4.4	4.5	4.4	4.3
$P_{bounce, max}$ (bar)	9	10.7	10.5	10.3
η_{vol} (%)	60.8	59.3	59.6	59.9
ODP (mm)	475	497	495	492
IDP (mm)	33	33	33	33
Turbine Work (kJ/cycle)	83.3	90.4	87.9	85.5
Turbine Inlet T (K)	780	830	820	805
M_{engine} Trapped Ratio	0.47	0.44	0.44	0.44
IMEP (bar)	8.7	9.8	9.7	9.6
Heat Losses (% of fuel)	19.7	13.4	16.1	18.7
Friction (% of comp. work)	12.0	12.0	12.0	12.1

Table 3-6 shows the results for the different heat transfer levels. It can be seen that efficiency improves with lower heat transfer. This benefit comes directly from the turbine inlet conditions, where the pressure and temperature remains higher due to lower heat losses. Overall, the results show that heat transfer is not highly sensitive to the system performance. With the heat transfer rate enhanced by 150%, efficiency drops by 2%. Note that 2% in efficiency may be significant, but the extra loss has little effect on other volumes. This study was trying to observe the system response to the variables, but

not the performance. In other words, it eliminates the possibility of experimental measuring error on heat transfer. Considering that the stroke, compression ratio, frequency and mass flow rate remain similar, heat transfer is not a large factor on system behavior.

3.5.2 Sensitivity to Friction

The friction model containing static and kinetic components is described in Section 2.6. The coefficients were chosen arbitrarily to match the given data, as mentioned in Section 3.4. The following study tries to understand two key points related to the friction model; first, the effect of absolute friction force on the system behavior; and second, the isolated effects of kinetic friction and static friction. For the first test, a simply scaling factor was used to vary the friction force.

Table 3-7 Sensitivity study of total friction amount effect

Model	London	UM model 80% Friction	UM model 100% Friction	UM model 120% Friction
Brake Efficiency (%)	34.6	36.7	36.1	35.6
CR	8.5	8.57	8.45	8.33
Freq (Hz)	10.2	11.6	11.5	11.4
Mass flow rate (kg/compressor/cycle)	0.176	0.176	0.174	0.173
$P_{comp,delivery}$(bar)	5.1	5.1	5.0	5.0
$P_{in,turbine,avg}$ (bar)	4.4	4.4	4.3	4.3
$P_{bounce,\ max}$ (bar)	9	10.5	10.3	10.1
η_{vol} (%)	60.8	59.9	59.9	59.9

ODP (mm)	475	495	492	490
IDP (mm)	33	33	33	33
Turbine Work (kJ/cycle)	83.3	86.8	85.5	84.2
Turbine Inlet T (K)	780	803	805	807
M_{engine} Trapped Ratio	0.47	0.44	0.44	0.44
IMEP (bar)	8.7	9.5	9.6	9.7
Heat Losses (% of fuel)	19.7	18.8	18.7	18.5
Friction (% of comp. work)	12.0	9.6	12.1	14.7

Table 3-7 shows that the amount of friction had minor effect on the system performance. The relative friction work was 9.6%, 12.1%, and 14.7% for scaling factors of 80%, 100%, and 120%, respectively. It makes sense that the higher the friction, the slower the pistons movement and the shorter the stroke. However, the frequency only dropped 0.2 Hz, or 12 rpm from 80% to 120% of the baseline case. Since the changes are small, the friction is not considered an important term for system behavior. Furthermore, the free-piston engine has no rotating crankshaft assembly, so this is most of the friction seen in this device aside from that encountered in the turbine.

The second study focused on the individual effects of the kinetic and static components of friction. As mentioned in Section 2.6, the ratio of static to kinetic friction was chosen arbitrarily. Only London's relative friction reported as 12% of compressor work was available for calibration. Therefore, it was desired to examine the individual effects of each component of friction. To achieve this, the total friction work was fixed at the reference value and the coefficients C_k and C_s in Eq. 2.18 were varied independently. The friction forces acting on the piston throughout the cycle are shown below.
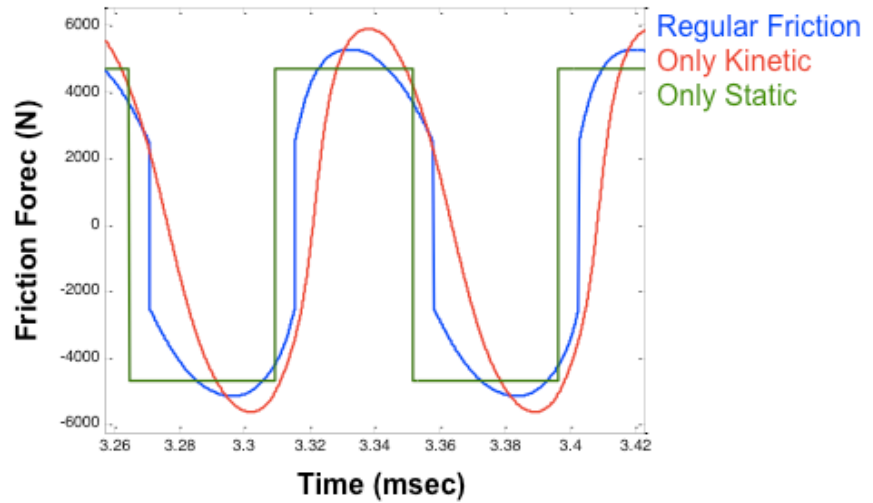
Figure 3-13 Different friction force models

It can be seen in Figure 13-3 that the kinetic friction is a smooth curve because it is only a function of piston velocity. Static friction is a constant value with the sign determined by piston's direction of motion. The values were properly adjusted to make the total friction work remain 12% of compressor work for a fair comparison. The results are shown in the following table.

Table 3-8 Sensitivity study of friction force models

Model	London	UM model Reg. Friction	UM model Only Kinetic	UM model Only Static
Brake Efficiency (%)	34.6	36.1	36.1	36.1
CR	8.5	8.45	8.46	8.45
Freq (Hz)	10.2	11.5	11.5	11.5
Mass flow rate (kg/compressor)	0.176	0.174	0.174	0.174
$P_{comp,delivery}$(bar)	5.1	5.0	5.0	5.0

$P_{in,turbine,avg}$ (bar)	4.4	4.3	4.3	4.3
$P_{bounce, max}$ (bar)	9	10.3	10.3	10.3
η_{vol} (%)	60.8	59.9	59.9	59.9
ODP (mm)	475	492	493	493
IDP (mm)	33	33	33	33
Turbine Work (kJ/cycle)	83.3	85.5	85.5	85.5
Turbine Inlet T (K)	780	805	805	805
M_{engine} Trapped Ratio	0.47	0.44	0.44	0.44
IMEP (bar)	8.7	9.6	9.6	9.6
Heat Losses (% of fuel)	19.7	18.7	18.7	18.7
Friction (% of comp. work)	12.0	12.1	12.1	12.0

This study showed the least sensitivity in the system, where most of the results remained unchanged. Therefore, the exact shape of the friction forces minimally affects the piston dynamics. Combined with the results from the first friction study, it can be concluded that the system behavior would change only when considering the energy dissipated by friction.

Bibliography

[1]   G. Flynn, "25,000 hours of Free-Piston Engine Operation", SAE National West Coast Meeting, San Francisco, 1956

[2]   A. L. London, A. K. Oppenheim, "The Free-Piston Engine Development – Present Status and Design Aspect", Transactions of the ASME, 1952:74(2):1349–1361

[3]   A. K. Oppenheim, A. L. London, " The Free-Piston Gas Generator – A Thermodynamic-Dynamic Analysis", Technical Report under Navy Contract N6-ONR-251 Task Order 6, NR-035-104, 1950

[4]   L. A. Welge, "The Free Piston Gas Generator – A Verification of The Oppenheim-London Design Method", Master's thesis, United State Naval Postgraduate School, 1952

[5]   D. R. Olson, "Simulation of A Free-Piston Engine With A Digital Computer", SAE paper 580276, 1958

CHAPTER 4

TCFPLA Engine Configuration and Operation

The previous chapter has proven that the numerical model can predict the physical behavior of the free-piston engine with the addition of alternator model. One goal of this study is to develop a proper device for the use of automotive vehicle. Therefore, GS-34, as the stationary engine for power plant, is too large for the purpose. The GM Hyprex, on the other hand, was originally built for the automotive use, so its dimensions are employed for initial study. This chapter determines the size of the device based on the power requirement by a step-by-step examination and optimization. The idling condition, or low load operation is also tested to complete the operating range. At the end, the engine map is generated to see the efficient region of the TCFPLA engine.

4.1 Parametric Study on Dimensions of Hyprex

The goal of this study is to develop the TCFPLA engine, which outputs 100 kW of power for the vehicle use. The original GM Hyprex produces 125 HP through gas turbine according to the reference [1]. Although the power seems to fit the demand, it is desired to use the alternator to potentially increase the efficiency. However, in order to understand the free-piston engine, the linear alternator is currently removed for a deeper study on the dimensions of the original GM Hyprex. There are four critical dimensions: bounce chamber offset, compressor offset, exhaust port opening position and compressor-to-combustion bore ratio. These dimensions can be presented in the simple sketch in Figure 4-1. Similar as some reported works [2][3], the piston mass is another important factor to impact the system. After the parametric studies, the final geometries can be determined based on the results. It is noteworthy that one should focus on the difference

among the cases under an individual parameter sweep, but not across different sweeps, since a base setting for one sweep may differ from one another.
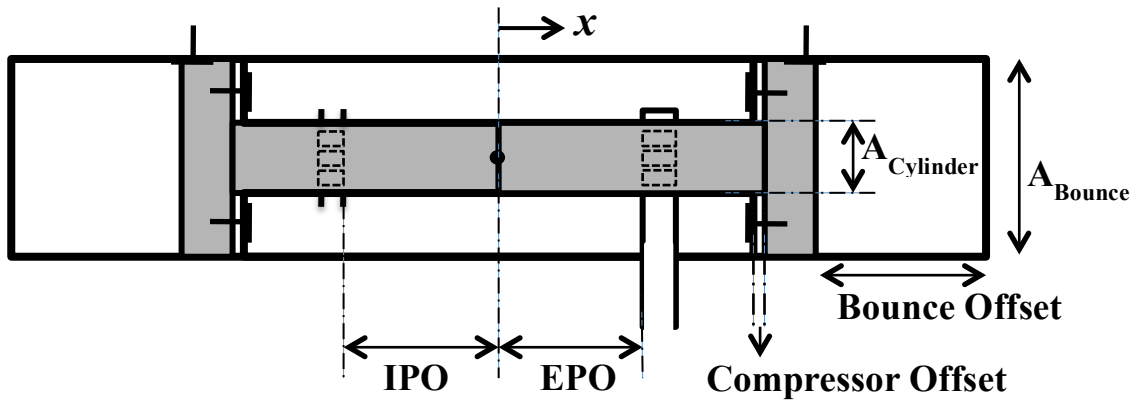
Figure 4-1 TCFPLA symbols for dimensions

4.1.1 Bounce Chamber Offset

The bounce chamber offset is defined as the distance from the piston head on the air piston (bounce chamber side) to the end the bounce chamber while the piston head on the combustion chamber at the centerline, as seen in Figure 4-1. The bounce chamber offset determines its maximum volume. For easily describing the offset value, it is normalized by the cylinder bore. The GS-34 has the value of Offset/Bore = 2.0, and this is the initial value for test. In the following results, all conditions are fixed except the fueling rate for the purpose of finding the full-load capacity, which is defined as the most fuel that can be burned without exceeding the 250 bar peak pressure limit. This limit is a common restriction for the modern compression ignition engines.

Table 4-1 Fuel sweep for Bounce Offset/Bore = 2.0

$M_{fueling}$	130	140	150	mg/cycle
Brake Efficiency	50.6	51.6	52.4	%
Effective CR	14.7	16.4	19.9	
Frequency	30.0	31.6	33.7	Hz

ODP	0.162	0.167	0.172	m
IDP	0.008	0.007	0.006	m
Turbine Power	83	96	112	kW
$P_{eng,max}$	173	214	295	bar

The results in Table 4-1 show that 150 mg/cycle has the cylinder peak pressure at 295 bar, which violates the 250 bar limit. Although the turbine powers are close to the reported 125 HP [1] from the original GM Hyprex, the fueling rate was never mentioned in that paper.

The Bounce Offset/Bore = 2.2 is tested as shown below:

Table 4-2 Fuel sweep for Bounce Offset/Bore = 2.2

$M_{fueling}$	150	160	170	mg/cycle
Brake Efficiency	50.3	51.4	52.4	%
Effective CR	12.3	13.3	15.1	
Frequency	27.6	28.8	30.4	Hz
ODP	0.181	0.185	0.189	m
IDP	0.009	0.009	0.008	m
Turbine Power	88	100	115	kW
$P_{eng,max}$	141	167	212	bar

Compare Table 4-2 with 4-1, the fueling rate has been increased but the peak pressure, effective compression ratio and frequency are lower with the Offset/Bore value of 2.2. On the other hand, the stroke, or more specifically, the outward dead center, significantly increases. The lower frequencies have similar power outputs with the higher fueling rates resulting in a brake efficiency that is nearly the same.

Geometrically, larger Offset/Bore value means the overall engine size is larger in the longitude direction, and the piston can travel a longer distance. Thermodynamically, a bigger bounce chamber reduces the relative compression in the bounce chamber for a given piston displacement, and therefore the bouncing force becomes smaller resulting in a smaller compression ratio. It consequently reduces the peak pressure in the combustion chamber and the steady state condition shows an overall lower pressure with a reduction in the frequency and speed. This can be clearly seen in the pressure profiles below:
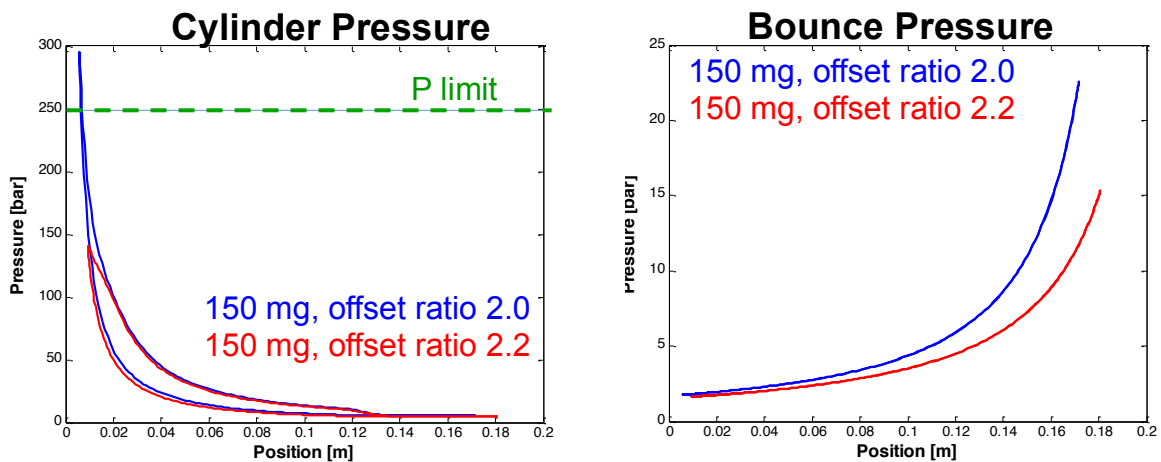
Figure 4-2 Cylinder and bounce chamber pressure with different Offset/Bore values

According to Frey [4], the max stroke in the Ford engine is about 0.173 m, which falls between the results of these two. Considering the advantage of a lower frequency and a higher load capacity, 2.2 is chosen as the value of the Bounce Offset/Bore ratio.

4.1.2 Piston Mass

It may not be difficult to imagine that the piston mass is an important parameter in the free-piston engine, because the piston motion, based on Newton's Second Law, is a function of pressure forces applied on the piston. The mass of the piston is not arbitrary but determined by its material and volume. Furthermore, solidity, mentioned in GS-34 reference [5], is the level of porousness in the metal structure. Table4-3 and a sketch below show the information of the piston in GS-34 and Hyprex.

Table 4-3 Piston dimensions of GS-34 and Hyprex

	GS-34	Hyprex
Engine Bore (m)	0.34	0.1016
Bounce Bore (m)	0.89	0.2794
Comp. Offset (m)	0.03	0.009
Bnc. Offset (m)	0.68	0.20
Turbine Orifice (m)	0.09	0.027
Piston Volume (m^3)	0.2636	0.0075
Piston Density (kg/m^3)	8000	8000
Solidity (%)	24.1	24.1
Piston Mass (kg)	508	15
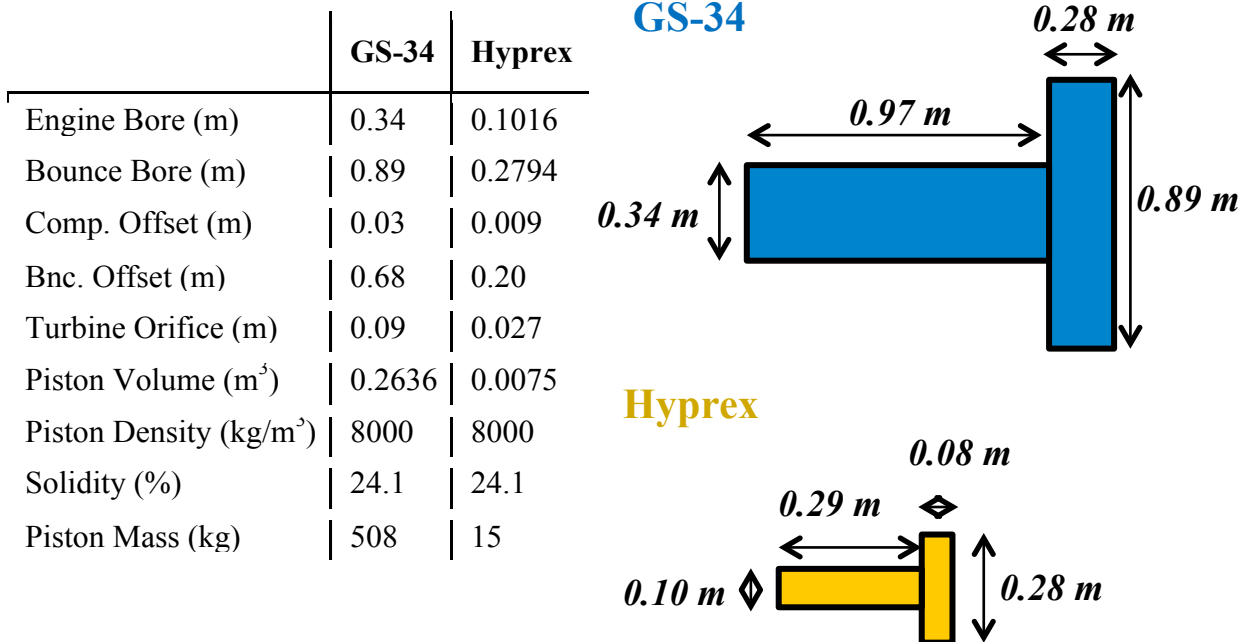
GS-34

Hyprex

As seen in Table 4-3, if the density and solidity is the same as the GS-34's piston, the Hyprex piston mass is 15 kg. The volume and materials may not be changed, but the solidity can be flexible. If the solidity is 100%, the corresponding mass becomes 60 kg. The following table shows the results of various piston masses under the same operating settings.

Table 4-4 The effects of piston mass with same fueling rate 110 mg/cycle

M_{Piston}	15	30	60	kg
Brake Efficiency	44.4	48.3	50.2	%
Effective CR	8.0	13.9	30.3	
Frequency	36.4	27.9	22.2	Hz
ODP	0.146	0.154	0.164	m
IDP	0.014	0.008	0.004	m

Pow$_{\text{Turbine}}$	75	63	52	kW
P$_{\text{eng,max}}$	70	137	358	bar

The results in Table 4-4 tell that the heavier piston tends to travel longer distance with reduced speed. It is because the heavier piston has less acceleration around the dead centers, and carries more inertia when the negative force applied on it to decelerate. This would increase compression ratio and peak in-cylinder pressure, increasing the potential to violate the restrictions. The piston motion profiles show this clearly as below.
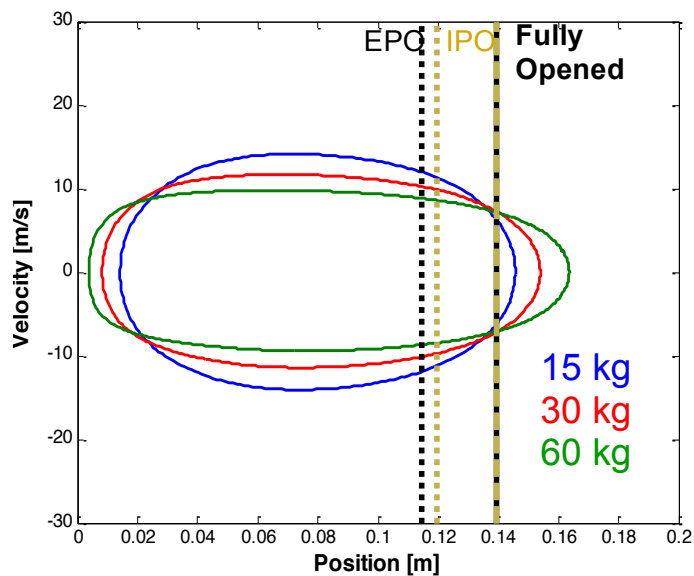
Figure 4-3 Piston velocity vs. position show the effects of piston mass

The lightest piston has very high speed, leading to high friction and low stability. The heaviest piston reduces the full-load capacity because of high cylinder pressure. Therefore, to avoid the disadvantage of both extremes, the piston mass 30 kg is then chosen for the engine in the size of Hyprex.

4.1.3 Compressor Offset

Similar to the bounce chamber offset, the compressor offset is defined as the distance between the piston head at the compressor side and the compressor head (see

Figure 4-1) while the power piston at the centerline of combustion chamber. If the compressor offset increases, the compressor becomes larger in size to accommodate more air during the intake process, but overall lower pressure in the compressor during the compression stroke may require more traveling to deliver sufficient air into air box. The results are shown below.

Table 4-5 The effects of compressor offset at the same fueling rate

Offset$_{Compressor}$	8.7	10.0	11.2	12.4	mm
Brake Efficiency	51.4	51.8	52.0	52.1	%
Effective CR	13.3	15.1	16.8	18.3	
Frequency	28.8	29.6	30.4	30.9	Hz
ODP	0.185	0.187	0.189	0.190	m
IDP	0.009	0.008	0.007	0.006	m
Turbine Power	100	104	107	109	kW
P$_{eng,max}$	167	200	233	260	bar

According to Table 4-5, larger compressor offset returns higher compression ratio in the combustion chamber. Because the lower pressure in the larger compressor reduces the stopping force, the piston travels more during the inward stroke. Since the piston is a single piece compressing both compressor chamber and combustion chamber at the same time, the combustion chamber compression ratio therefore increases and leads to higher peak in-cylinder pressure. However, overall the effect is small, compared with other dimensional numbers as seen in the piston motion profile.
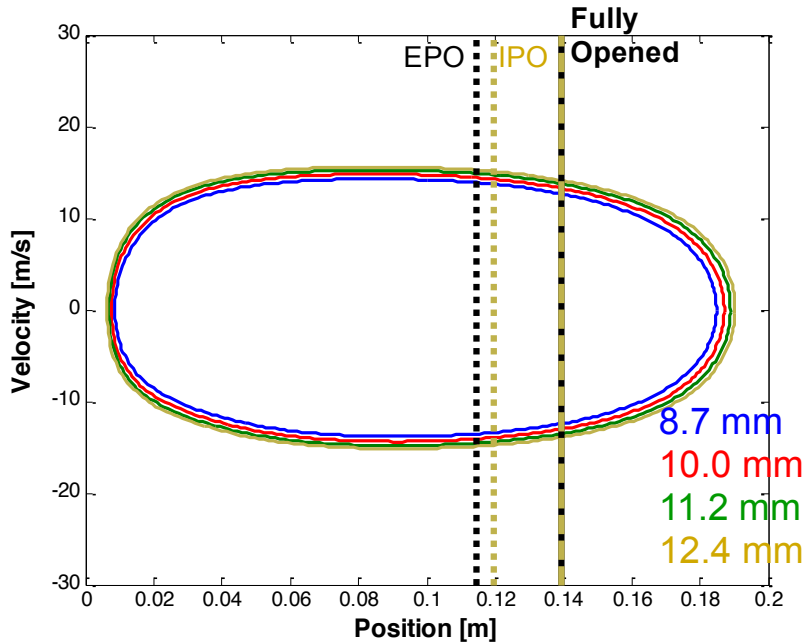
Figure 4-4 Piston velocity vs. position profile on different compressor offsets

Since the differences are small, and the power outputs are around the full-load condition for the 125-HP Hyprex engine, it is appropriate to pick a number that does not exceed the maximum allowed in-cylinder pressure. Therefore, the compressor offset = 11.2 mm is chosen. As described before, this number is normalized by combustion chamber bore so this dimensionless factor is Compressor Offset/Bore = 0.11.

4.1.4 Exhaust Port Opening Position

The exhaust port opening (EPO), shown in Figure 4-1, is defined as the distance from the centerline to the port initial opening position. It determines the position where the high-pressure combustion products inside the cylinder will be released into the exhaust manifold. Therefore, the later the port opens, the further the piston will travel during the outward stroke. The intake port opening (IPO) is always 5 mm further than the EPO to prevent too much backflow into air box and ensure an efficient scavenging process. The results for different EPO positions are shown in Table 4-6 below.

Table 4-6 The effects of EPO at the same fueling rate

EPO	114	134	144	164	mm
Brake Efficiency	51.4	52.9	53.2	52.5	%
Effective CR	13.3	14.8	14.8	15.4	
Frequency	28.8	31.4	32.3	34.8	Hz
RGF	11.4	15.6	17.4	22.3	%
Φ	0.46	0.40	0.37	0.34	
ODP	0.185	0.192	0.194	0.199	m
IDP	0.009	0.009	0.010	0.011	m
Turbine Power	100	112	116	123	kW
$P_{eng,max}$	167	215	225	265	bar

More information is shown in Table 4-6 in order to explain the effects of EPO position. The residual gas fraction (RGF) is the exhaust residual left in the combustion chamber from previous cycle as the percentage of total mixture inside. RGF increases with increased EPO, because larger EPO leads less time for scavenging. On the other hand, the equivalence ratio, Φ, is reduced with larger EPO. This is because the exhaust ports close earlier, and the volume at that moment is larger to accommodate more air.

As expected, high pressure remains in the cylinder if the EPO is further from the centerline. Therefore, pistons would travel further outwardly with larger ODP shown in the table. Moreover, the frequency increases as the higher pressure makes the piston move faster. This can be seen more clearly in the velocity profile.
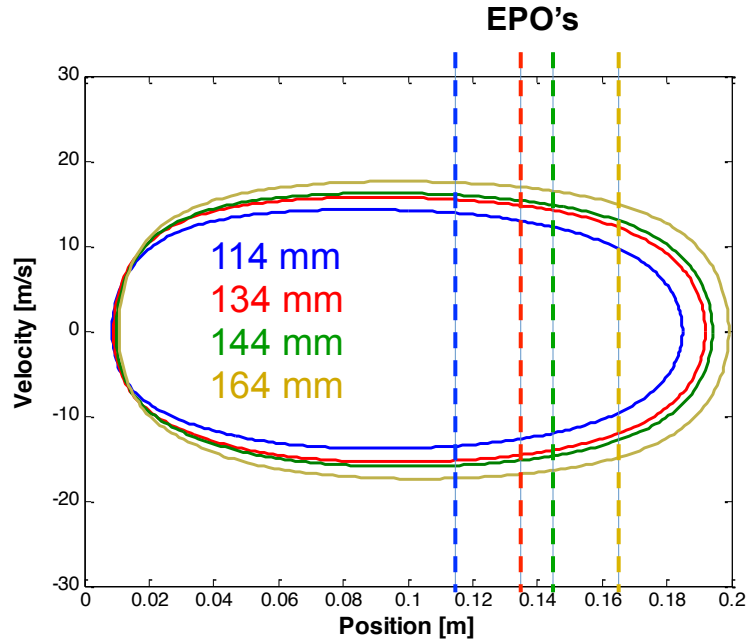
Figure 4-5 Piston velocity vs. position profile on different EPO's

In Figure 4-5, the dash lines refer to corresponding EPO positions distinguished by colors. It is obvious that the later the exhaust open, the larger the outward dead center, leading higher bounce chamber pressure and effective compression ratio. Again, the high compression ratio at high load results to in high peak pressure, which should be avoided in the operation. Therefore, the value of EPO is chosen as 144 mm, or normalized as EPO/Bore = 1.42.

4.1.5 Compressor-to-Combustion Area Ratio

The compressor-to-combustion area ratio determines the size of the compressor in the radial direction, instead of longitude direction as offsets in the previous sections. The engine bore remains the same to maintain the load range. As shown in Figure 4-1, the area of compressor is the difference between bounce chamber and combustion chamber. The GS-34 had the ratio of $A_{compressor}/A_{cylinder} = 6.56$, and Hyprex used 7.56 for its design. 8.56 is also tested in order to get a more complete picture. To

isolate the area effect, the piston mass also remains the same even though the piston volume changes.

Table 4-7 Effects of the area ratio at the same fueling rate = 160 mg/cycle

A_{Ratio}	6.56	7.56	8.56	
Brake Efficiency	50.9	49.0	46.8	%
Effective CR	17.7	11.2	8.4	
Frequency	33.9	30.9	29.3	Hz
ODP	0.197	0.192	0.188	m
IDP	0.008	0.013	0.017	m
Turbine Power	123	108	98	kW
$P_{eng,max}$	286	156	106	bar

The results in Table 4-7 show that the larger area ratio reduces both the compression ratio and stroke. The pressure is overall lower in compressor and bounce chamber because both volumes are larger. More fuel has to be burned to generate higher pressure to operate the larger device. Therefore, the power output can be extended and shifted to another range. It is not desired to increase the power at the current stage. Although the area ratio = 6.56 has violated peak pressure, and high power, it is possible to reduce the fueling rate and make the power close to 100 kW while lowering the peak pressure at the same time. The area ratio 6.56 is used for the future design.

4.2 Resizing for 100-kW TCFPLA

Since the dimensions determined in the previous section are similar to the GM Hyprex, this is called Hyprex TCFPLA engine. A linear alternator can be easily integrated with the free-piston engine model to test the effects. It is found that the power output can be further expanded, because the reduced piston kinetic energy, extracted by the alternator, allows more fuel to be burned. The power extraction coefficient for the

alternator, defined in Section 2.7, can be varied. More detailed energy and efficiency analysis for the alternator will be further discussed in Chapter 5.

The current goal is to determine the size of a device, whose peak power is 100 kW. Therefore, integrating the 100-kW free-piston engine with various linear alternator power extractions can define the load range. The sweep of fueling rate is performed to eliminate the unfeasible points which violates the restrictions. The power output as a function of BSFC can be seen in Figure 4-6.
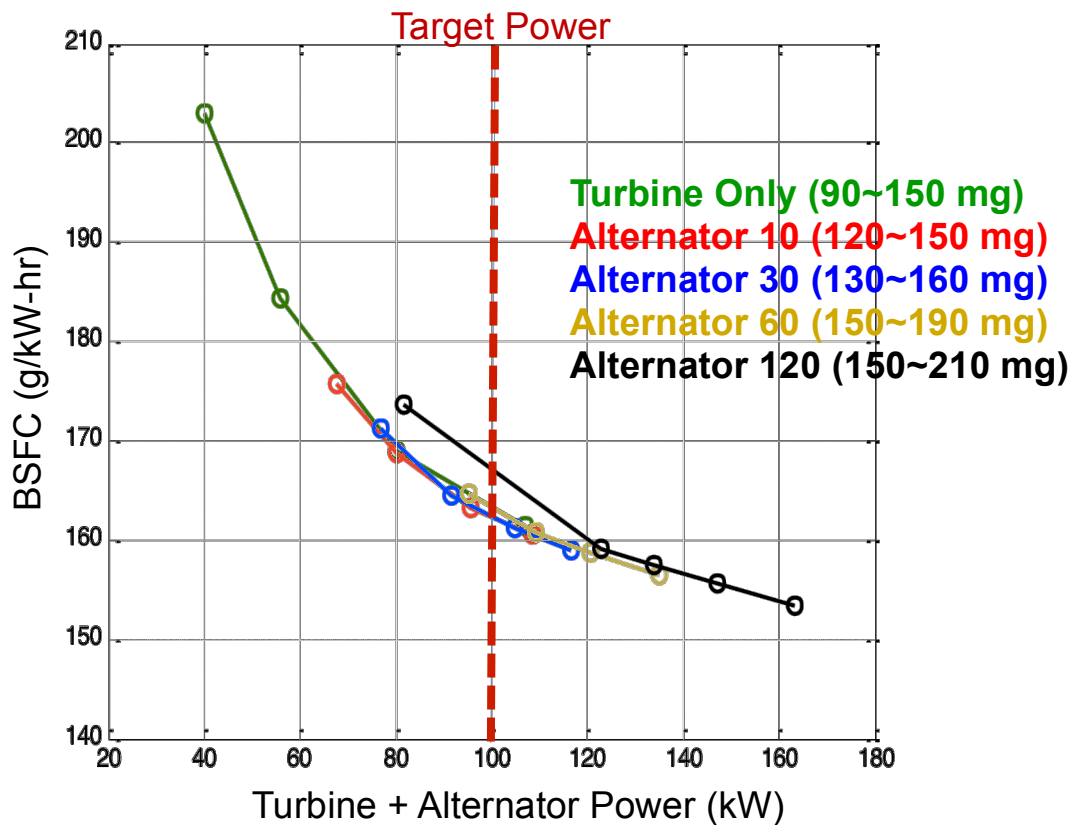
Figure 4-6 BSFC as a function of total power for Hyprex TCFPLA engine

In Figure 4-6, the colored curves represent different alternator power extractions as noted in the legend, and the numbers in the parenthesis are the range of fueling rate for corresponding alternators. The green curve shows the free-piston gas turbine without alternator. As in previous section, the full load is slightly higher than 100 kW at 150

mg/cycle fueling rate. The addition of alternator allows more fuel to be burned without violating the peak pressure restriction. The reduced BSFC keeps at higher load clearly shows the benefit of linear alternator on efficiency. Both turbine and alternator real behaviors are accounted for by assuming 85% efficiencies. At this stage, it is unclear on the limit of the alternator power extraction coefficient. Based on the results shown in Figure 4-6, more alternator power is desired, but higher alternator output may not be realistic, considering the physical limitation of the linear alternator.

The linear alternator enhances the efficiency with increased power output, which also returns higher total power. As seen in Figure 4-6, the target power 100 kW has become the mid load for the Hyprex TCFPLA engine. Since the alternator has the ability to increase the load, the original size of Hyprex is too big for the target. According to the current results, the alternator can output 30% of total power at full-load condition, which indicates that the target turbine power for the downsized engine should be around 70 kW.

Table 4-8 Further downsized TCFPLA for target of 100 kW

	GS-34	Hyprex	100kW
Engine Bore (m)	0.34	0.1016	0.0762
Bounce Bore (m)	0.89	0.2794	0.2095
Comp. Offset (m)	0.03	0.009	0.0084
Bnc. Offset (m)	0.68	0.20	0.1676
Turbine Orifice (m)	0.09	0.027	0.0207
Piston Volume (m^3)	0.2636	0.0075	0.00306
Piston Density (kg/m^3)	8000	8000	8000
Solidity (%)	24.1	24.1	62
Piston Mass (kg)	508	15	15
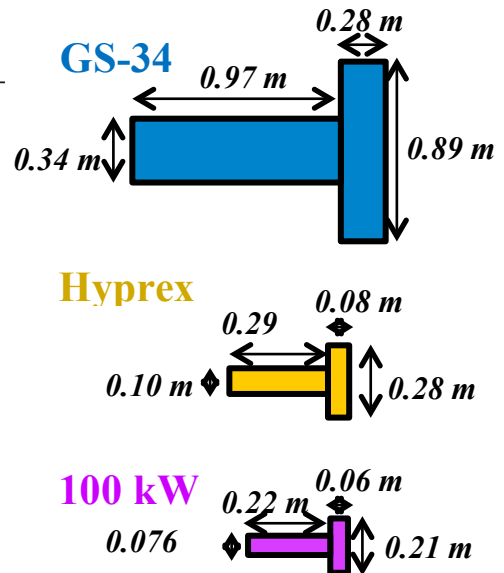
Going down from 100kW to 70 kW of turbine power, the combustion chamber should reduce its volume to 70% of the original Hyprex, assuming the efficiency remains similar. However, it is found that the bounce chamber mass is controllable and it helps

75

burning more fuel but not raising cylinder pressure too much, this downsized engine needs only 50% of combustion chamber volume but sufficient for 70 kW power through turbine. In addition, running the alternator requires extra fuel, which thereby enhances turbine power at the same time. This downsized TCFPLA is called 100-kW TCFPLA engine in the later sections.

4.3 Detailed Linear Alternator Model and Validation

Stony Brook University has developed the linear alternator model for this special TCFPLA engine, based on the Sandia alternator design [6]. The detailed alternator model, unlike the simplified one described in Section 2.7, has real electrical voltage and current measurement inside the alternator and battery circuits. The model uses Simulink® with its SimPowerSystems toolbox, which provides the connection for electric components, such as capacitor, resistor, inductance, diode, and simple battery model, etc. A simple alternator structure can be seen below:
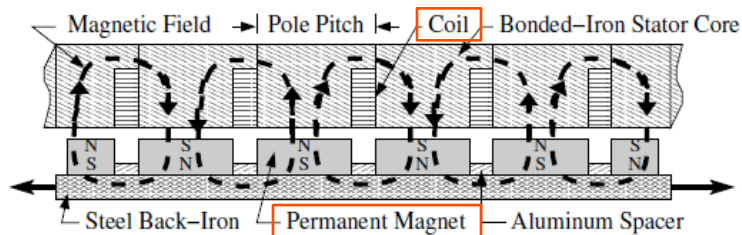
Figure 4-7 Coils and magnets in an alternator [6]

As seen in Figure 4-7, the coils and magnets have fixed location on their structurally supporting materials. The magnet set consists of four full pieces and two half pieces as total of five magnets. The distances between two coils and two magnets determine the magnetic flux at given magnets position. Removing some of the coils or magnets, however, reduces the amount of involved coils that generate the induced voltage, but the magnetic flux as a function of mover position remains the same. Recalling Eq. 2.20:

$$V_{ind} = -\frac{d\Phi}{dt} = -\frac{d\Phi}{dx}\frac{dx}{dt} = iR_{coil} \qquad \text{(Eq 4.1)}$$

$d\Phi/dx$ is the magnetic flux as a function of the piston position in the TCFPLA engine. It is a design parameter that should be considered at the early stage of alternator development. To establish this alternator characteristic, commercial finite element software, Flux2D, was used to simulate the magnetic flux effects on the coils. The Flux2D model and alternator dimensions [6] can be seen below in Figure 4-8.
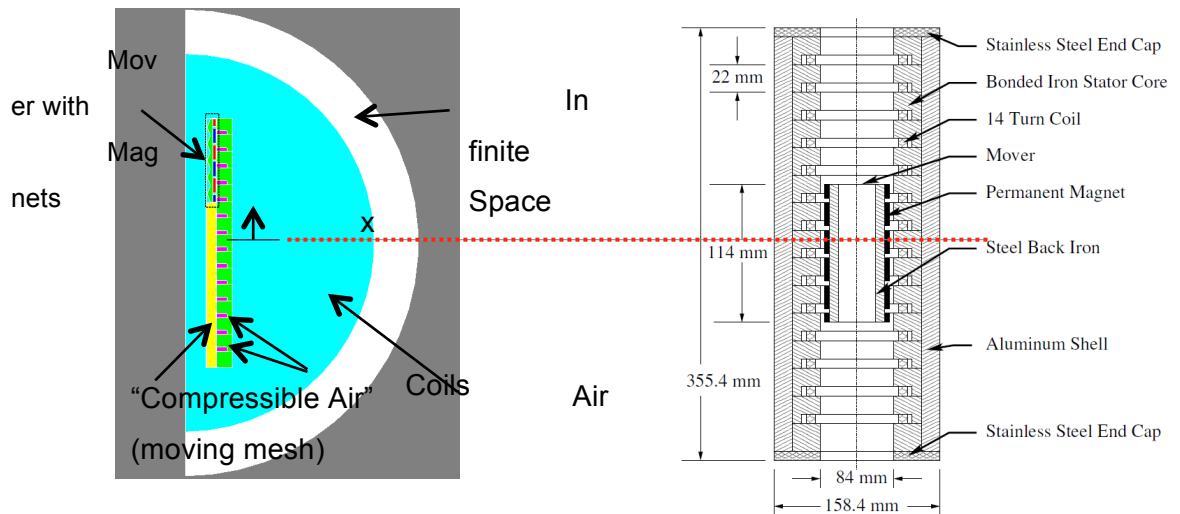
Figure 4-8 Flux2D model and the geometry information of Sandia alternator [6]

As seen in Figure 4-8, the Sandia alternator has 14 coils with a 22mm gap between each two coils. The overall length of this alternator is 355mm, which may fit the larger Sandia device well, but it may be too large for current much smaller 100kW device. The results of Flux2D simulation define the magnetic flux based on the magnet assembly's relative position to any given specific coil. Therefore, there are 14 $d\Phi/dx$'s generated, and some examples are then shown in Figure 4-9 below.
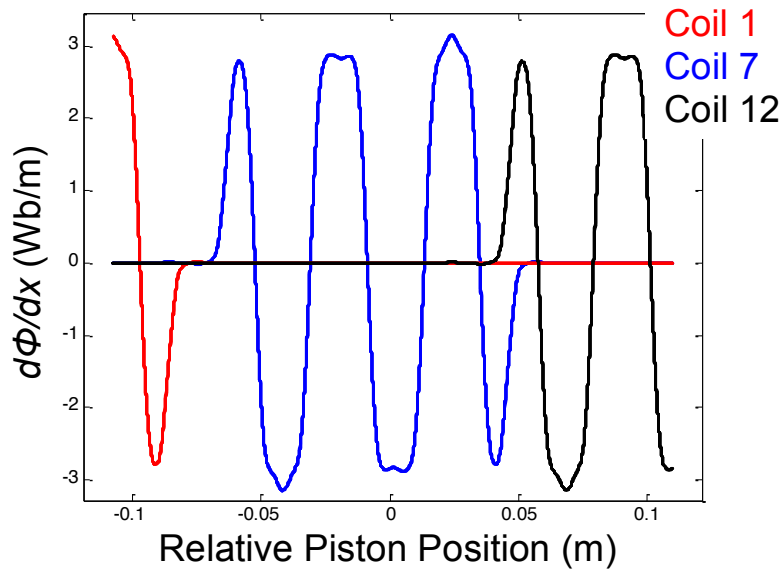
Figure 4-9 Magnetic flux for coil 1, 7 and 12 as examples

Notice that the x-coordinate is noted as piston position relative to the coil, instead of magnet assembly position, because there is an offset between piston and the magnet assembly. It is convenient to use piston position since it relates to piston velocity and volume of each chamber directly in the simulation process. In Figure 4-9, coil 1 refers to the coil closest to centerline and coil 14 is the furthermost, as plotted in Figure 1-9. One can see that coil 1 has only some peaks when the piston gets close to the left end, and similar result occurs with coil 12. Coil 7, however, shows the full curve of magnetic flux for the given piston position, while the other two only show a portion of that, because the intensity of magnet field is weak at both ends. For example, coil 1 is at the very left, and only one or two magnets on the very left supplies the magnet flux going through this coil, and the rest of them are too far. Coil 7 is in the middle position and get the magnets engaged in both traveling directions.

A look-up table giving $d\Phi/dx$ for coils directly replaces the simplified alternator model in the original TCFPLA model. In addition, the alternator generates alternating current (AC) that is not suitable for battery charging. Therefore, a simple rectifier consisting of 4

diodes that transforms the AC into direct current (DC) is necessary. An inductance and a capacitor as filters to correct the power factor are also important to keep the voltage and current in phase for maximum power. The Simulink® model for the alternator and rectifier can be seen below.
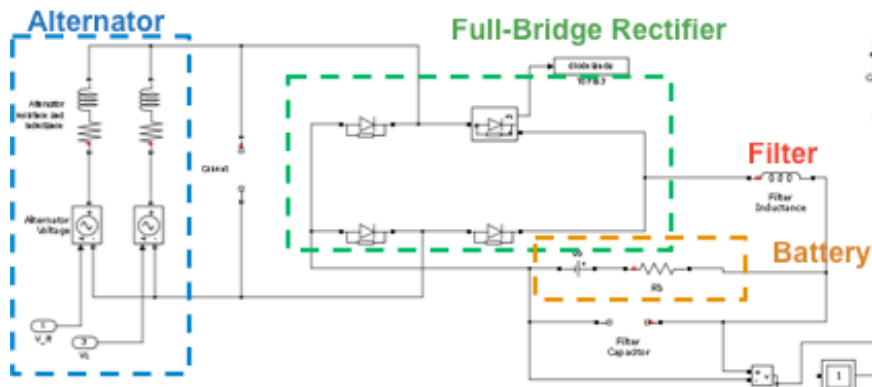
Figure 4-10 Simulink® model for alternator and rectifier, developed by SBU
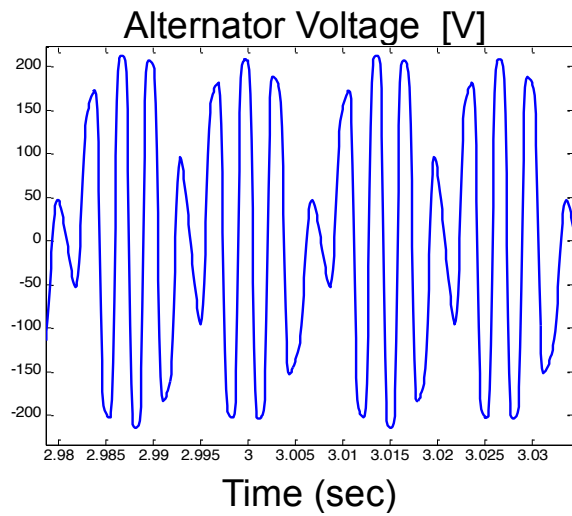
Figure 4-11 Alternator voltage, sum of 14 coils in 100 kW TCFPLA device
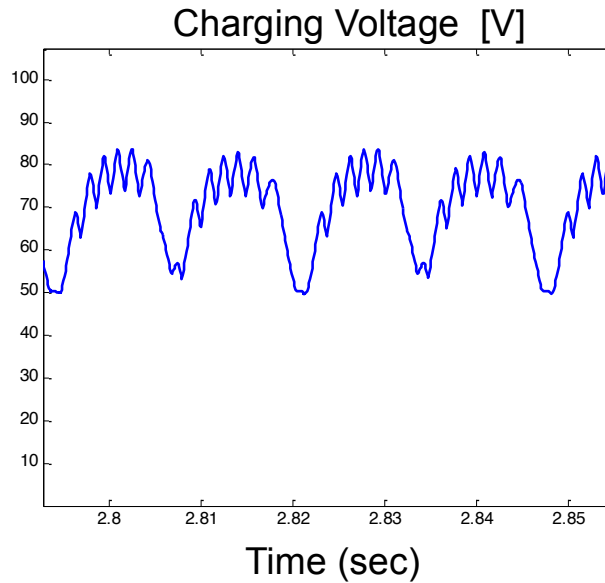
Figure 4-12 Battery charging voltage (DC) after the rectifier and filters

After linking this alternator model with the TCFPLA model, a sample voltage before and after rectifier can be obtained as shown in Figure 4-11 and 4-12, respectively. It is desire to know how the more realistic alternator affect the free-piston turbine. Table 4-9 shows the alternator effect.

Table 4-9 Comparison of performance numbers for the addition of alternator

Alternator	With	Without	
Brake Efficiency	49.7	49.3	%
Effective CR	10.9	14.4	
Frequency	37.2	41.8	Hz
ODP	0.1557	0.1590	m
IDP	0.0100	0.0075	m
$P_{Turbine,in}$	4.8	5.7	bar
$W_{Turbine}$	1.52	1.76	kJ/cycle

80

W$_{Charging}$	0.25	0	kJ/cycle

From this table, it is clear that the alternator reduces the piston speed and stroke, because the electromagnetic force applies against the piston's movement. The turbine energy output is also reduced because the overall operating pressure drops. Note that a part of turbine energy is transferred to the alternator output, but the higher total energy returns better efficiency. A very important point can be made here. The turbine model in both cases is the same. The one coupled with the alternator still has the potential to produce more power, as the inlet pressure is not as high as the one without alternator. This implies that if the pressure can be boosted to the higher level, the turbine power can be improved. This can be achieved with a higher fueling rate, and this explains why the alternator can extend the full-load condition.

4.4 Parametric Study for Detailed Alternator and Comparison with Simplified Model

As discussed in the previous section, the magnetic flux as a function of magnet position is based on alternator design, including the gap between each two coils, the gap between each two magnets, turns of coils, materials of magnets, etc. When these design parameters change, the magnetic flux through coils changes and a new finite element analysis is needed to calculate the new function. However, if some coils or magnets at the end of assembly are taken away, the shape of magnetic flux should remain the same but the number of engaged coils would decrease. Based on this, the number of coils and magnets can be reduced for the downsized 100-kW TCFPLA engine. This section also compares the detailed model with the simplified one to see the difference between these two, and finalize the model that would be used afterwards.

4.4.1 Parametric Study for Number of Coils and Magnets in Alternator

First, the number of coils in the alternator is varied. Fewer coils should produce lower power output, reducing the alternator force against the piston movement. The table below shows the sweep of coil numbers.

Table 4-10 Coil number sweep for the study of alternator

Coil Number	7	8	9	10	14	
Fueling / M_{bounce}	80 / 6	80 / 6	80 / 6	80 / 6	80 / 6	
Brake Efficiency	51.8	51.6	51.5	51.4	51.3	%
Effective CR	13.8	12.8	12.1	11.7	11.5	
Frequency	41.7	40.4	39.5	38.9	38.7	Hz
ODP	0.1587	0.1579	0.1573	0.1569	0.1567	m
IDP	0.0079	0.0085	0.0090	0.0093	0.0094	m
$P_{Turbine,in}$	5.6	5.4	5.2	5.1	5	bar
$W_{Turbine}$	1.70	1.65	1.61	1.59	1.57	kJ/cycle
$W_{Alternator}$	0.15	0.19	0.22	0.25	0.26	kJ/cycle

As seen in Table 4-10, the coil number directly affects the strength of the alternator. Similar to Table 4-9, more energy extracted by the alternator would cause the reductions of frequency, stroke compression ratio and the turbine output, as a stronger alternator applies more force against the piston. One may notice that the difference between 10 coils and 14 coils are very minor. This is because the original alternator containing 14 coils, which is too large for this 100-kW TCFPLA engine. Therefore, the last two coils, coil 13 and 14, never engage with the magnets and produce almost zero voltage. In other words, the stroke is too short that the magnet assembly cannot reach to the point where its magnetic field is able to pass through the last two coils. The evidence of this can be seen in the magnetic flux below.
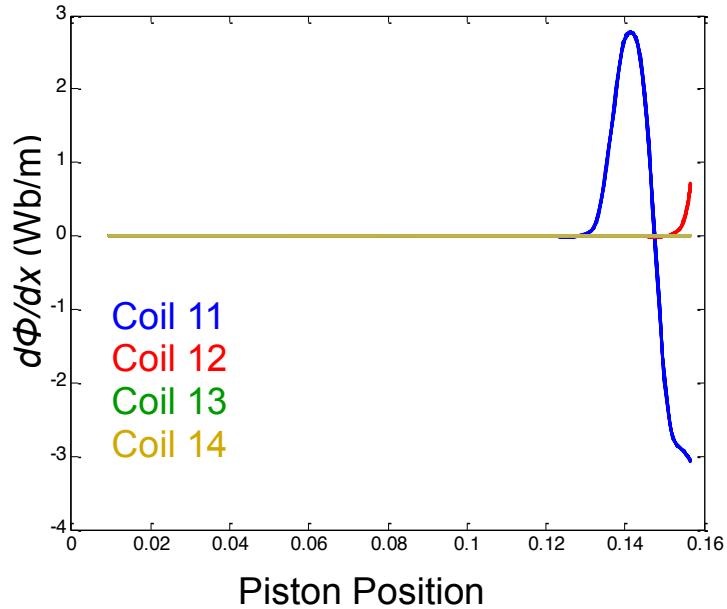
Figure 4-13 Magnetic flux as a function of piston position for coil 1, 6, and 13

As mentioned before, coil 13 has almost no flux throughout under this stroke. The flux may show up if the piston travels further so that the magnets can induce the voltage in these end coils. However, the piston stroke may be limited by the size of the TCFPLA engine.

The number of magnets can also be reduced. Reduced magnets weaken the intensity of the magnetic field, reducing the induced voltage.

Table 4-11 Magnet number sweep for the study of alternator

Magnet Number	5	4	3	
Fueling / M_{bounce}	80 / 6	80 / 6	80 / 6	
Brake Efficiency	51.5	51.6	51.8	%
Effective CR	12.1	12.9	14.5	
Frequency	39.5	40.6	42.5	Hz
ODP	0.1573	0.1580	0.1591	m

83

IDP	0.0090	0.0084	0.0075	m
$P_{Turbine,in}$	5.2	5.4	5.7	bar
$W_{Turbine}$	1.61	1.66	1.72	kJ/cycle
$W_{Alternator}$	0.22	0.18	0.13	kJ/cycle

Similar to the coil number, the decrease of magnet number reduces the ability to take power out from the alternator. Therefore, both of the components of the alternator have direct effects on energy extraction. To complete the study of the alternator, various combinations of coils and magnets are cross-compared.

Table 4-12 Alternator comparison with different combinations of coil/magnet number

Coils / Magnets	10 / 5	10 / 4	10 / 3	9 / 5	9 / 4	9 / 3	8 / 5	8 / 4	8 / 3	
Fueling / M_{bnc}	80 / 6	80 / 6	80 / 6	80 / 6	80 / 6	80 / 6	80 / 6	80 / 6	80 / 6	
Brake Eff	51.4	51.5	51.8	51.5	51.6	51.8	51.6	51.7	51.9	%
Effc. CR	11.7	12.6	14.5	12.1	12.9	14.5	12.8	13.5	15.1	
Frequency	38.9	40.2	42.5	39.5	40.6	42.5	40.4	41.3	43.1	Hz
ODP	0.1569	0.1578	0.1591	0.1573	0.1580	0.1591	0.1579	0.1585	0.1595	m
IDP	0.0093	0.0086	0.0075	0.0090	0.0084	0.0075	0.0085	0.0081	0.0072	m
$P_{Turbine,in}$	5.1	5.4	5.7	5.2	5.4	5.7	5.4	5.6	5.8	bar
$W_{Turbine}$	1.59	1.64	1.72	1.61	1.66	1.72	1.65	1.69	1.74	kJ/cycle
$W_{Alternator}$	0.25	0.19	0.13	0.22	0.18	0.13	0.19	0.16	0.12	kJ/cycle

By comparing the frequency, stroke (ODP & IDP), turbine energy and alternator energy, the results shown in Table 4-12 can be separated into several groups (by color). The cases in the same group return very similar alternator performance and system

performance. For example, coils/magnets = 10/4, 9/4, and 8/5 as a group (in green color) have the alternator work around 0.19 kJ/cycle, frequency 40 Hz, and turbine inlet pressure 5.4 bar. Those results indicate that those alternators, even with different numbers of coils and magnets, are very similar on their ability to extract power. The results of coils/magnets = 10/4 and 9/4 are similar, because 4 magnets as a shorter assembly has difficulty to reach coil 10 for induced voltage. It is similar to the cases between 10 coils and 14 coils in Table 4-10. This can be fixed by moving the magnet assembly away from the centerline to make itself closer to coil 10, but studying the best position for placing the alternator is outside the scope of the present work.

Two important conclusions can be drawn here for the alternator. First, the coils and magnets number have no effect on the system behavior and performance. The only important thing is the amount of energy extracted by the alternator, because the piston does not know how the energy was extracted. The alternator takes the kinetic energy from piston, and the piston dynamic determines the system performance, so only the cyclic alternator energy extraction matters. Second, based on the coils/magnets = 10/5 case, this may be the maximum energy this alternator can extract if applying the Sandia design on this TCFPLA machine. It was found that 10 coils would have no difference with 14 coils due to the stroke is too short. Therefore, 13.5% of total energy from the alternator may be the maximum value for this design on the 100-kW TCFPLA engine. A re-designed alternator, such as narrower gap between coils and magnets, is necessary if more power is required. This also concludes that some points in Figure 4-6 are not reasonable for too much energy is extracted from alternator.

4.4.2 Comparison of Detailed Alternator Model and Simplified Alternator Model

According to previous discussion, it is found that the number of coils and magnets do not matter as long as the energy extracted by alternator is similar. This motivates the interest for the difference between the detailed model, described in Section 4.3, and the simplified model in Section 2.7. The simplified model can easily change the power

extraction level, and it has no complicated electric components that slow the computing time. The biggest concern is the electromagnetic force generated by the alternator since they behave very differently as seen in Figure 4-14 below.
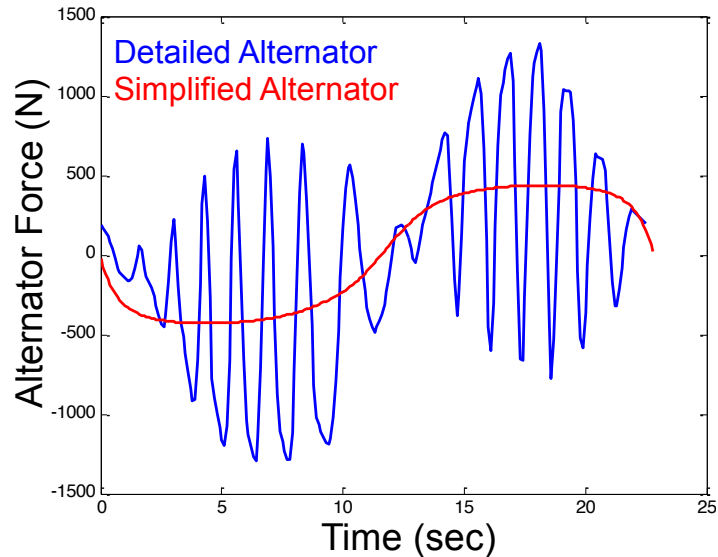
Figure 4-14 Alternator electromagnetic force acting on the traveling piston

Section 2.7 describes the simplified model which multiplies the piston velocity by a constant to estimate the alternator force. As seen in Figure 4-15, it tries to fit the mean value of the real alternator force that oscillates many times in a stroke. Notice that the simplified alternator force only changes sign while the piston changes direction. However, the detailed alternator force changes sign several times during a stroke. This means that the force does not work against the piston traveling direction all the time in reality. It is the physics of electromagnetics from the magnets assembly, as the magnetic flux would increases or decreases based on the position. Therefore, it is assumed a constant can be found to best represent the mean value of the real alternator. The following table shows the comparison of the detailed model side by side with the corresponding simplified model that extracts similar power from the alternator.

Table 4-13 Comparison between detailed and simplified alternator model

Coils / Magnets (or Alt. gain)	14 / 5	35	10 / 4	23	8 / 4	18	9 / 3	15	
Fueling / M_{bnc}	80 / 6	80 / 6	80 / 6	80 / 6	80 / 6	80 / 6	80 / 6	80 / 6	
Brake Efficiency	51.3	50.8	51.5	51.2	51.7	51.4	51.8	51.5	%
Effective CR	11.5	11.3	12.6	12.5	13.5	13.4	14.5	14.1	
Frequency	38.7	38.2	40.2	40.1	41.3	41.2	42.5	42.0	Hz
ODP	0.1567	0.1563	0.1578	0.1577	0.1585	0.1584	0.1591	0.1589	m
IDP	0.0094	0.0096	0.0086	0.0086	0.0081	0.0081	0.0075	0.0077	m
$P_{Turbine,in}$	5.1	5.0	5.4	5.3	5.6	5.5	5.7	5.7	
$W_{Turbine}$	1.57	1.55	1.64	1.64	1.69	1.68	1.72	1.71	kJ/cycle
$W_{Alternator}$	0.26	0.26	0.19	0.18	0.16	0.15	0.13	0.13	kJ/cycle
Charging Eff.	86	N/A	89	N/A	90	N/A	92	N/A	%

In Table 4-13, the paired columns with the same color produce close amount of alternator work. The detailed alternator models contain different coil and magnet numbers to vary the ability to extract power. The simplified cases change the multiplier, also called alternator gain, to alter the alternator power. Interestingly, as long as the alternator energy is close (within 0.01 kJ/cycle), the system behaves very similarly. Look for example at the values of the stroke and frequency, stroke indicates the volume change in each chamber, and the frequency represents the rate of volume change. Therefore, the pressure and heat transfer profiles are expected to be similar, and the system energy flows would consequently be similar.

Other operation conditions, such as temperature profiles and friction, are also compared and confirmed that the paired cases are very comparable. Although the electromagnetic forces generated by alternator are in different shapes, they seem not to

affect the piston dynamic significantly since the simplified model presents the mean value. Considering the extra computing time is needed for the detailed alternator model, it is favored to use the simplified model for easy adjustment on the alternator output. Furthermore, rectifier circuit and battery model are not included in the scope of current research. A more refined design such as an actively controlled rectifier, reducing the loss from the fast change of electric current, can be developed in the future.

However, the alternator energy transformation into the battery charging power has to be considered as the truly useful energy. Table 4-13 shows the charging efficiency in the last row for the detailed alternator cases. According to the test of various combinations of coils and magnets number, the charging efficiency varies from 85% to 92%. The lowest number 85% is chosen as the "alternator efficiency" as a conservative estimate to prevent over-predicting the efficiency.

4.5 Low Load Strategy

The cranked engine has the connecting rod to retain the compression ratio for combustion. However, the free-piston engine operates under the pressure forces acting on the piston, so the engine could stall if the pressures do not achieve the desired value. At low load condition, the fuel energy is not sufficient to raise the in-cylinder pressure. The outward traveling distance is then reduced, causing the bounce chamber to be less compressed. Consequentially, the bouncing force is not large enough to drive the piston to the desired compression ratio. Once the misfire occurs, the engine stalls for failure to open the scavenging port properly.

One remedy is to throttle the exhaust gas entering the turbine. This increases the residual gas inside the combustion chamber, and therefore helps the combustion trigger even when the fueling is low. The direct effects of exhaust restriction can be seen in the following comparison.

Table 4-14 Throttled turbine inlet effect

	50/21	40/13	
Fueling / $D_{turbine}$	50/21	40/13	mg / mm
M_{bnc} / Inj. Pos.	6 / 20.5	6 / 90.5	g / mm
Brake Efficiency	42.0	42.9	%
Effective CR	9.8	4.7	
Frequency	31.0	29.2	Hz
RGF	11	31	%
Φ	0.36	0.35	
ODP	0.1484	0.1440	m
IDP	0.0111	0.0233	m
$P_{Turbine,in}$	3.3	4.7	bar
$T_{Turbine,in}$	650	820	K
$W_{Turbine}$	0.94	0.77	kJ/cycle

With the current geometry setting, 50 mg/cycle is the lowest fueling rate this device can run without any special technique, so the left column is for the unchanged turbine. Changing the orifice size is a simple way to mimic the throttling effect. As can be seen in Table 4-14, the case with 40 mg/cycle has to reduce the turbine inlet orifice size from 21 mm to 13 mm, whose flow area is less than 40% of the wide open throttle. It is worth noticed that the compression ratio is only 4.7 for the throttled case, because too much residual exhaust remains in the cylinder. One may think the compression ratio is too low for the ignition, but it is important to realize the air has been compressed twice -- first time in the compressor chamber and secondly in the combustion chamber. In addition, the reduced exhaust flow area increases the residual gas fraction significantly, raising the in-cylinder temperature in the closed-cycle for the combustion. Low compression ratio also means low expansion ratio, which increases the turbine inlet temperature. As the results, the break efficiency can be maintained even when the

89

compression ratio is highly reduced. However, the extra control of the throttle may increase the complexity and cost in the real system.

The original GM Hyprex applies a special technique, called "recirculation", to operate the low load condition especially for idling. It simply dumps the air from the air box into the intake manifold to reduce the pressure in air box. By doing this, the delivery reed valve would open earlier at lower pressure, decreasing the pressure force against the piston while traveling inwardly. In addition, the hot gas from the air box heats the intake air, and it increases the overall temperature that helps the combustion triggered at lower compression ratio. Recirculation recovers the compression ratio with the cost of efficiency, as it takes the already-compressed air out of the system.

The recirculation valve is modeled as an orifice. The air in the air box is slowly conducted into the intake manifold through a fixed orifice during the whole engine cycle, and it expands to the ambient pressure while entering the intake manifold. This orifice size can be changed based on the load. Generally, the lower the load, the larger the recirculation port is needed. The recirculation model also includes the heat losses occurring during the recirculate air throughout the pipe. However, there is no actual heat transfer model in order to simplify the calculation. Instead, the heat loss is modeled as the flow enthalpy reduction before entering the intake manifold.

The "low load" defined in the model is based on the fueling rate which would misfire without recirculation, but this fueling rate may vary if a different combustion model is used. As mentioned before, 50 mg/cycle is the smallest fueling rate requiring no special technique for the smaller 100-kW TCFPLA engine. Some recirculation results as examples can be seen in the table below.

Fueling / D_{Recir}	40/15	30/20	20/25	mg / mm
M_{bnc} / inj.Pos.	6 / 25.5	6 / 30.5	5 / 40.5	g / mm
Brake Eff	27.9	13.5	5.6	%
Effc. CR	14.9	8.8	11.6	

Frequency	28.9	23.0	20.6	Hz
ODP	0.1443	0.1280	0.1287	m
IDP	0.0070	0.0123	0.0093	m
$P_{Turbine,in}$	2.3	1.9	1.3	bar
$T_{max,cylinder}$	118	64	59	K
$W_{Turbine}$	0.50	0.18	0.05	kJ/cycle

Table 4-15 Sample results for low load condition with recirculation

The size of recirculation valve is not dedicatedly chosen in this demonstration. The values here only ensure the engine can run with given fueling rate, so no clear trend can be seen other than the reduction of turbine output. Several observations can be made from Table 4-15. First, the lower the load, the larger the recirculation valve is needed to reduce the pressure in the air box. Second, the engine has lower speed with less fuel, but the recirculation helps maintain the compression ratio and stroke, both of which help maintain the engine operation. Third, the efficiency drops to 5% at 20mg fueling rate with almost no energy output, meaning most of the fuel energy is used to drive the free-pistons and compensate for the losses.

4.6 100-kW TCFPLA Operation

The dimensions of TCFPLA has been determined in the previous sections, and the engine map can be defined at different operating points with various fueling rate and alternator power takeout. Unlike the conventional cranked-driven engine controlled by the load, the TCFPLA engine speed is the results of Newton's 2nd Law based on the pressure forces on both sides of the piston. Therefore, the bounce chamber pressure, or mass, is an important operating variable for the engine performance. In addition, conventional engines use either spark plug or fuel injector to control the combustion phasing, so the injection position in TCFPLA determines the best firing timing.

Therefore, the bounce chamber mass and injection timing, are two active ways to control the operation and the effects are discussed in the following sections.

4.6.1 Bounce Chamber Mass Effects

In order to isolate the bounce chamber effects, all other operating parameters are fixed. For 60 mg/cycle of fuel injected when pistons move to 75 mm from the center line, the results of bounce chamber mass variation can be seen below.

Table 4-16 Effects of different bounce chamber mass at given operating condition

M_{bnc}	10	12	14	g
Brake Efficiency	45.5	47.3	48.5	%
Effective CR	11.7	14.5	17.2	
Frequency	34.6	36.5	38.0	Hz
ODP	0.1485	0.1448	0.1408	m
IDP	0.0093	0.0075	0.0063	m
$P_{turb,in}$	4.2	4.4	4.6	bar
$T_{turb,in}$	682	679	681	K
Mass flow	3.02	3.06	3.07	g/compressor
$W_{Turbine}$	1.22	1.27	1.30	kJ/cycle
$P_{eng,max}$	141	186	235	bar

In Table 4-16, the higher the bounce chamber mass, the better the efficiency. This higher efficiency comes from the higher turbine output at the same fueling rate. So it is desired to know why the turbine can produce more power. To answer this, it is important to recall the turbine work equation from Section 2.8.

$$W_{turbine} = \dot{m} \cdot \eta_{turbine}(h_{in} - h_{ex,i}) \qquad \text{(Eq 4.2)}$$

According to Eq. 4.2, turbine energy is proportional to mass flow rate, isentropic efficiency, and the enthalpy difference between inlet and isentropic exit. The turbine isentropic efficiency is fixed at 85%. The inlet temperature determines the inlet enthalpy, and the inlet pressure determines how low the outlet enthalpy can be throughout the expansion. Table 4-16 shows that the mass flow rate increases with the increased bounce chamber mass and turbine inlet pressure. This explains why the turbine has more output. However, this does not explain why the mass flow rate and turbine inlet pressure become higher. The reason is the higher compression ratio help deliver more air into the air box, so the air box pressure is higher before the scavenging process. When the scavenging ports open, more flow goes through the combustion chamber, increasing the turbine inlet pressure.

In summary, proper change in the bounce chamber can increase the efficiency up to 3% in Table 4-16. The in-cylinder pressure is increased correspondingly, meaning the bounce chamber mass has to be adjusted to an optimum value, which returns the highest efficiency without exceeding the upper limit of 250 bar for the cylinder pressure.

4.6.2 Injection Position Effects

The injection is a parameter that directly controls the combustion in compression ignition engines, generally referring to diesel engine. Although the combustion model is the commonly used Wiebe function, the injection is the trigger of ignition delay calculation that subsequently determines the combustion phasing. It is an important factor affecting the system response in all aspects. For 80 mg of fuel and 6g of bounce chamber mass, a sweep of injection position can be shown below.

Table 4-17 Comparison of injection position effects on system performance

Inj. Pos.	22	17	13	mm from center
Brake Efficiency	48.5	46.2	43.9	%
Effective CR	13.0	11.4	10.5	

Frequency	40.6	38.0	36.0	Hz
ODP	0.1592	0.1576	0.1562	m
IDP	0.0083	0.0096	0.0103	m
$P_{turb,in}$	5.5	5.1	4.7	bar
$T_{turb,in}$	787	799	817	K
Mass flow	3.2	3.1	3.0	g/compressor
$W_{Turbine}$	1.73	1.65	1.57	kJ/cycle
$P_{eng,max}$	176	133	112	bar

The efficiency drops with the delay of injection position as shown in Table 4-17. The effective compression ratio shows apparent contradicting results, as it is expected that later combustion leads to higher compression ratio. This is because the delayed combustion suffers more expansion penalty, reducing the in-cylinder pressure. Lower in-cylinder pressure results in less bouncing energy stored in the bounce chamber. Eventually, the compression ratio becomes smaller due to less bouncing force.
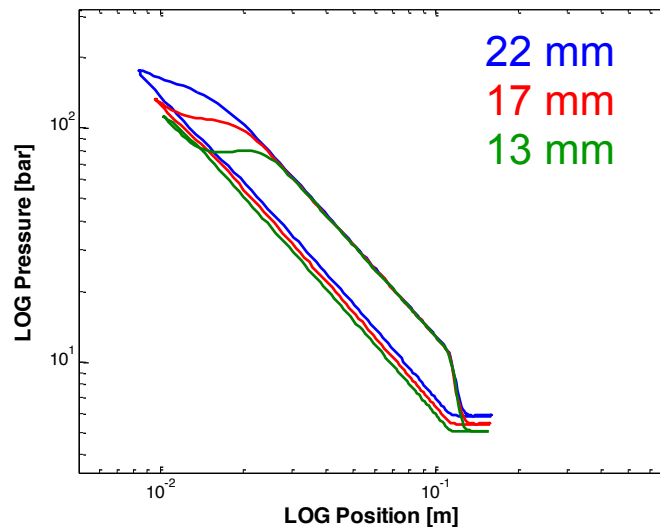
Figure 4-15 LogP-LogX diagram showing the pressure profile affected by combustion

In Figure 4-15, the green curve (13 mm injection position) shows an extremely late combustion happening during the expansion process, which suffers a large penalty. From the energy point of view, this reduces the indicated work, or combustion chamber boundary work, that would be delivered to bounce chamber and turbine, and therefore decreases the turbine output and compression ratio. On the other hand, the blue curve with 22 mm injection position has less expansion penalty to maintain the stroke, compression ratio and mass flow rate, providing healthy turbine operation. Similar to the bounce chamber mass, the injection can be carefully chosen for best performance output.

4.6.3 Engine Map

The way to plot the engine operation map of TCFPLA would look different from the conventional engine. First, the TCFPLA engine has two power extraction devices, so the output can be split into two ways at a given load. Moreover, several levels of alternator power takeout can be employed for one fueling rate. Second, the engine speed is not pre-determined because of the characteristics of free-piston engines. The alternator reduces the speed more due to the electromagnetic force acting against the piston.
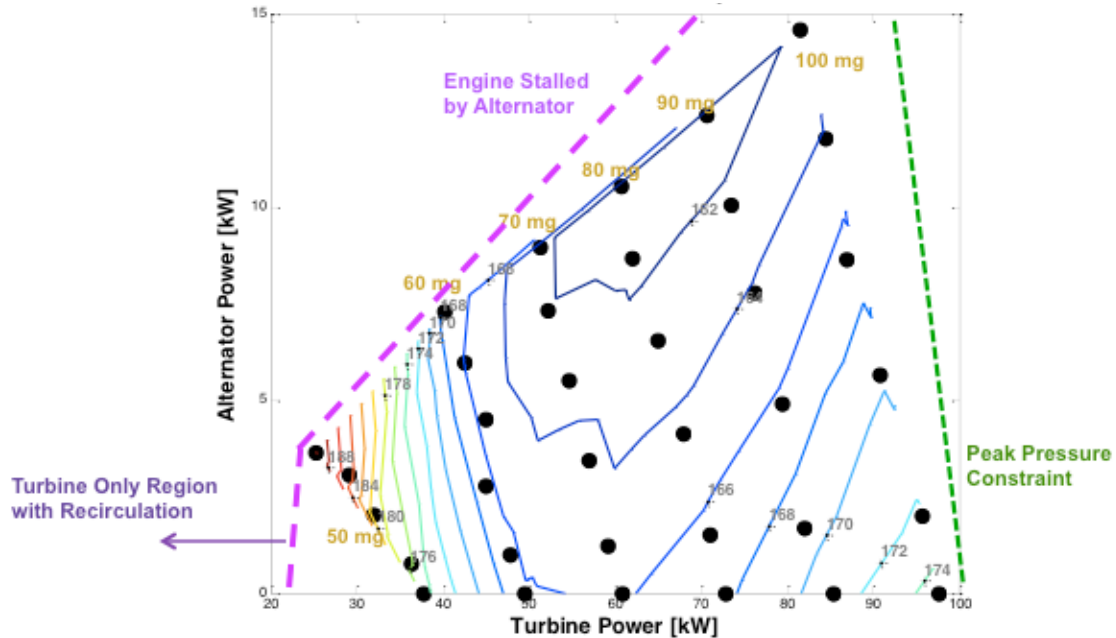
Figure 4-16 BSFC contour for TCFPLA operation at different power extraction ratio

Figure 4-16 above shows the BSFC contour for the 100-kW TCFPLA. This is a relatively complicated figure containing a significant amount of information. The values of BSFC are shown near the contour lines, ranged from 162 to 182 g/kW-hr. The black dots represent the operating points, whose locations indicate corresponding turbine (X-axis) and alternator (Y-axis) power. The fueling rates are marked on top of each group whose turbine powers are similar. For example, the dots on the very right column are all for the fueling of 100 mg/cycle, and the higher points on y-axis signify larger alternator power takeout. Several constraints are also shown here. The right boundary is the peak pressure constraint, as the fueling is too high to lower the in-cylinder pressure under the limit (250 bar). The upper left boundary is the engine stall constraint caused by alternator, because large electromagnetic force prevents the scavenging port from opening. The lower left boundary is similar, causing the engine stall by alternator, but this borderline only limit the use of alternator. As discussed before, the "recirculation" as the remedy can remain the engine operation for turbine output at low load with the cost of efficiency, but the BSFC is not shown.

Based on the discussion in the previous two sections, there are two important variables that need to be chosen carefully: bounce chamber mass and injection timing. The parameter sweeps of those two variables has been performed to pick relatively optimum values for any given point. Those values are not true optimums, but they are fairly good values for showing the reasonable results without running a full multi-variable optimization process.

In Figure 4-16, the first observation is that the most efficient points are the mid load condition with high alternator power takeout. It shows that the linear alternator is favorable when the engine runs on medium to high load. For the fueling rate of 60 mg/cycle, it is remarkable that the efficiencies are almost the same no matter how large the alternator is. The trend reversed as the alternator becomes unfavorable for the low load condition, 50 mg/cycle as the example here, because the fuel energy is the source running this device; at mid or high load, the fuel energy is sufficient to run both the alternator and turbine. On the other hand, at low load the fuel energy is just enough to run the turbine healthily under proper pressure. In other words, the addition of alternator that increases the piston resistance would stall the engine because the stroke becomes too small.

Alternator plays an important role on piston speed due to the electromagnetic forces. Therefore, a similar map with frequency as the contour is plotted below.
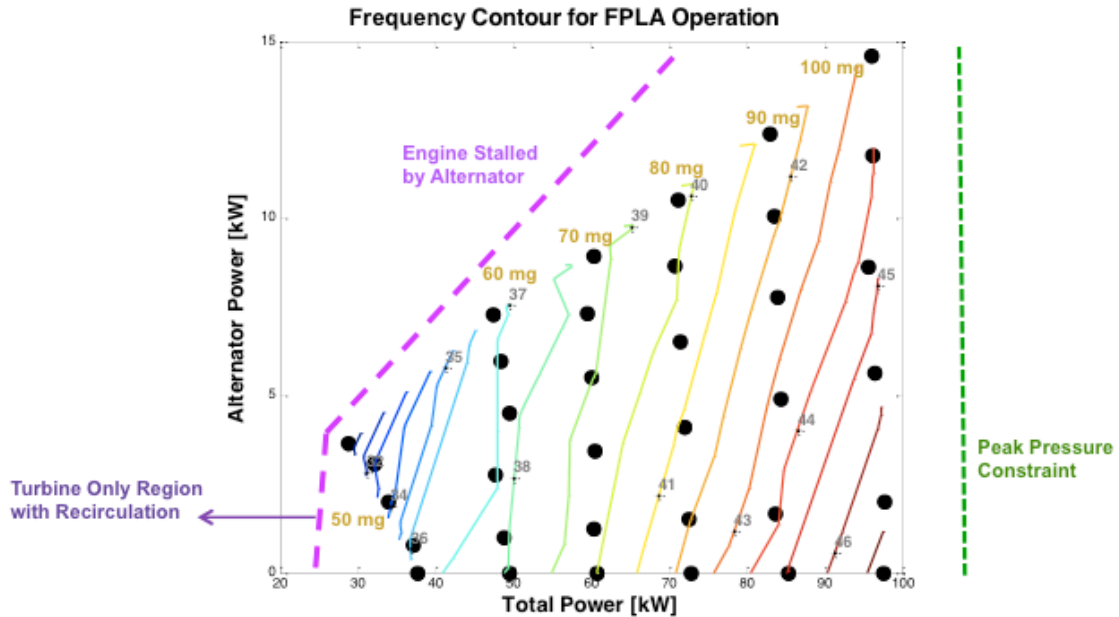
Figure 4-17 Frequency contour for TCFPLA operation at different power extraction ratio

Instead of plotting the turbine power as the x-axis, the total power (turbine plus alternator) is used to see the alternator effects. The contour lines present the frequency in Figure 4-17, and the restrictions in Figure 4-16 still apply here. Clearly, the alternator does not change the total power output since all the dots form a vertical line at their given fueling rates, except the lowest load points for 50 mg/cycle. The reason for that is similar as before; the fuel energy is not sufficient to drive the alternator and the turbine works inefficiently while the alternator power is still increasing.

One key effect of the alternator showing here is that the alternator slows down the piston. At the same fueling rate, the more power extracted by the alternator, the slower the frequency is, even though the total power output is the same. The total power remains the same for most of the load range, but the frequency goes down when the alternator extracts more power. This implies that the system has to be more efficient to produce more energy to compensate the smaller frequency. Figure 4-16 also showed the consistent results that support this.

Figure 4-16 presents the BSFC with the relation of turbine and alternator output. This figure can be simplified and transformed into a 2-D plot showing the relation between BSFC and total power output.
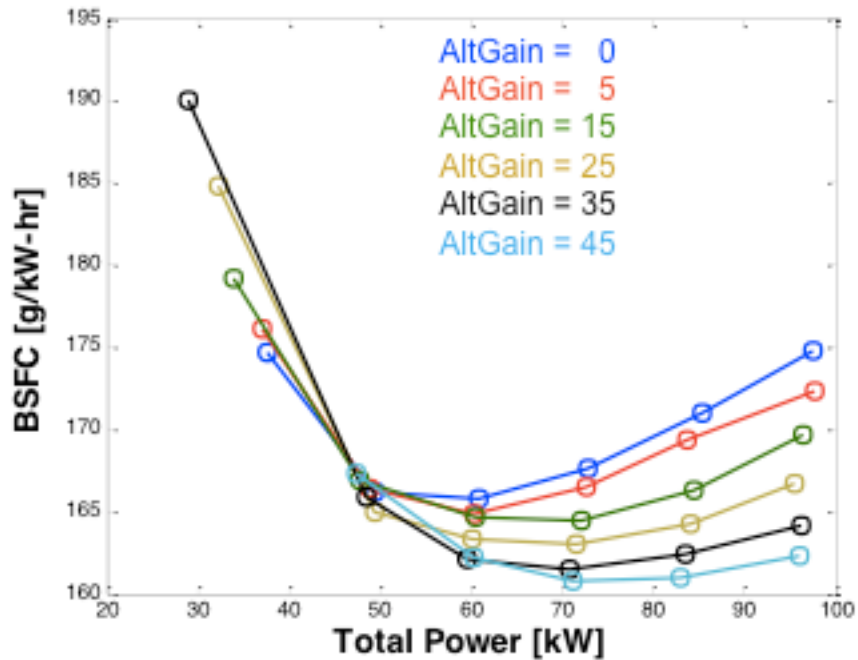
Figure 4-18 BSFC vs. total power at different fueling and alternator power takeout

This plot shows two trends more clearly than the contour plot; first, with total power more than 60 kW, the alternator increases the efficiency, which has been seen in Figure 4-16 if a vertical line is plotted at a given load. This effect has been explained before. Second, the BSFC goes down and up with the increase of load. This can also be seen in Figure 4-16 if a horizontal line is plotted at a given alternator power output. It is because the turbine produces power less efficiently. It is somehow confusing because the turbine isentropic efficiency is set at 85%.

Recall that in Eq. 4-2 the turbine work is a function of mass flow rate, isentropic efficiency, and the difference between the inlet and outlet enthalpy. Any of these terms decrease would result in the loss of thermal efficiency. Efficiency is fixed at 85%, and the enthalpy difference is expected to increase since the inlet pressure goes up with the

increased fueling rate. Therefore, the mass flow rate may drop at the higher load points that lead to the drop of efficiency.
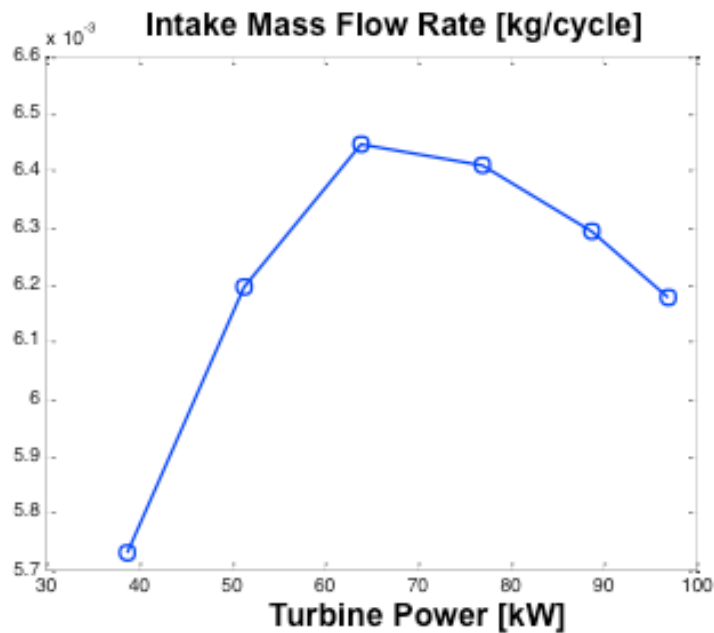
Figure 4-19 Mass flow rate for turbine only operaion

As seen in Figure 4-19, The mass flow rate indeed goes up and down with the increased of load. The initial climb of mass flow rate is due to the increase of stroke and compression ratio, both of which increase the vacuum inside the compression chamber, so the intake mass flow increases. After 60 kW, the mass flow rate drops because the increase of frequency reduces the duration of intake valve opening. The reed valves close too fast to allow the air to move into the compressor.

Bibliography

[1]   A. F. Underwood, "The GMR 4-4 'HYPREX' Engine, A Concept of The Free-Piston Engine for Automotive Use", SAE 570032, 1957

[2]   L. Li, Y. Luan, Z. Wang, J. Deng and Z. Wu, "Simulations of Key Design Parameters and Performance Optimization for a Free-piston Engine", SAE 2010-01-1105, 2010

[3]   L. Huang, "An Opposed-Piston Free-Piston Linear Generator Development for HEV", SAE 2012-01-1021, 2012

[4]   D. N. Frey, P. Klotsch, A. Egli, "The Automotive Free-Piston-Turbine Engine",

[5]   SAE 570051, 1957

[6]   A. L. London, A. K. Oppenheim, "The Free-Piston Engine Development – Present

[7]   Status and Design Aspect", Transactions of the ASME, 1952:74(2):1349–1361

[8]   Aichlmayr, H. T., Van Blarigan, P., "Modeling and Experimental Characterization of a Permanent Magnet Linear Alternator for Free Piston Engine Applications," ASME 2009 3rd International Conference on Energy Sustainability, Vol. 1, ES2009-90396, 2009

CHAPTER 5

TCFPLA Analysis by First Law of Thermodynamics

In Chapter 4, the geometry and operation of the TCFPLA engine were discussed. The model shows reasonable and consistent results. By performing the parametric sweeps, the values of bounce chamber mass and injection position were obtained for most efficient results at given load. However, the reasons behind the selected values rely on the analysis of thermodynamics. This chapter will present the viewpoint of Frist Law of thermodynamics. Various approaches for analyzing the energy flows will be discussed for better understanding the TCFPLA engine at the system level.

5.1 Introduction

The First Law of thermodynamics applied to a cyclic process, such as internal combustion engine, is the energy balance equation for the control volumes. The physical chamber volume does not limit the definition of control volume. Instead, it can be arbitrarily chosen from the combination of several chambers to the whole system. While the TCFPLA engine system at the steady state condition, the following energy balance equations have to be satisfied:

$$0 = \oint (\dot{H}_{in} - \dot{H}_{out} + \dot{Q} - \dot{W})dt \qquad\qquad \text{(Eq 5.1)}$$

$$\oint \dot{W}_{cylinder}dt = \oint (\dot{W}_{compressor} + \dot{W}_{bounce} + \dot{W}_{alternator} + \dot{W}_{friction})dt \qquad\qquad \text{(Eq 5.2)}$$

Eq 5.1 is the First Law, or conservation of energy, in steady state with no energy storage term in a control volume. Cyclic integral has to be performed for the balance of one full cycle. Eq. 5.2 presents the energy terms transferred out of the combustion chamber (cylinder). In the TCFPLA engine, the alternator extracts work from the piston kinetic energy, which is directly transferred from the cylinder boundary work. Similarly,

kinetic energy is used to overcome friction. Bounce chamber work is zero at steady state in a full cycle, only if an adiabatic condition is applied. With heat losses from the bounce chambers, the energy gained from the combustion chamber is simply used to compensate for the loss. Therefore, considering the losses through bounce chamber and friction are small, boundary work of combustion chamber is mainly transferred to compressor and alternator.

Thermal efficiency is generally defined as a ratio of useful energy to the energy source. In the TCFPLA engine, the useful energy is the combination of alternator and turbine outputs, and the energy source is the amount of fuel injected.

Thermal Efficiency: $\qquad \eta_{thermal} = \dfrac{W_{turbine} + W_{alternator}}{Q_{fuel}}$ (Eq 5.3)

Other energy terms, such as the heat losses, Q_{losses}, and the exhaust lost, $H_{exhaust}$, are summed onto the numerator in Eq. 5.3 to form the conservation of energy equation.

Energy Balance: $\qquad \dfrac{W_{turbine} + W_{alternator} + Q_{losses} + H_{exhaust}}{Q_{fuel}} = 1$ (Eq 5.4)

Eq. 5.4 is significantly important for the later discussion because the thermal efficiency will be plotted based on this equation.

The key benefits of TCFPLA come from two parts. First, the heat recovery from the air box recovers the heat due to TCFPLA's special structure. The air box fully covers the surface area of combustion chamber, so the heat from the combustion is able to directly transfer into the air box if there is no extra cooling channel around the combustion chamber. The heat, being seen as a loss in the conventional engine, is mostly saved inside the TCFPLA, although small amount of heat still leave the system through the wall of air box. Second, the linear alternator improves the efficiency as discussed in Chapter 4. The improvement comes from the selected bounce chamber mass and injection position for most efficient operation. The following sections will discuss the energy flow in the TCFPLA engine to understand more about these two benefits.

5.2 Air Box Heat Recovery

When heat losses through the combustion chamber wall in the conventional engine, the loss is unable to be recovered. The TCFPLA engine, on the other hand, can recover the lost heat from the combustion chamber by the air box, fully surrounding the cylinder heat transfer surface. Because the model has no solid wall thickness for conduction, it is assumed the heat would not go into the wall but transfer between volumes. The effect of high wall temperature, such as breakdown of lubrication, is ignored. 100 % of heat loss out of combustion chamber is treated as heat addition into the air box. The model can also adjust the percentage of heat transferred into the air box to simulate the situation where the heat flows into some solid materials, but this is outside of the scope in this study for now. The purpose of this study is to understand the heat recovery without any extra complexity.

Based on Eq. 5.4, the thermal efficiency breakdown comparing the cases with and without heatrecovery can be seen below.
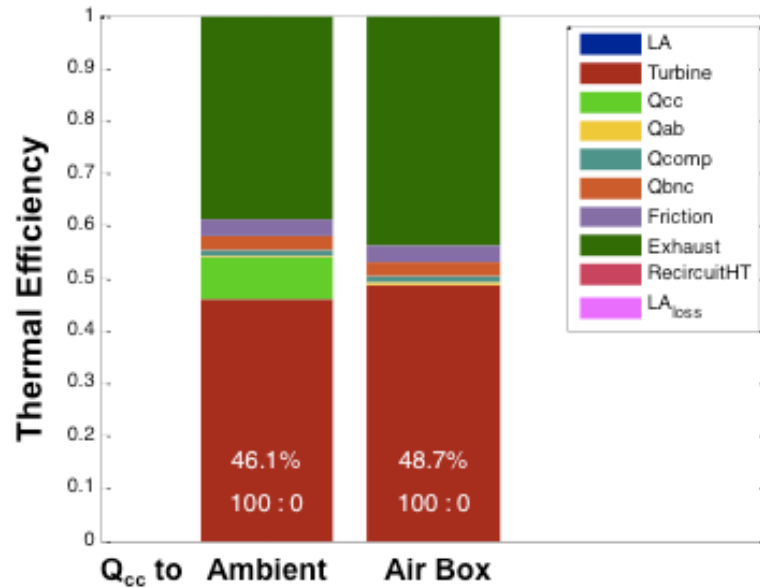
Figure 5-1 Energy distribution for comparison of heat recovery

In Figure 5-1, the percentages printed on the bars reflect the thermal efficiencies. The ratio "100:0" presents the proportion of turbine output to alternator output. Therefore, it is obvious the comparison made in Figure 5-1 use only turbine. All the colored bars present the corresponding energy terms normalized by fuel energy. "LA" is the linear alternator work. "Turbine" is the turbine work. All the Q terms are the heat losses; subscription "cc" is for combustion chamber, "ab is for air box, "comp" is for compressor chamber and "bnc" is for bounce chamber. "Friction" is the friction loss. "Exhaust" shows the wasted enthalpy of exhaust outlet. "RecircuitHT" is the heat transferred out of the recirculation pipe to the ambient during the transition, but it is not applied in this comparison. "LA$_{loss}$" is the energy loss due to the circuit inside the alternator whose efficiency is a constant 85%, same as the isentropic turbine efficiency. Both cases burn the same amount of fuel for a fair comparison.

The left bar shows the scenario where the heat losses from the combustion chamber into the ambient. In other words, the heat is simply a loss of energy and never recovered. The right bar is the heat recuperating case, showing that the light green bar (heat losses from combustion chamber, or Q$_{cc}$) disappeared. The heat comes from the engine heat up the air inside the air box, and higher temperature in the air box enhances its heat losses, so the yellow bar is slightly thicker. Exhaust waste also at higher temperature contains more enthalpy, shown as a larger green bar on the top. The retrieving heat increases the temperature in the air box and all its downstream volumes, including combustion chamber, exhaust manifold, and turbine. As the results, the turbine inlet pressure remains similar, but the higher temperature increases the turbine work. Note that the stroke is not affected by this reroute of heat flow, and so do the compression ratio and frequency. Therefore, the increase of turbine work mainly comes from the higher temperature condition due to the heat recovery.

The only downside of the overall higher temperature is the potential to violate the peak cylinder temperature limit of 2200K. That means the injection may have to be delayed and suffer the expansion penalty on purpose to lower the temperature. In

conclusion, the heat recovery offers the chance to recover the heat that is otherwise lost to the coolant. Even though the surface area of air box is large, its low heat transfer coefficient and relatively low temperature make the heat losses a small portion, as seen in Figure 5-1. This is a significant advantage over the conventional engine, and it happens naturally at no cost due to the TCFPLA engine's special structure.

5.3 Energy Transformation for Alternator

The effects of alternator have been discussed in Chapter 4. The alternator extracts energy from the piston's kinetic energy, and therefore reduces the piston speed and stroke in the free-piston engine. Previously in Figure 4-16, it is clear that the alternator increases the efficiency at mid to high load. However, the reason behind this was never explained and could not be easily seen. The following energy breakdown in this section may be appropriate to understand the influence caused by the linear alternator.

In the following comparison, the fueling rates are constant 90 mg/cycle, but the values of alternator power extraction coefficient are varied. The change of energy in terms of thermal efficiency can be seen in Figure 5-2.
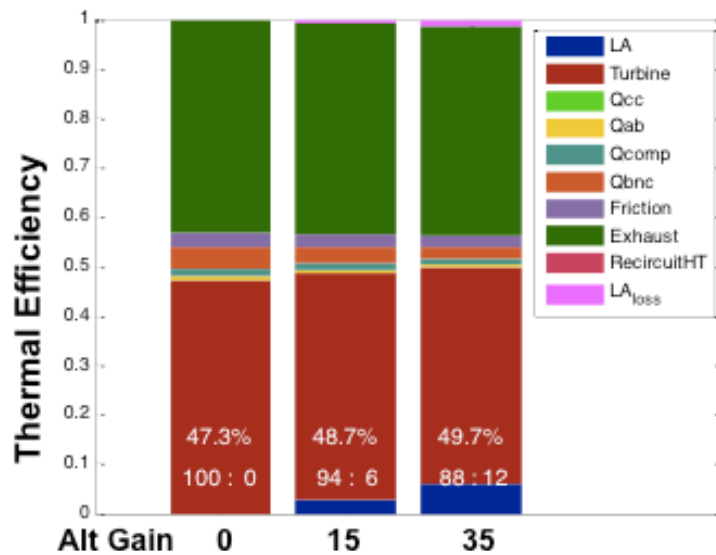
Figure 5-2 Thermal efficiency breakdown for comparison of alternators

As mentioned in Section 4.4, the alternator requires a rectifier for charging the battery and the internal resistance causes some losses. This loss is shown in pink (LA$_{Loss}$) and on the top of the thermal efficiency bar for those cases with alternator in Figure 5-2. The one with alternator coefficient 15 has 6% of useful work comes from the alternator, and coefficient 35 has 12%. The following table shows the cyclic energy generated by turbine and alternator:

Table 5-1 Useful work generated by turbine and alternator

Alternator Gain	0	15	35	
M$_{bounce}$	8	10	12	g
Turbine Work	1.90	1.84	1.76	kJ/cycle
Alternator Work	0.0	0.11	0.24	kJ/cycle

Based on Table 5-1, the alternator power extraction coefficient (alternator gain) increases from 0 to 35, and the turbine output drops. However, the increase of alternator output is larger than the reduction in turbine work. It is desired to know why the alternator produces work, in this case, more efficiently. In the simplified alternator model, the AC-to-DC conversion efficiency is 85% as mentioned before, so why the alternator is more efficient than turbine whose efficiency is also 85%? It may be confusing because the turbine efficiency is isentropic efficiency. The isentropic efficiency is not simply an input-to-output conversion efficiency as the one in the alternator. These two efficiency equations are listed below:

Turbine Isentropic Efficiency:
$$\eta_{turbine} = \frac{h_{in} - h_{ex,actual}}{h_{in} - h_{ex,isentropic}}$$
(Eq 5.5)

Alternator Efficiency:
$$\eta_{alternator} = \frac{W_{charging}}{W_{induced}}$$
(Eq 5.6)

In Eq. 5.5, h_{in} is the inlet enthalpy and h_{ex} is the outlet enthalpy with subscription "i" for isentropic and "a" for actual state. This efficiency defines the turbine expansion ability to convert the inlet enthalpy into useful work. In this case, the inlet enthalpy is not a single term in the denominator, unlike Eq. 5.6. Therefore, 85% of turbine efficiency is not equivalent to 85% alternator efficiency. While the alternator extracting power out of the piston's kinetic energy, the turbine inlet enthalpy decreases and less output is produced. Even if it is assumed the reduction of inlet enthalpy is 100% transferred to alternator work, different outputs will be produced due to different efficiency definitions. In fact, the energy transfer from turbine inlet to alternator is not a direct route because the piston dynamics being altered by the alternator influences the whole system behavior. Consequently, according to Table 5-1, using the linear alternator may be a more efficient route to deliver the useful work at the given efficiencies.

One more concern is if the efficiency is adequately chosen and in that respect a turbine isentropic efficiency of 85% is fairly common for most turbines. The 85% alternator efficiency, however, is a conservative option based on the detailed alternator model with a bridge rectifier, as described in Section 4.4. As a reminder, most cases have higher than 85% efficiency, and some of them even reach 90%. The overall efficiency is potentially higher by using the linear alternator.

Another important observation from Figure 5-2 is that the heat loss through the bounce chamber reduces with the increased alternator power. Since the alternator has no direct effect on the bounce chamber heat transfer coefficient and wall temperature, the decrease of bounce chamber heat loss comes from more bounce chamber mass. This is confusing because generally more mass implies higher pressure and temperature when being compressed. However, the free-piston engine has no fixed stroke, but the pressure on both ends of the piston determines its stroke. The piston changes traveling direction at the points where the piston kinetic energy in this direction reduces to zero by the pressure force against it. Consequently, an overall higher pressure in the whole compression event alters the piston direction in a shorter stroke. In the bounce chamber, more mass results

in higher pressure raise rate during compression, cancelling the piston kinetic energy faster. In addition, this leads to less compression in the bounce chamber, and lower peak pressure and temperature in the bounce chamber result in less heat transfer. A more detailed discussion on bounce chamber mass will follow in the next section.

5.4 Energy Distribution

Eq. 5.2 shows the balance of the cylinder work in the TCFPLA. This equation tells that the boundary work of combustion chamber, or indicated work, is split into four other terms: boundary work of compressor chambers, boundary work of bounce chambers, linear alternator, and friction. The indicated work partly presents the quality of combustion that raises the in-cylinder pressure. It is therefore interesting to understand how the indicated work is distributed into these four terms, and conduct more energy into the alternator and compressor for useful work output. To clarify, here the compressor work is useful because it is not a loss, based on Eq. 5.2. It does not mean the work put into the compressor can be useful as output.

In the following discussion, three comparisons will be made to see the change of energy distribution through isolating different operating parameters, including injection position, alternator gain and bounce chamber mass.

Table 5-2 Energy distribution at different injection positions

A_{gain}	M_{bnc}	Injection Position	$\dfrac{W_{alt}}{W_{cyl}}$	$\dfrac{W_{fric}}{W_{cyl}}$	$\dfrac{W_{bnc}}{W_{cyl}}$	$\dfrac{W_{comp}}{W_{cyl}}$	W_{cyl}	η_{brake}
45	10 g	95 mm	18 %	5 %	5 %	72 %	2.01 kJ	49.8 %
45	10 g	24 mm	18 %	5 %	5 %	72 %	1.85 kJ	47.6 %
45	10 g	15 mm	18 %	6 %	4 %	72 %	1.62 kJ	44.1 %

The operating conditions are listed on the first three columns in Table 5-2 followed by the energy distribution terms, which are normalized by the indicated work.

The amount of indicated work and brake efficiency are also shown for reference. The injection position is noted as the distance from the centerline of the combustion chamber. The fueling rate for these three is a constant 90 mg/cycle.

The injection position, as mentioned in chapter 4, is used to improve the performance. The better performance, as commonly known in the conventional engine, comes from better combustion phasing with less expansion penalty. In Table 5-2, it is evident that the change of injection position improves the indicated work, favored from healthier combustion. Log-P-Log-V plotted below represents this idea clearly.
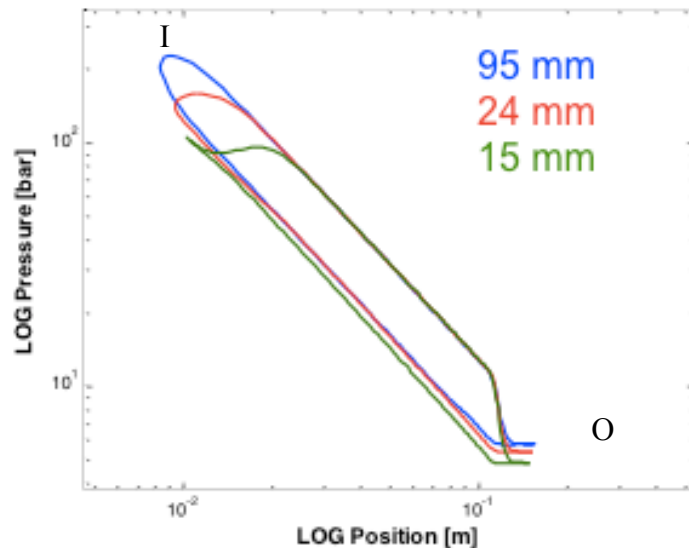
Figure 5-3 Log-P Log-V diagram showing the combustion phasing

The injection position, however, does not significantly change the energy distribution, especially the useful alternator and compressor work, remaining at 18% and 72%, respectively. With more delay of injection, the slight increase of friction is simply because the indicated work as the denominator becomes smaller, even with the fact that the amount of friction should be smaller for shorter stroke (green curve). The slight drop of bounce chamber work is the bounce chamber is compressed less, as can be seen on the outward dead points (ODP) in Figure 5-3. The 15 mm case curve has the smallest ODP due to the low pressure from the late combustion.

110

It can be easily imagined that the adjustment of alternator gain would shift the energy distribution more into the alternator, but how this affects other terms is the question to be answered.

Table 5-3 Energy distribution for different alternator power takeout

A_{gain}	M_{bnc}	Injection Position	$\dfrac{W_{alt}}{W_{cyl}}$	$\dfrac{W_{fric}}{W_{cyl}}$	$\dfrac{W_{bnc}}{W_{cyl}}$	$\dfrac{W_{comp}}{W_{cyl}}$	W_{cyl}	η_{brake}
0	10 g	23 mm	0 %	6 %	7 %	87 %	1.81 kJ	47.0 %
25	10 g	32 mm	11 %	5 %	6 %	78 %	1.98 kJ	49.2 %
45	10 g	95 mm	18 %	5 %	5 %	72 %	2.01 kJ	49.8 %

As expected, Table 5-3 shows that the alternator energy increases from 0% to 18% with the usage of alternator, and so does the efficiency. The injection positions have been tuned for best performance at the given fueling rates and alternator gains. In other words, the indicated work almost reaches its maximum at the given condition. For the first case with no alternator, the indicated work cannot go higher even if the fueling is the same. This is because the limitation of peak pressure forces the delay of combustion that lowers the pressure.

The reduction of losses will be in favor of either compressor or alternator. As seen in Table 5-3, the friction and bounce chamber work both reduce with the increase of alternator. The absolute amounts of bounce chamber loss through heat transfer remain similar among these three cases, but the increase of indicated work reduces the percentages. Moreover, the amount of friction loss is decreasing with alternator because the alternator shortens the stroke. As a result, the total percentages of useful work (compressor and alternator) are increasing from 87% to 90%, combining with the increase of indicated works return better overall efficiency at this given fueling rate.

The last parameter for discussion is the bounce chamber mass.

Table 5-4 Energy distribution for operation under different bounce chamber mass

A_{gain}	M_{bnc}	Injection Position	$\dfrac{W_{alt}}{W_{cyl}}$	$\dfrac{W_{fric}}{W_{cyl}}$	$\dfrac{W_{bnc}}{W_{cyl}}$	$\dfrac{W_{comp}}{W_{cyl}}$	W_{cyl}	η_{brake}
45	10 g	95 mm	18 %	5 %	5 %	72 %	2.01 kJ	49.8 %
45	12 g	32 mm	18 %	5 %	4 %	73 %	2.01 kJ	50.2 %
45	14 g	25 mm	17 %	5 %	3 %	74 %	1.95 kJ	49.8 %

Again, injection positions are tuned for given operating conditions. Therefore, the combustion here suffers the least expansion penalty. The bounce chamber mass is not related to the useful energy directly, since it only plays a role for energy storage. However, the mass would determine the pressure profile that has great influence on heat transfer. Table 5-4 suggests the more the bounce chamber mass, the less the heat loss. More importantly, the compressor work increases from the benefit of less heat loss.   A similar discussion was raised in Section 5.3, but it was hard to isolate the bounce chamber mass effects because the alternator was also different as seen in Figure 5-2.

As a reminder, the heat transfer model for the bounce chamber is Woschni's correlation, described in Section 2.5.   This correlation estimates the heat transfer coefficient according to the pressure and temperature profile. Hence, higher pressure results in higher heat transfer coefficient. In Table 5-4 with three mass settings, 14 g would have highest pressure if all were compressed to the same volume.   However, higher mass supplies more resistance that forces the piston to turn with less compression, resulting in smaller peak pressure in the bounce chamber. This causes the variable stroke as one special characteristic of the free-piston engines.   The following figure shows the bounce chamber pressure profiles and the various stroke caused by mass in the bounce chamber.
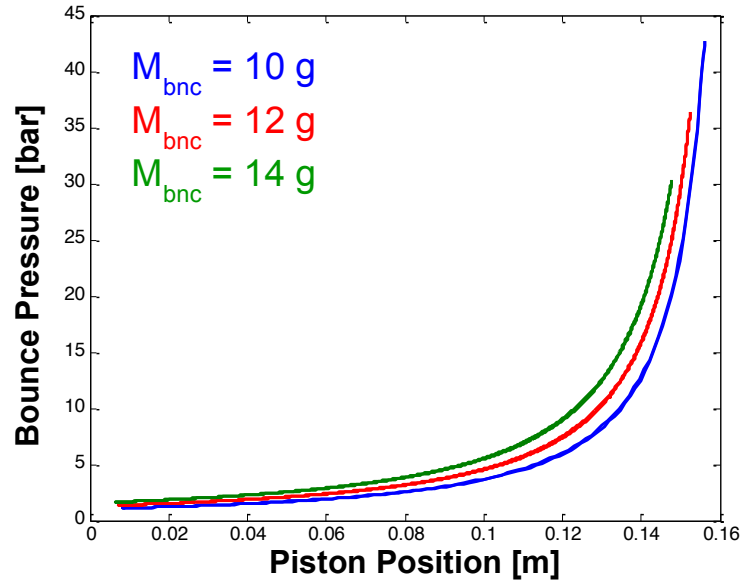
Figure 5-4 Bounce chamber pressure profile for different mass setup

In this figure, it is clear to see that 14 g of mass has the highest pressure at any given piston position, but the shortest stroke makes the peak pressure the lowest. This also implies that the temperature is lowest in the bounce chamber. The combined effects of these two lead to the lowest overall heat transfer coefficient and the smallest temperature difference between the gas and wall. As a result, the loss through heat transfer is reduced. However, the lowest heat transfer does not promise the best efficiency. In Table 5-4, although the difference in efficiency is very small, it can be seen that the indicated work drops for the case with 14 g of bounce chamber mass. This is because the overall higher pressure leads to higher cylinder compression ratio, raising the in-cylinder pressure, so the indicated work has to be reduced to keep the operation under restrictions. In this case, the lower heat loss compensates the loss of indicated work, and therefore the efficiency remains similar.

In conclusion, the change in one operating parameter causes more than one effects on the system behavior. The selected injection position and bounce chamber mass both maximize the indicated work and minimized the heat losses through the bounce chamber.

Generally, the bounce chamber mass effects are small, as shown in Table 5-4, but the amount of mass cannot be arbitrary. It has to be within a range, combined with the injection timing to adjust the indicated work for best performance and satisfy the restrictions. The injection position has no effect on the energy distribution, while the alternator transforms the compressor work into output directly. This is believed as one of the most important benefits of the TCFPLA engine because the alternator takes some energy out during compression and expansion. This means more fuel energy can be converted into indicated work without suffering the expansion penalty. In conclusion, the linear alternator, combined with the injection timing and bounce chamber mass, retains the desired compression ratio and extracts work during strokes.

5.5 Useful Work

In the conventional engine, the useful work is simply the boundary work of the combustion chamber minus the friction. In the TCFPLA engine, however, the boundary works are internally transferred from combustion chamber to bounce chamber, and transferred for the compressor. The useful work is produced by turbine and alternator. The alternator extracts the piston kinetic energy coming from the indicated work. The turbine utilizes the exhaust gas and its output is not explicitly seen in Eq. 5.2. Turbine inlet pressure determines the difference of the inlet and outlet enthalpy. Higher pressure helps produce more work and enhances the overall thermal efficiency. In addition, mass flow rate and inlet temperature would affect the turbine output as well. Many energy flows and thermodynamic data make the analysis very difficult.

Therefore, it is desirable to find the relations between the turbine output and other energy terms to understand where the potential is for improvement. The following figure shows the relation between the compressor work as the very upstream, and the turbine work as the very downstream.
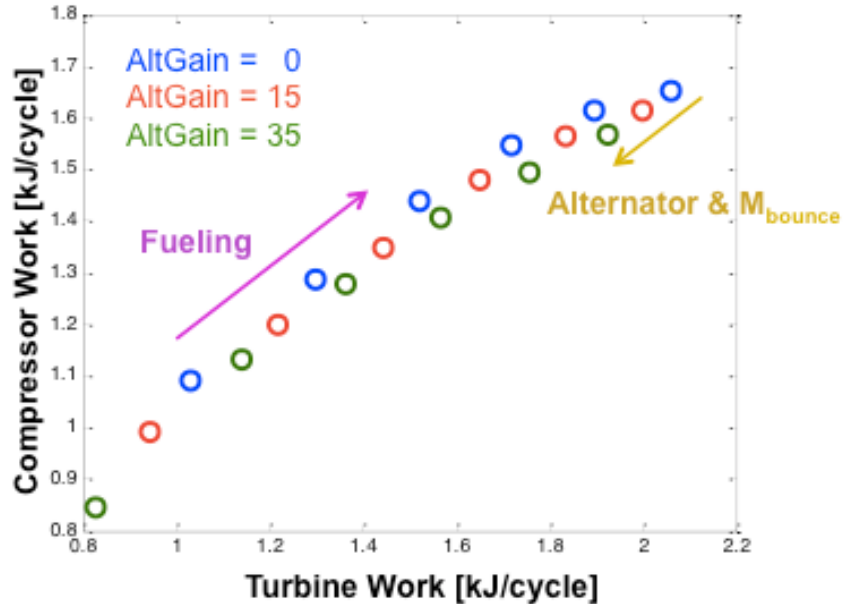
Figure 5-5 Relation between compressor work input and turbine work output

In Figure 5-5, every three data points with different colors (for different alternator gain) forms a group whose fueling rate is constant. The overall trend shows that the turbine output is highly proportional to the compressor work. As the fueling rate increases, more work is transferred into the compressor and raises the overall pressure in the system.   When the alternator turned on, part of compressor work is used to drive the alternator, so the turbine work drops.

Therefore, to increase the turbine work, the most direct way is to increase the compressor work. According to Section 5.4, the compressor work is supplied by the cylinder indicated work minus the alternator output, bounce chamber heat loss, and friction. Without the alternator, as long as the losses are similar, the amount of indicated work directly reflects the compressor work. Based on this, the relation between the indicated work and compressor work might be important.

115
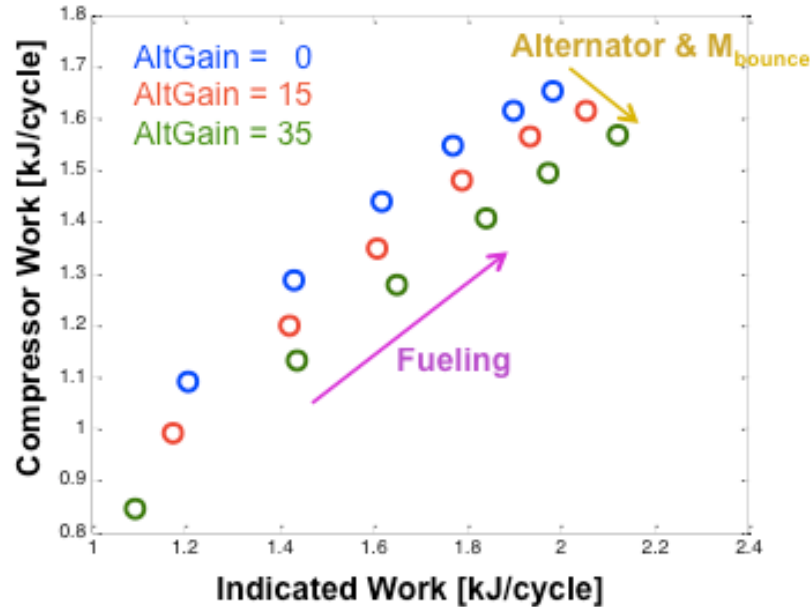
Figure 5-6 Relation between indicated work and compressor work input

As seen in Figure 5-6, the compressor work is generally proportional to the indicated work, and this is very straightforward as the compressor work is delivered by the bounce chamber as the energy storage during the combustion expansion.   In Figure 5-6, every three points with different colors at similar x-axis as a group has the same fueling rate, but the alternator separates them away. Most interesting part of this figure is the addition of the alternator.   All green points for alternator gain 35 have lower compressor work than the blue points which have 0 alternator gain. It is understood because the alternator takes some part of work out from the indicated work, based on Eq. 5.2. At the low-to-mid load condition, it can be observed that the indicated works reduce or remain similar as the alternator gain increases. On the other hand, the indicated work is higher for the high load cases.

This brings up another important concept about the operation of the TCFPLA engine.   The alternator is a load directly applied on the piston, so the low fueling makes the piston traveling difficult, reducing the stroke and indicated work thereafter. Combined with the BSFC contour in Figure 4-16, this explains why the alternator lowers

116

the efficiency at low load condition but improves for high load. It presents the fact that the alternator only benefits on mid-to-high load where the fuel energy is sufficient to drive both compressor and alternator properly. Compressor work has the maximum allowed value at a given load, because too much work would lead to the exceeding of peak pressure constraint in the combustion chamber. Assuming a maximum compressor work occurs at the highest blue point in Figure 5-6. Because the injection timing and bounce chamber are tuned, any fueling rate higher than this point will be prohibited by the constraints. However, with the help of alternator, more fuel energy can be released before the combustion dead center to increase the indicated work. For example, if the operation at 100 mg/cycle of fuel without the alternator reaches the peak combustion pressure, to burn 110 mg/cycle without exceeding this pressure, only two options are available. One way is to delay the combustion for less indicated work. This obviously reduces the efficiency. The other way is to use the alternator to extract the compressor work. The reduced compressor work keeps the cylinder peak pressure below the restriction, while the alternator enhances the indicated work and efficiency.

All in all, the compressor work is proportion to the turbine output energy. Alternator helps reduce the compressor work to maintain the peak pressure level with extra energy extraction by itself. However, the extension of the indicated work is unlimited by adding a very large alternator, because there are still two other restrictions. First, the physical limit of the alternator, as the room is not unlimited for extra coils and magnets. Second, the peak temperature restriction is still there to limit the equivalence ratio and therefore the fueling cannot be increased infinitely.

CHAPTER 6

TCFPLA Analysis by Second Law of Thermodynamics

The First Law of thermodynamics, presenting the relations between several important energy terms, has been discussed in Chapter 5. Most of the predecessor's works for the internal combustion engine stopped at the First Law analysis. One main reason is that the thermodynamic analysis for the conventional engine mainly was applied to only the combustion chamber [1]. The intake and exhaust flow are commonly assumed adiabatic, meaning no loss of enthalpy. In addition, the combustion release the energy based on the given combustion efficiency and the amount of fuel. However, both the flows and combustion have losses with regards to the Second Law. The entropy generation comes from any irreversible process, such as mixing, heat transfer or chemical reaction. In this chapter, a detailed Second Law analysis for the TCFPLA engine will be presented to see the loss that is unseen by the First Law approach.

6.1 Introduction

In the conventional engine analysis, the main focus is on the combustion chamber volume that produces power and experiences losses. Intake and exhaust may be considered, but their thermodynamic states are generally constants, containing single flow with no mixing or change of composition. However, this is not true in the TCFPLA engine. It has many subvolumes connected by valves that include several mixing, heat transfer and throttle processes. For example, two inflows enter the air box from the compressor chamber and will mix with the mixture already inside. The scavenging air also flows out of the air box. Two heat transfer processes are involved: one is from the combustion chamber through the heat recovery and the other one is loss through the outer

wall. It is extremely complicated, so a detailed Second Law analysis is useful to evaluate the available energy for potential improvement.

The second law of thermodynamic is expressed in the entropy balance equation written for a selected control volume. Generally, entropy tends to increase whenever the thermodynamic equilibrium changes due to the outside source, mainly the flow and heat, or the chemical reactions changing the composition. This is explained by the entropy generation due to the irreversible processes in the system. The entropy generation can be calculated by the entropy balance equation in a control volume, and the irreversibility can be determined.

Entropy Balance: $\qquad \dfrac{d}{dt}(m \cdot s)_{CV} = \sum \dot{m}_i s_i - \sum \dot{m}_e s_e + \sum \dfrac{\dot{Q}_{CV}}{T} + \dfrac{dS_{gen}}{dt}$ $\qquad$ (Eq 6.1)

Irreversibility: $\qquad\qquad\qquad\qquad \dfrac{dI}{dt} = T_0 \cdot \dfrac{dS_{gen}}{dt}$ $\qquad\qquad$ (Eq 6.2)

In the TCFPLA engine model, entropy generation can be easily obtained from Eq. 6.1 as the information for the flows and heat transfer are known. The control volume entropy $(ms)_{CV}$ is differentiated numerically with known thermodynamic states at each time step to obtain the rate of change. The mass flow rates with their associated entropy are known for the first two terms on the right hand side. Heat transfer is estimated by given heat transfer models, and the heat is leaving the control volume at a certain wall temperature. All volumes in the TCFPLA engine can use Eq. 6.1 to estimate the entropy generation. The irreversibility can be obtained by Eq. 6.2 to satisfy the availability balance equation as below.

Availability Balance: $\qquad \dfrac{dA_{CV}}{dt} = \dot{\Psi}_{in} - \dot{\Psi}_{ex} - \dfrac{dA_w}{dt} + \dfrac{dA_q}{dt} + \dfrac{dA_f}{dt} - \dfrac{dI}{dt}$ $\qquad$ (Eq

6.3)

$\qquad where \qquad \dot{\Psi}_{in/ex} = \dot{m}\left[(h - h_0) - T_0(s - s_0)\right]$ $\qquad\qquad$ (Eq 6.4)

$\qquad\qquad\qquad \dfrac{dA_w}{dt} = P\dfrac{dV}{dt}$ $\qquad\qquad\qquad$ (Eq 6.5)

$$\frac{dA_q}{dt} = \dot{q}(1 - \frac{T_0}{T}) \qquad\qquad \text{(Eq 6.6)}$$

$$\frac{dA_f}{dt} = x_b \cdot m_{cyl} \cdot \Delta G^0 \qquad\qquad \text{(Eq 6.7)}$$

$\dot{\Psi}_{in/ex}$ in Eq. 6.4 is the inflow/outflow exergy, or flow availability represented in the rate form. Eq. 6.5 is the availability of the boundary work, whose value is exactly the same as the work. The availability transfer associated with heat transfer is shown in Eq. 6.6, where T is the boundary temperature where the heat transfer occurs. Eq. 6.7 is the rate of fuel availability release by correlating with the burn rate. The only unknown in Eq. 6.3 is the irreversibility, which can be calculated from Eq. 6.2. Under the steady state condition, cyclic integral of the left hand side of Eq. 6.3 should be zero for no availability storage. If Eq. 6.3 is used to calculate the irreversibility, the control volume availability needs to be calculated by the following equation.

$$A_{CV} = (U_{CV} - U_0) + P_0(V_{CV} - V_0) - T_0(S_{CV} - S_0) \qquad \text{(Eq 6.8)}$$

It is noteworthy to mention the calculation for the combustion irreversibility. Based on Eq. 6.1, there is no flow during the combustion event, so the entropy generation depends on the control volume entropy and the heat transfer term. The combustion reactants are transformed to combustion products as CO_2 and H_2O, causing the change of composition. In addition, the pressure changes significantly during the combustion period. Therefore, the entropy before and after combustion should be calculated based on the thermodynamic properties alone and should avoid an evaluation of the detailed changes during the combustion.

Using the availability balance is the other approach to obtain the combustion irreversibility. Many references [2] [3] calculate the fuel availability by multiplying the lower heating value of fuel with a constant, which is claimed as a conversion factor between the fuel heating value and availability. This is based on the empirical data as a very rough estimation. Considering the fuel is burned at different compression ratio,

timing, or any other factor that affecting the condition of ignition, the pressure and temperature would end up differently after combustion. With the full access to the thermodynamic properties in the TCFPLA engine model, the actual fuel availability should be estimated based on Gibbs Free Energy, as in Eq. 6.7.
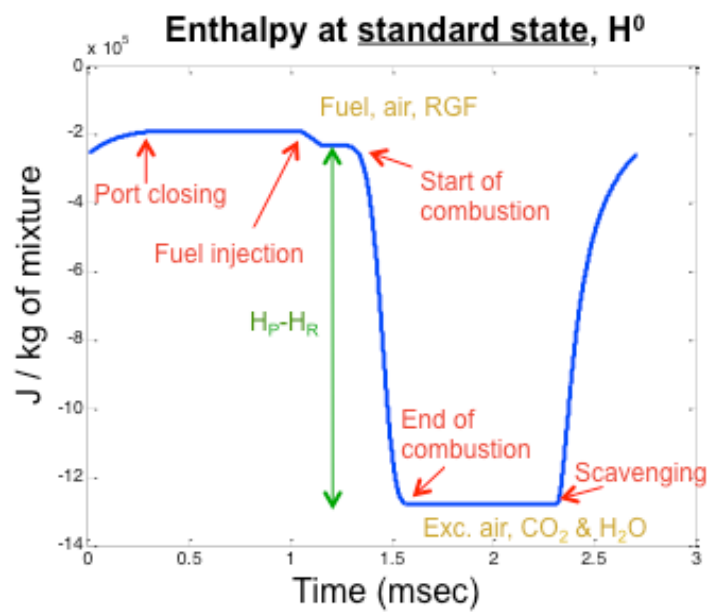

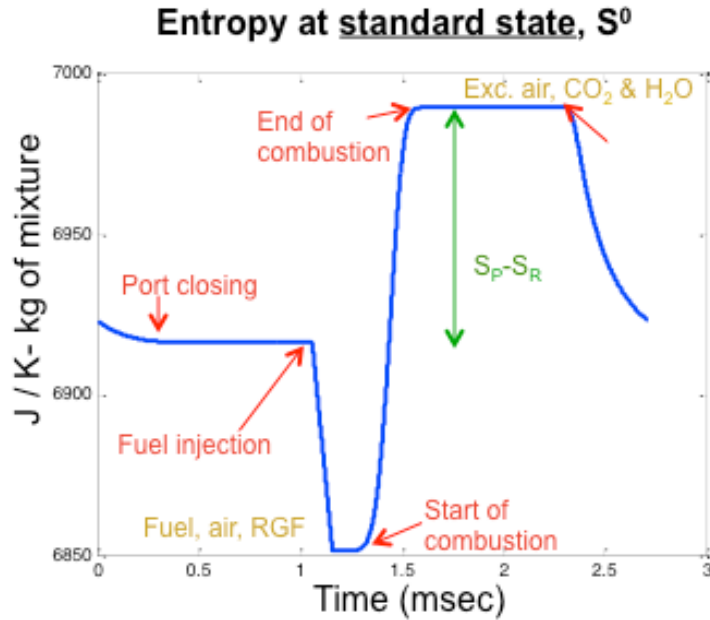Figure 6-1 System standard enthalpy profile shown in one full cycle

Figure 6-2 System standard enthalpy profile shown in one full cycle

Figure 6-1 and 6-2 shows the enthalpy and entropy at standard state, which is 298K and 1 atm, in the combustion chamber. The Gibbs Free Energy is defined as:

$$\Delta G = (H_p^0 - H_R^0) - T_0(S_p^0 - S_R^0) \qquad \text{(Eq 6.9)}$$

where H^0 is the standard enthalpy and S^0 is the standard entropy. The subscripts of "P" and "R" denote the combustion products and reactants, respectively. T_0 is the standard reference temperature 298 K. As can be seen in these two plots, the numbers for the right hand side of Eq. 6.8 are all available for the fuel availability calculation by Eq. 6.7.

One important comment is made about the combustion irreversibility. Due to the single-zone combustion model used in the TCFPLA engine, the estimation for the availability in the combustion chamber is not perfect. The single-zone model unifies the combustion chamber as a homogeneous thermodynamic condition during the combustion event. Therefore, the burned and unburned mixtures are at the same averaged pressure and temperature, even though their compositions are different. As a result, the unburned gas is brought to a higher pressure and temperature than it should be. Respectively, the

burned gas is at lower pressure and temperature. The averaged temperature and pressure are involved in the calculation of U_{CV}, V_{CV} and S_{CV}, leading to an inaccurate estimation. The solution for this is to switch the single-zone model to a two-zone model. The two-zone model has the unburned and burned zones with their corresponding states, which enables the calculation without using the averaged values. The availability of combustion chamber is the sum of availabilities in the unburned and burned zone. The error from the single-zone model, however, is not significant. As the irreversibility due to the combustion process cannot be avoided this period is treated in a simplified manner in this study to facilitate an expedient model formulation.

6.2 Availability in Volumes

Based on Eq. 6.3 through 6.7, each availability term in a control volume through a whole cycle can be plotted in cumulative value.
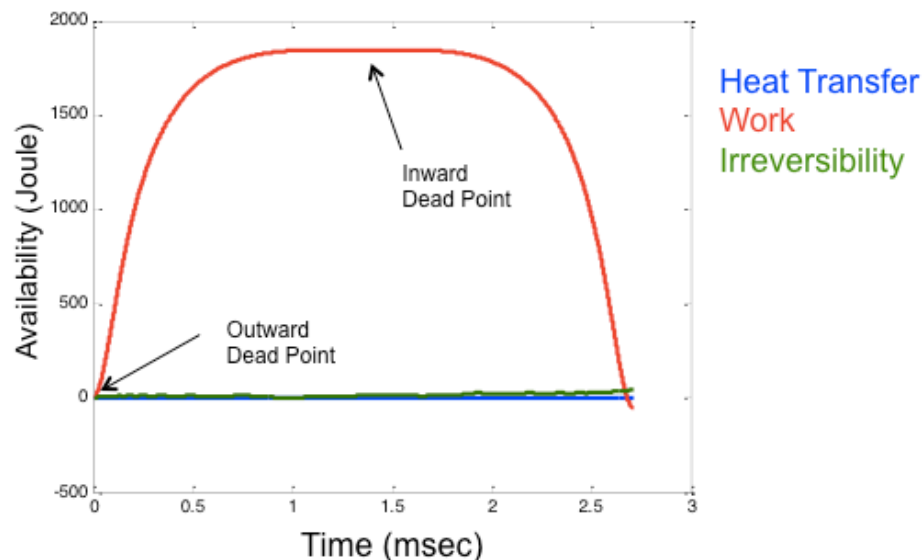

Figure 6-3 Cumulative availability of bounce chamber

Figure 6-3 shows all non-zero terms on the right hand side of Eq. 6.3 for the bounce chamber. All lines start from zero since they are cumulative values. Bounce chamber is relatively simple because there is no flow in or out. Therefore, the difference

123

between the boundary work, which is transferred from the combustion chamber, and heat transfer is the irreversibility. Since the value here is cumulative, the work (red) starts at 0 at outward dead point (ODP) and increases due to expansion. When the piston reaches the inward dead point (IDP) and changes direction, the bounce chamber is compressed with negative work. The curve goes down and ends at a point lower than zero to finish the cycle. As the bounce chamber is not adiabatic, the First Law in chapter 4 tells the extra work put in for compression is used to compensate the heat loss. The Second Law presents that other than heat transfer, the irreversibility is associated with to reduce the system availability.
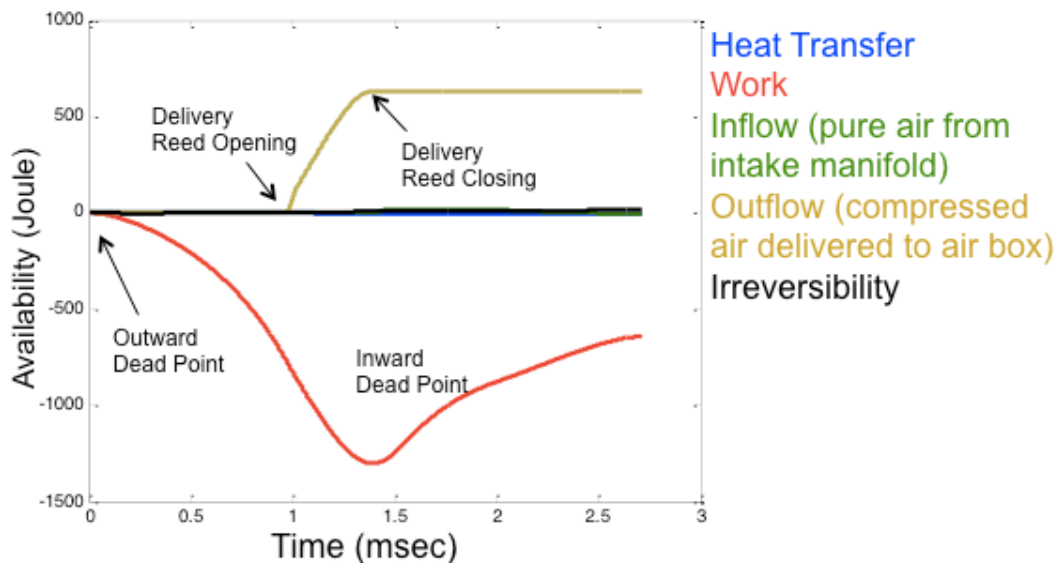

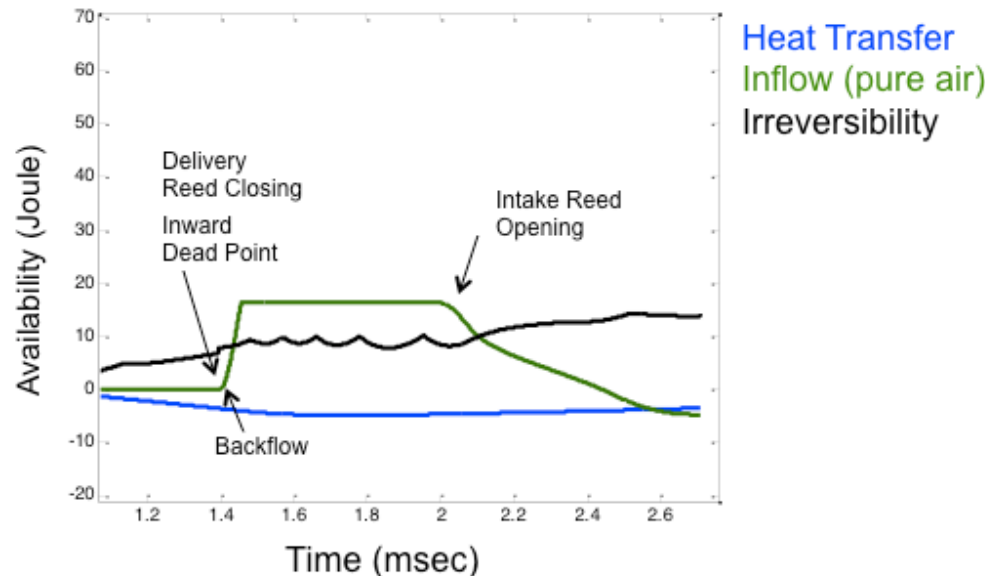Figure 6-4 Cumulative availability of compressor chamber

Figure 6-5 Cumulative availability of compressor chamber (zoom-in)

Figure 6-4 shows the contribution of each availability term in the compressor chamber. Starting from the ODP, the compressor is doing negative work to compress the air. The yellow curve shows that the cumulative outflow exergy increases until the valves close at IDP. The outflow has positive sign, because it is subtracted in Eq. 6.3. After IDP, the compressor expands and produces some positive work until the ODP. The inflow contains mostly ambient air with zero availability, and this explains why the green line is always near zero. Fresh air comes in and mixes with the leftover hot air in the compressor. This mixing process is where the irreversibility generates. Figure 6-5 shows the zoom-in of Figure 6-4 after the IDP for a clear view of irreversibility. The increase of the intake is caused by the backflow from the air box, as the reed valves do not close instantly. The intake curve goes toward negative when the intake reed valves open, because the air whose pressure is lower than the ambient contains negative availability. The heat transfer (blue) seen in Figure 6-5 is negative, as the heat is defined as positive if entering the volume.

One may question the small fluctuation of irreversibility shown in Figure 6-5. This comes from the entropy calculation, which contains both parts of temperature and

125

pressure. The temperature part including the estimation of specific heat is based on a look-up table with 50K intervals. Therefore, if the temperature changes within two consecutive time steps is smaller than 50K, the temperature part of entropy remains the same. However, the pressure part changes continuously on time step. The inconsistence of these two parts causes the oscillations, but overall it is increasing. This small error may occur in other volumes too.
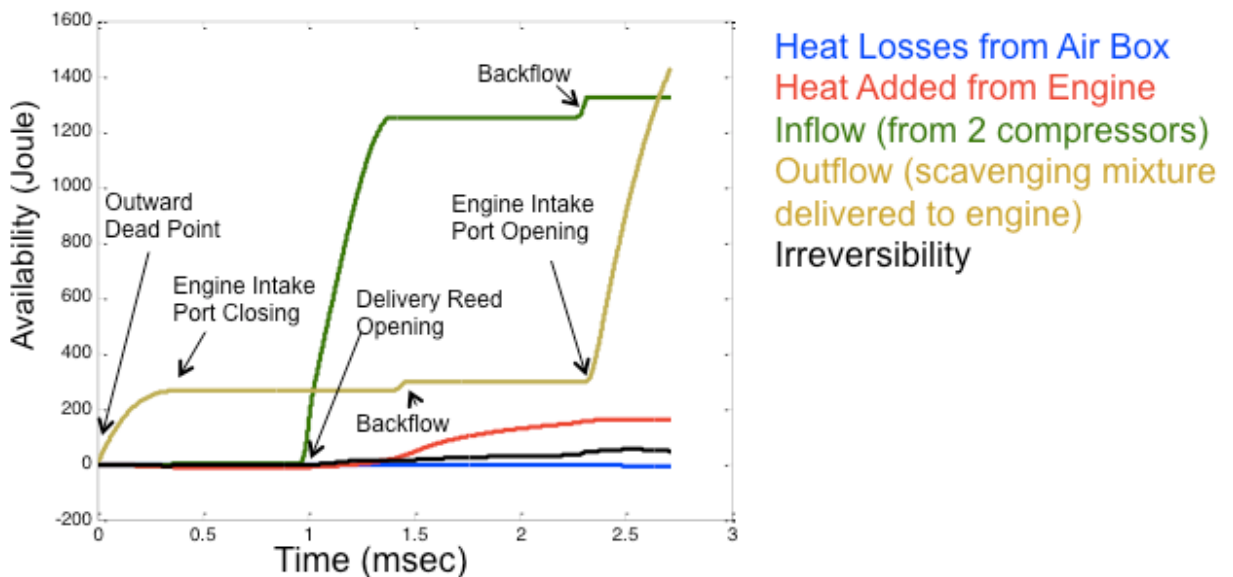
Figure 6-6 Cumulative availability of air box

The air box has no boundary work but only flows, as shown in Figure 6-6. The green curve as the inflow represents the compressed air entering into the air box. This figure only shows one inflow curve but it contains the exergy from both compressors. A backflow as a small hump occurs when the intake scavenging port opens, as marked on the figure. Some combustion products flow back into the air box and contribute to the inflow exergy. Similarly, the backflow shown on the outflow (yellow) is the flow returns to the compressor chambers while the delivery reed valve closing. It is not as hot as the backflow from combustion chamber, so the hump is smaller. Two heat transfers are involved in this volume: one is the loss (blue) in negative, and the other is the heat recovery (red) from the combustion chamber and that is positive. The irreversibility

126

takes place during the heat transfer and mixing processes. The scavenging flow into the combustion chamber is not a mixing event in air box, and the irreversibility curve remains at a similar value at the end of the cycle. It is a mixing event though in the combustion chamber, which can be seen next. The backflow from the combustion chamber is at high temperature, and it causes a visible increase of irreversibility in Figure 6-6.
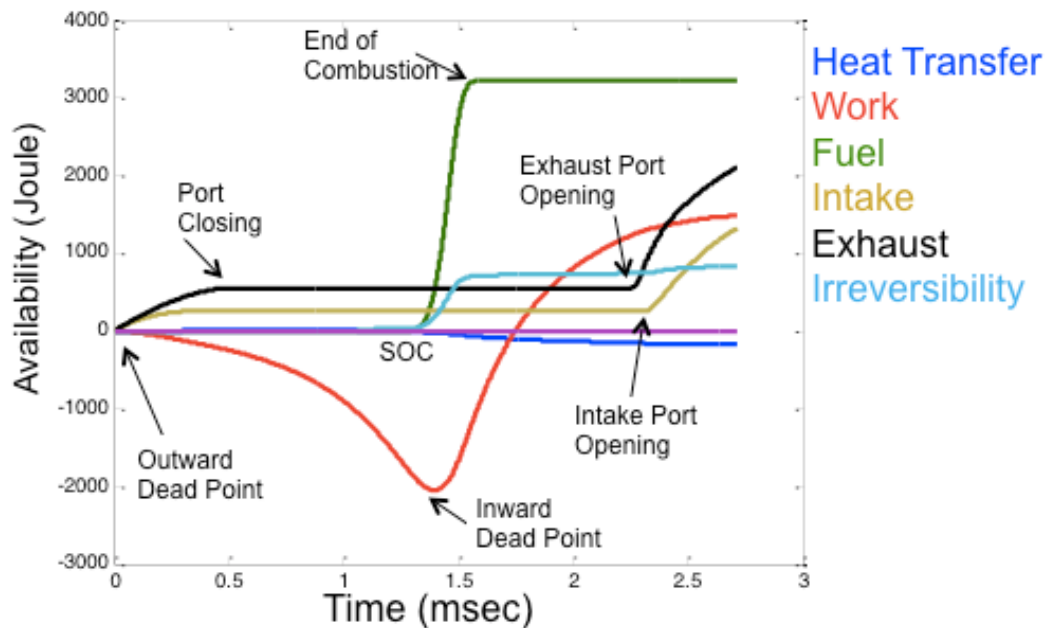
Figure 6-7 Cumulative availability of combustion chamber

The combustion cylinder is the most complicated volume, as shown in Figure 6-7. It includes the boundary work, flows, heat transfer, and fuel availability. The work (red) goes down first because the compression stroke produces negative work, and it goes up after IDP at a faster rate for the high-pressure expansion. Heat transfer is negative as it transfers out of the volume, and it accumulates faster after the IDP where the heat transfer is more intense. The combustion releases the fuel availability (green) that raises the irreversibility (light blue) most. Scavenging flows cause a hump on the irreversibility

because it is a strong mixing process. The exhaust carries high availability from the combustion, and this availability will be converted into useful work in turbine afterward.
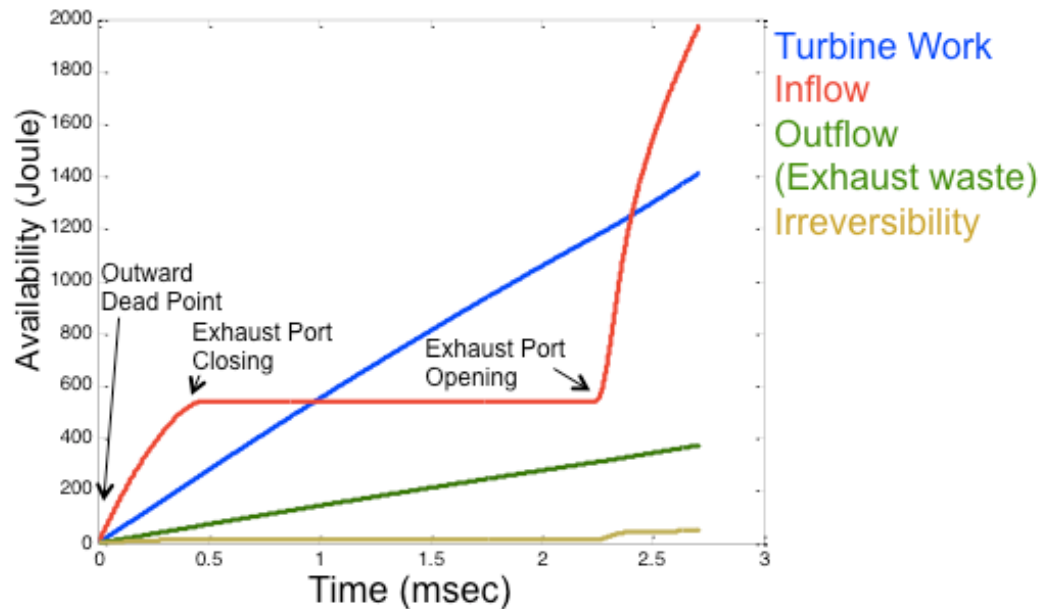
Figure 6-8 Cumulative availability of combustion chamber

The turbine is modeled as an orifice with steady flow from the exhaust manifold. The constant work is generated as the blue line with constant slope shown in Figure 6-8. The combustion exhaust as the inflow has high availability for being converted into turbine work. The gas entering the turbine is expanded for work production, so the exergy is low at ambient pressure. The irreversibility mainly occurs when the hot gas coming from the engine mixes with the existing gas in the manifold.

This section brought a full analysis for the contribution of each availability term in Eq. 6.3. It is hard to reduce the irreversibility in the control volumes, especially the combustion as the most irreversible process. Therefore, as mentioned before, most conventional engine analysis has no significance to determine the Second Law loss. For the free-piston engine, no Second Law analysis has been. Moreover, the TCFPLA engine involves more flows and heat transfer than the conventional engine, so the Second Law analysis is more desired for system diagnose.

6.3 Irreversibility of Flow

The irreversibility, or called destruction of availability, is namely the loss of the potential ability to produce useful work. In the previous section, the irreversibility was focused on control volumes. This section will stress on the irreversible processes taking places during mass transfer activities.

6.3.1 Flow Through Restricted Area

The mass transfers between volumes through a restricted area, such as valves and orifices. The flow rate is determined by the flow area and discharge coefficient, as described in Section 2.3. In the First Law point of view, the flow contains enthalpy as a form of energy. Generally, the flow through the restricted area can be seen as adiabatic, so the flow energy remains the same before and after the area. However, in the Second Law point of view, the pressure drop after the restricted area means the generation of entropy, or the destruction of availability. To define the loss, the equation for flow availability, or exergy, need to be introduced.

Exergy: $$\dot{\Psi} = \dot{m}[(h - h_0) - T_0(s - s_0)] \qquad\qquad \text{(Eq 6.10)}$$

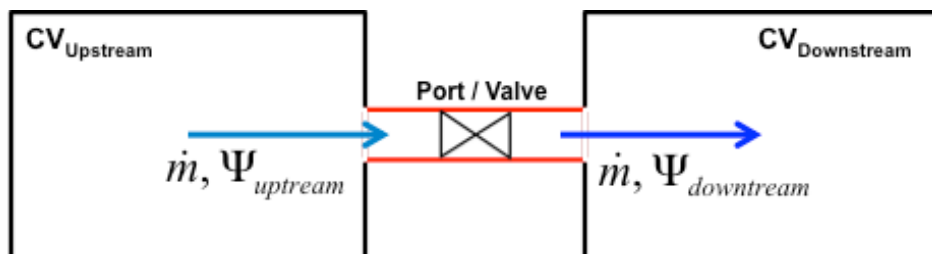The flow before the flow area is defined as the upstream, and after as the downstream.

Figure 6-9 Flow exergy before and after a port / valve

As seen in Figure 6-9, the mass flow rate is constant through the port, according to the conservation of mass. The process is assumed adiabatic, so the enthalpy remains

the same as well. However, the exergy is not conserved due to the throttle process and this leads to entropy generation. The exergy flow rates are listed for the upstream and downstream locations, and the Second Law loss is the difference between these two.

$$d\Psi_{upstream} = \dot{m}[(h_{upstream} - h_{0,upstream} - T_0(s_{upstream} - s_{0,upstream})] \qquad \text{(Eq 6.11)}$$

$$d\Psi_{downstream} = \dot{m}[(h_{downstream} - h_{0,upstream} - T_0(s_{downstream} - s_{0,upstream})] \qquad \text{(Eq 6.12)}$$

$$Loss = \oint_{cycle} d\Psi_{upstream} - d\Psi_{downstream} \qquad \text{(Eq 6.13)}$$

This loss is generally small, but considering many flows in the TCFPLA, the entire amount of flow losses may account for 4% of fuel availability, which will be shown later in Section 6.4.

6.3.2 Flow throughout Turbine

As the turbine is a machine utilizing the available energy by expanding the flow, the inlet and outlet must have a pressure difference. This failure of proper use of the pressure drop to produce work would generate entropy and destroy availability.
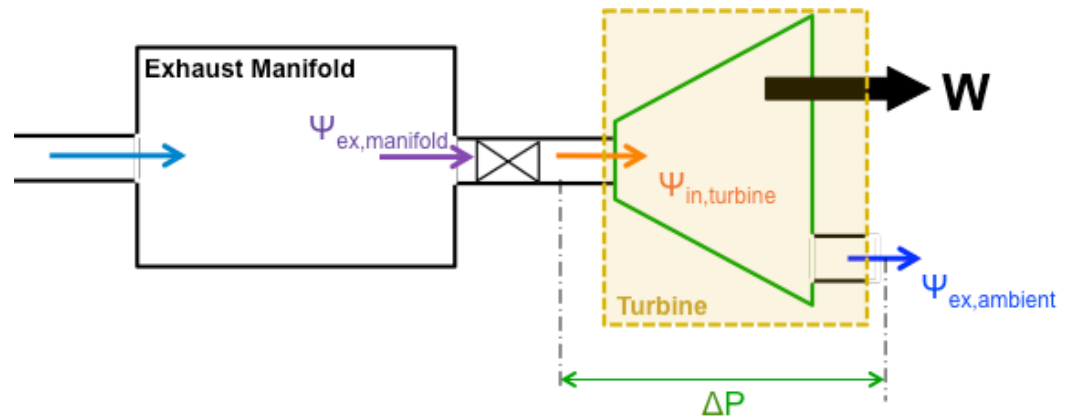

Figure 6-10 Exergy flow through a turbine

A simple sketch describing the flow exergy through a turbine is shown in Figure 6-10. The exhaust manifold is simply an adiabatic volume, so the inflow and outflow are assumed to contain the same energy and exergy. The Second Law loss of turbine comes from the ΔP marked in figure. Ideally, the difference between inlet and outlet exergy

130

should be the energy extracted by the turbine. However, 85% of turbine isentropic efficiency reduces the energy output. The turbine loss can be calculated bsaed on the equation below.

$$Loss = \Psi_{in,turbine} - \Psi_{ex,ambient} - W \qquad \text{(Eq 6.14)}$$

The Second Law efficiency of turbine can be defined as the ratio of useful work to exergy difference.

$$\eta_{2nd} = \frac{W}{\Psi_{in,turbine} - \Psi_{ex,ambient}} \qquad \text{(Eq 6.15)}$$

Generally, the Second Law efficiency is higher than the First Law efficiency. In most current modeling results, the turbine Second Law efficiency is about 90%.

6.4 Irreversibility of Heat Recovery

As discussed in Section 5.2, the heat recovery is a significant advantage of the TCFPLA engine. The model assumes that 100% of heat out of combustion chamber is conducted into the air box to preserve the energy. However, even though the energy is 100% retained, the exergy drops due to the transfer of heat from a higher temperature to a lower temperature environment. This transfer is therefore associated with an irreversible process that destroys the exergy.
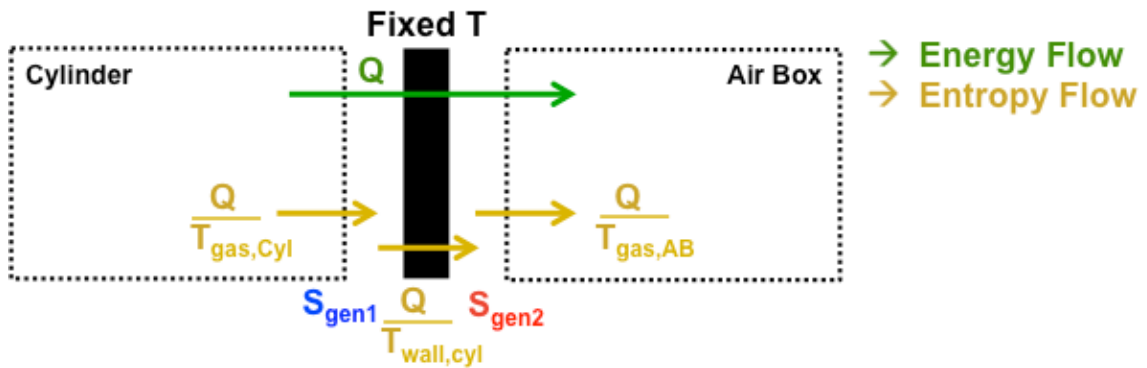

Figure 6-11 Heat recovery showing the entropy generation during energy transfer

The entropy generation comes from the heat transferring through a finite temperature difference. The model ignores the thermal boundary layer, and assumes the temperature is uniform in the control volume. Figure 6-11 describes the process of heat recovery in terms of entropy. From the left the flux of entropy (Q/T) is at the cylinder gas temperature then it moves through the wall at the wall temperature so the flux is larger (Q/T, same Q but smaller T). Last, the flux arrives in air box at the air box gas temperature which is the lowest T. The increase in the flux equals the rate of entropy generation and is directly proportional to the exergy destruction.

As the heat transfer passes through several layers it gives rise to entropy generation in different locations. Considering a control volume as the boundary layer between gas and wall, the heat coming in and out at different temperatures generates the entropy as seen in Figure 6-11. In the boundary layer, there is no inflow or outflow, so the entropy generation is simply caused by heat transfer. The following plot shows the entropy generations seen in Figure 6-11.
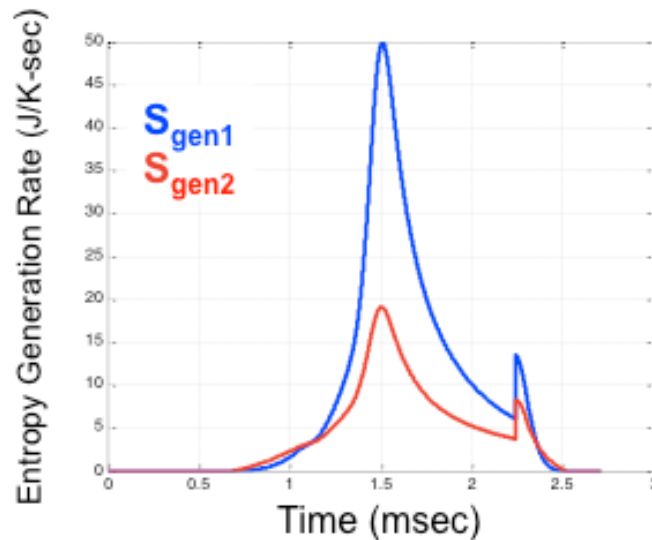

Figure 6-12 Entropy generation rate during the heat recovery process

In Figure 6-12, S_{gen1} is the entropy generation between the cylinder gas and the wall, and S_{gen2} is between the wall and the air box gas. S_{gen1} is larger than S_{gen2} because

the temperature difference between the cylinder gas and the wall is larger than that between the wall and the air box gas. The shape of this rate follows the shape of heat transfer rate, estimated by the Woschni model. Therefore, the heat out of the combustion chamber suffers two destructions of availability before arriving the air box. To see how much is actually destroyed, heat availability and the irreversibility are plotted.
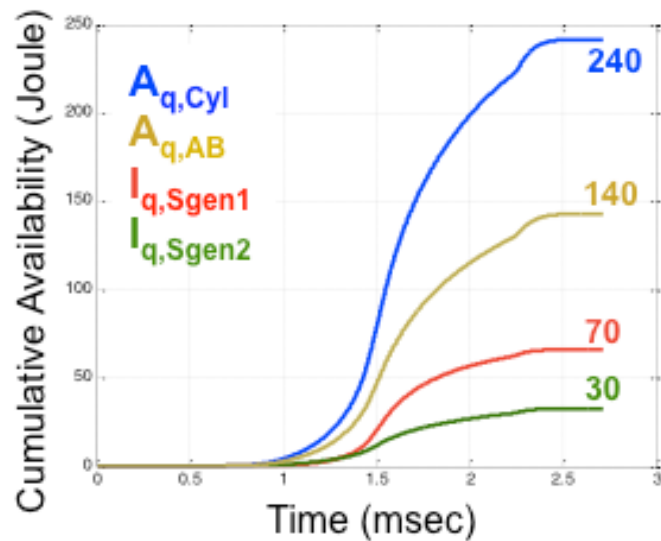
Figure 6-13 Cumulative availability and irreversibility for heat recovery

In Figure 6-13, $A_{q,Cyl}$ is the heat availability transferred out of combustion chamber, and $A_{q,AB}$ is that into the air box. As can be seen, from 240 J to 140 J, only 60% of availability is transferred into the air box. That is, 40% of available energy is destroyed due to the irreversible process.

From the First Law viewpoint, 100% of heat out of combustion chamber is transferred into the air box. This does not mean all the transferred energy can be turned into useful work. The heat increases the air box temperature which in turn increases the air box heat transfer loss to the outside wall. The energy moves from a high temperature environment and ends up in a lower temperature gas where it possesses less exergy for the same energy which explains the less than 100% recovery of exergy. The Second Law

clearly indicates that only 60% available energy is transferred. In other words, 40% of the heat availability is lost in the transfer process.

6.5 Potential Improvement Based on Second Law

The First Law analysis, in general, is able to point out the energy flow and determine the losses. However, it cannot determine if the energy transferred inside the system is available for use. The previous section gives a great example of the process with heat transfer where energy is recovered 100% but only 60% of availability is recovered. Therefore, reducing the lost energy seems to be reasonable to improve the efficiency, but reducing irreversibility makes a more direct improvement.

As for the purpose of comparison, Figure 5-2 is recalled here to see the energy distribution of the TCFPLA engine.

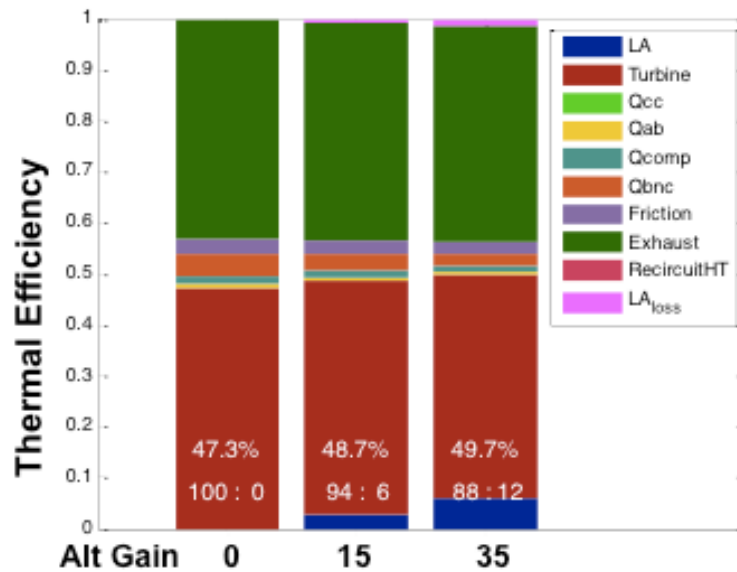Figure 6-14 Energy composition for different alternator setup

The results here in Figure 6-14 show the largest loss is the exhaust waste, which contains high temperature gas that cannot be utilized by this device. The second largest is either bounce chamber heat loss or friction. Friction is generally hard to be improved, but increased bounce chamber mass successfully reduces the heat losses, as discussed in

Chapter 5. The thermal Fractions sum up to 1 as all terms are normalized by fuel energy. Similarly, this can be altered into a Second Law based plot, normalized by fuel availability.
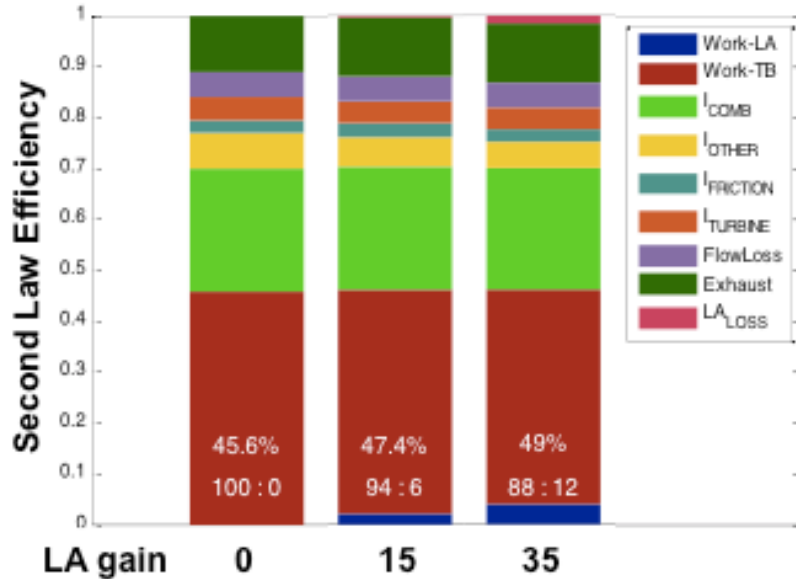
Figure 6-15 Availability composition for different alternator setup

As complex as Figure 6-14, Figure 6-15 has many terms regarding to Second Law consideration. Work terms are known for 100% transformation, so both the turbine and alternator work, marked as Work-TB and Work-LA, remain the same amount in terms of availability. The largest loss, however, is no more the exhaust waste (green) but I_{COMB}, as the irreversibility inside the combustion chamber (light green). This presents a fact that the combustion is a strong irreversible process that destroys a great amount of availability. Unfortunately, this irreversibility is hard to change because the combustion is an inherently intense irreversible chemical process. $I_{FRICTION}$ is the friction loss, whose value is the same as its energy. $I_{TURBINE}$ is the irreversibility in turbine, and FlowLoss is the irreversibility occurs when flow passes a restriction (valve), as discussed in Section 6.3. I_{OTHER} includes all the irreversibility in control volumes other than combustion

chamber. The control volume's irreversibility comes from heat transfer and flows, as completely discussed in Section 6.2.

These three cases look very similar in Figure 6-14. In order to clarify each case, Figure 6-15 is converted to a table that lists the percentage of each term as below.

LA gain	Work-LA	Work-TB	I_{COMB}	I_{OTHER}	$I_{FRICTION}$	$I_{TURBINE}$	FlowLoss	Exhaust
0	0 %	45.6 %	24.3 %	6.8 %	2.7 %	4.6 %	4.1 %	11.6 %
15	3.2 %	44.2 %	24.1 %	5.8 %	2.6 %	4.4 %	4.1 %	11.4 %
35	6.8 %	42.2 %	23.9 %	5.1 %	2.5 %	4.2 %	4.0 %	11.3 %

Table 6-1 Availabilities as the percentages of fuel availability

As shown in Table 6-1, the irreversibility in the combustion chamber are large portions but similar among all cases. Considering other irreversibility, the largest difference among these is I_{OTHER}, which is the irreversibility inside volumes other than combustion chamber. Since it contains many volumes, a further break out is necessary to address where the difference comes from.

LA gain	M_{bounce}	I_{OTHER}	$I_{COMPRESSOR}$	I_{AirBox}	$I_{ex\_manifold}$	I_{bounce}
0	8 g	6.8 %	0.9 %	1.1 %	1.0 %	3.8 %
15	10 g	5.8 %	0.8 %	1.1 %	1.1 %	2.8 %
35	12 g	5.1 %	0.7 %	1.1 %	1.2 %	2.0 %

Table 6-2 Irreversibility of volumes as the percentage of fuel availability

It is obvious in Table 6-2 that the largest irreversibility comes from the bounce chamber. Since bounce chamber is a closed volume, the only energies allowed for transfer are heat and work. This result is consistent with the First Law viewpoint, as shown in Figure 6-14, that the bounce chamber heat transfer is the second largest loss in the TCFPLA engine. Therefore, even though the First Law and Second Law determine different largest loss, they conclude the same second largest loss as the bounce chamber

136

heat transfer. This is where the potential improvement can be made. Considering the peak bounce chamber temperature is 550 – 750K, the heat transfer indeed can be significant. Proper insulation that reduces the heat loss certainly would help in the improvement of efficiency.

In the bounce chamber, the loss of heat means the pressure rise more slowly during compression, reducing the bouncing force for next cycle. In other words, the loss of heat undoubtedly decreases the available energy to drive the compressor. According to this, the bounce chamber has to be compressed more to gain more energy from the combustion chamber, and this reduces the available energy for the downstream turbine. Even if the loss of energy takes a long route from the fuel chemical energy to the bounce chamber heat transfer, a loss is a loss. Considering future experimental work of the TCFPLA engine, the bounce chamber loss can easily be overlooked, as most of the focal points must be on the combustion, turbine, or linear alternator. Combustion needs a delicate calibration, and any change in the system requires a retune of combustion. Without knowing the bounce chamber is the second largest loss and a simple insulation can improve the system, work may be wasted on trying to improve on processes that are less important. Therefore, a full thermodynamic study is helpful to determine the potential improvement for the future prototyping investment.

6.6 Exergy Flow Through TCFPLA

According to the study of alternator, it is found that more than 80% of the useful power is output from the turbine. As the turbine uses the flow to produce energy, the flow availability, or exergy, becomes an important indicator showing how much the potential energy the flow carries. From the First Law analysis, the flow enthalpy cannot fully represent the available energy, because enthalpy is only associated with the energy which for an ideal gas is only function of temperature. Generally, high pressure associates with high temperature, so one may easily be confused with enthalpy and neglect that it is lack of the pressure information. However, turbine utilizes the high

pressure to convert the flow enthalpy into mechanical work. Accordingly, exergy is the only way to indicate how much energy is available at a given state. The following plot shows the simplified schematic of TCFPLA with exergy flow through the whole system.
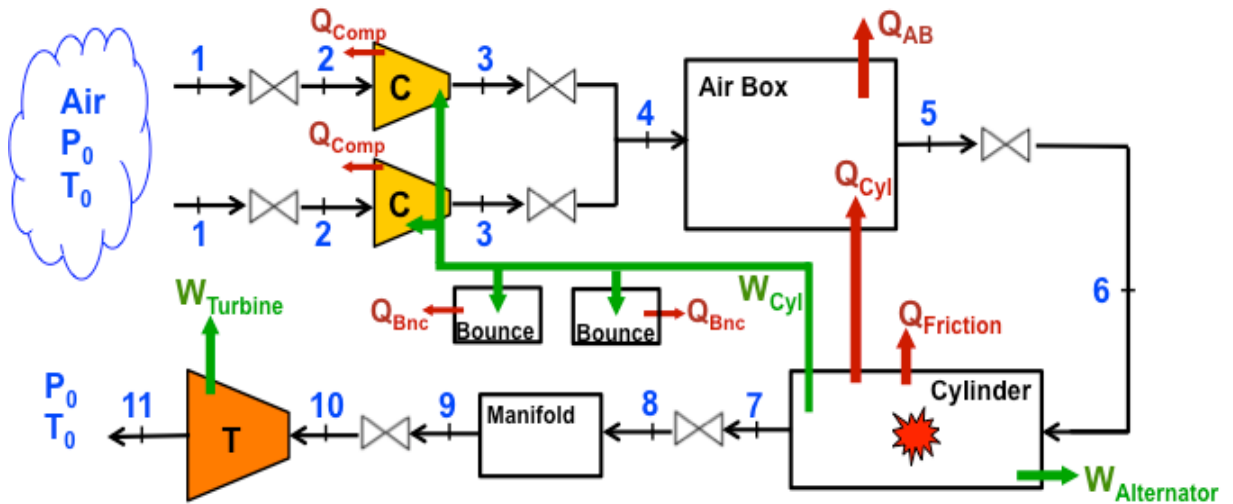
Figure 6-16 TCFPLA schematic with flow and energy transfer

In Figure 6-16, each flow state is marked with a number, ordered from upstream to downstream in the system. The "bow tie" symbols represent the reed valves or ports. The heat transfer terms Q's and work terms W's are subscribed with their corresponding information. The following table provides the cyclic integral of exergy at each state for the three cases with different alternator gain, as discussed before in Table 6-1.

LA gain	1	2	3	4	5	6	7	8	9	10	11
0	0	-27	798	1582	1827	1754	2660	2606	2606	2570	481
15	0	-26	769	1525	1768	1696	2592	2536	2536	2498	475
35	0	-24	727	1442	1684	1613	2503	2445	2445	2404	472

Table 6-3 Flow exergy at each state in the unit of [Joule/cycle]

State 1 is the intake air at the ambient, so there is no availability. After entering the compressor, state 2 contains negative availability because the pressure is lower than

138

the ambient due to the suction action of the compressor. The boundary work transferred from the combustion chamber compresses the air in the compressor chamber, boosting the availability at state 3. Two flows come from the two compressor chambers enter and mix in the air box. Because of the Reed valve, the compressed air comes to state 4 with a slightly drop of exergy. Air box receives heat from the combustion chamber as the heat recovery, increasing the exergy at state 5. The intake port of scavenging reduces the exergy due to a slight throttle effect before entering the combustion chamber at state 6. In the combustion chamber, the fuel releases the availability and significantly increases the exergy at state 7. Obviously, some of the fuel availability transfers to boundary work and some of it become a loss due to the highly irreversible combustion process and the heat loss through the walls to the air box. State 8 is the inflow after the exhaust port so the scavenging process results in a small pressure loss. As the exhaust manifold is assumed to be an adiabatic volume without actual valve and port, the flow does not lose exergy here at state 9. The turbine is considered as simple steady state device with an isentropic efficiency so there is an exergy loss in the turbine but otherwise it transfers most of the exergy into useful work. The exhaust flow contains the exergy as the part that cannot be used anymore at state 11.

With an increased alternator gain the work transferred into the compressor is reduced, so the exergy becomes less at state 3. The exergy difference between each two cases remains very close until state 7, where the combustion boosts the exergy. The exergy is highest at state 7 for the case without the alternator, and the values do not include the actual fuel exergy extracted from the piston into the alternator so the value drops as the alternator gain increases. As the alternator extract work and 100% of this work is available based on the Second Law, the real exergy increase by the fuel has to include this alternator work. According to Table 6-3, the increases of exergy from state 6 to 7 are 906, 896, and 890 Joule/cycle. Regarding the addition of alternator work, from state 6 to 7, the exergy gains are 906, 1030, and 1173 Joule/cycle for the alternator gain 0, 15, and 35, respectively. This signifies the TCFPLA with a larger alternator converts

more fuel availability into the useful work, namely the flow exergy before turbine and the alternator. Therefore, it is potentially more efficient.

Bibliography

[1]   J. Caton, "A Review of Investigations Using the Second Law of Thermodynamics to Study Internal-Combustion Engines," SAE Technical Paper 2000-01-1081, 2000

[2]   C.D. Rakopoulos, E.G. Giakoumix, "Second-law Analysis Applied on Internal Combustion Engines Operaion", Progress in Energy and Combustion Science 32 (2006) 2-47

[3]   J. Caton, "Results From the Second-Lae of Thermodynamics for a Spark-Ignition Engine Using an Engine Cycle Simulation", ICE-Vol. 33-3, 99-ICE-239, 1999

CHAPTER 7

Crank-Driven Opposed-Piston Gas Turbine

The TCFPLA has been fully analyzed based on thermodynamic laws in the previous two chapters. The arguments for the superiority between cranked-driven engine and free-piston engine were raised at the early stage of engine development. Other than the free-piston engine being more flexible with respect to the compression ratio, one of the arguments was it experiences less heat losses. However, the crank-driven engine won the battle due to its high controllability and simplicity. This short chapter will provide a straightforward comparison by using the existing TCFPLA engine model with proper modifications to move the piston in a crank/flywheel driven mode.

7.1 Configuration of Crank-Driven Opposed-Piston Gas Turbine

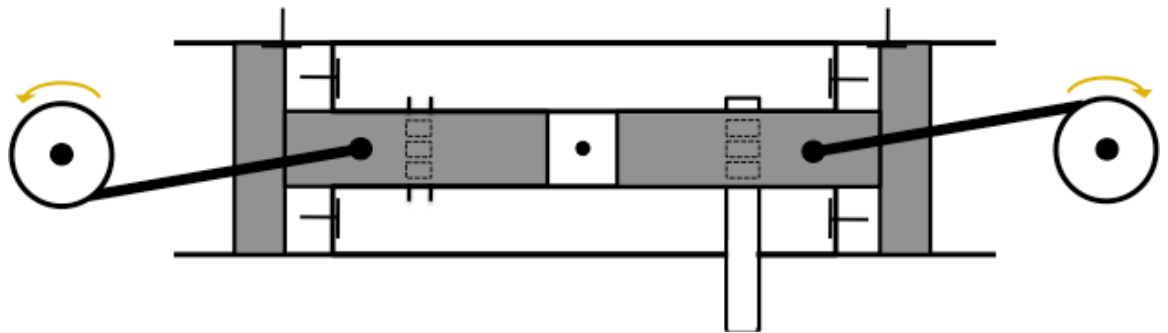The configuration of the cranked opposed-piston gas turbine can be sketched as below.

Figure 7-1 Configuration of cranked opposed-piston gas turbine

The bounce chambers in the TCFPLA engine supply the bouncing forces for the reciprocating piston movement, but replacing them with the crankshafts can achieve the same purpose, as seen in Figure 7-1. To make a fair comparison, the main structure of

this device remains the same as the TCFPLA engine. It still has two compression chambers, the air box, two-stroke combustion chamber, and gas turbine for work output. It also has two pistons traveling against each other, and this is known as the configuration of opposed-piston. By replacing the bounce chamber with the crankshaft, the piston motion profile is changed accordingly. This crank-driven engine is operated under a constant rpm equal to the given condition of the free-piston engine for fair comparison. The free-piston has larger acceleration near the turnaround point than the cranked piston, as can be seen below in the velocity profile plot.
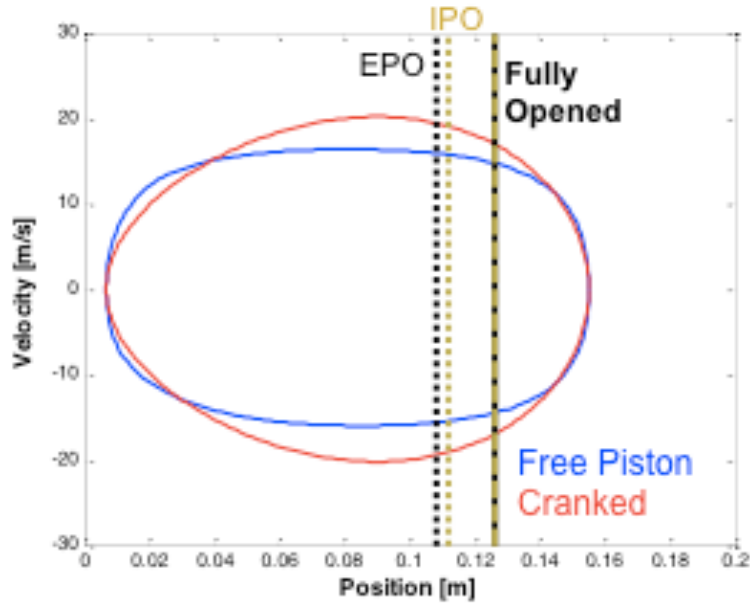
Figure 7-2 Piston position-velocity profile showing the difference of two type of pistons

Figure 7-2 clearly shows these two different piston dynamics. The stroke and compression ratio are set to be identical, as these can be easily specified for the crank-driven piston. After the inward dead point (IDP), the piston starts to accelerate. Near the IDP, the free piston shows higher acceleration, because the combustion blows the piston away. The speed remains nearly constant for free-piston, while the crank-driven piston keeps accelerating to the mid-stroke. Overall, the motion profile of free-piston is more like a rectangular, and the cranked piston is in a shape of egg.

7.2 Comparison of Operation

The stroke and frequency for the cranked engine configuration are picked from one TCFPLA engine operation. This ensures the comparison is not influenced by other factors. The thermal efficiency figure, as seen in Chapter 5, is plotted to show the difference between these two devices.
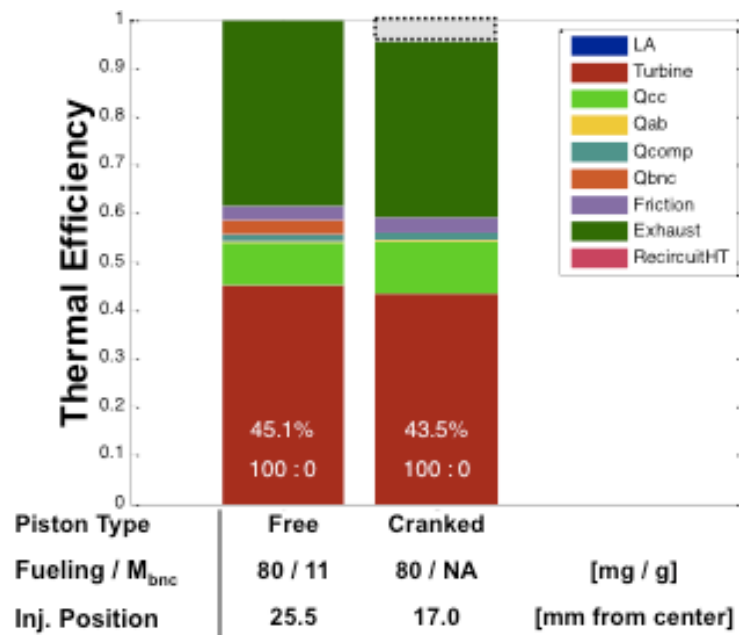
Figure 7-3 Thermal efficiency of free-pisron and cranked piston gas turbine

The operating conditions are listed in Figure 7-3. Both case burn 80 mg/cycle of fuel and their injection timing is tuned for the most efficient results. Several significant points can be made for the comparison. First, the bounce chamber heat loss shown in orange (Q_{bnc}) is absent for the cranked case. This is obvious because the cranked engine eliminates the use of bounce chamber. Second, the combustion chamber heat loss is not recovered by air box yet. This is on purpose to show the difference of heat transfer out of combustion chamber. As can be seen, the light green bar (Q_{cc}) on the crank-driven engine is larger, compared with the free-piston. This verifies the free-piston engines indeed experience less heat loss. The reason will be covered in the next section. Third,

there is a new gray bar, highlighted with dash line, appearing on top of the cranked engine bar. This gray bar is actually a new energy term that only appears in the crank-driven engine. Recall the energy balance equation in Chapter 5:

$$\oint \dot{W}_{cylinder} dt = \oint (\dot{W}_{compressor} + \dot{W}_{bounce} + \dot{W}_{alternator} + \dot{W}_{friction}) dt \qquad (Eq\ 7.1)$$

The gray bar happens to be the difference between the left hand side and the right hand side of Eq. 7.1. In the free piston, this equation can be balanced. However, in the crank-driven engine, the balance equation cannot be satisfied because the bounce chamber work no more exists. After overcoming the friction, the rest of the cylinder work is being transferred directly to the compressor. If the compressor requires less work, as in this case, the extra work can be useful with a small load on the crankshaft. This small load, for example, can be an electric generator. On the other hand, if the cylinder work is insufficient to compress the air to the given compression ratio, extra work has to be put in to drive the engine otherwise the engine will stall. Fourth, the injection positions shown in the figure are different between two cases. This is because the instantaneous speeds are different, and different injection timings are needed for the tuning to the most indicated work produced.

Based on Figure 7-3, the free-piston device looks more efficient, but the boundary work produced by the crankshaft is not accounted for efficiency yet. In addition, the heat loss for crank-driven engine is larger. Therefore, it is hard to draw any conclusion at this point.

7.2 Comparison of Heat Transfer

One of the arguments about the free-piston engine being more efficient comes from lower heat losses. The result shown in last section provides the same conclusion. In the past, researchers seemed to know this and mention the faster piston speed near the combustion top dead center reduces the heat loss. However, none of them gave a sound way to explain this or was able to conclude any definite results.

The crank-driven opposed-piston gas turbine shares the same heat transfer model with the TCFPLA engine. As a reminder, the Woschni heat transfer correlation use the in-cylinder temperature and pressure to estimate the heat transfer coefficient between the gas and wall. The comparison of the heat transfer coefficient as the function of piston position is shown below.
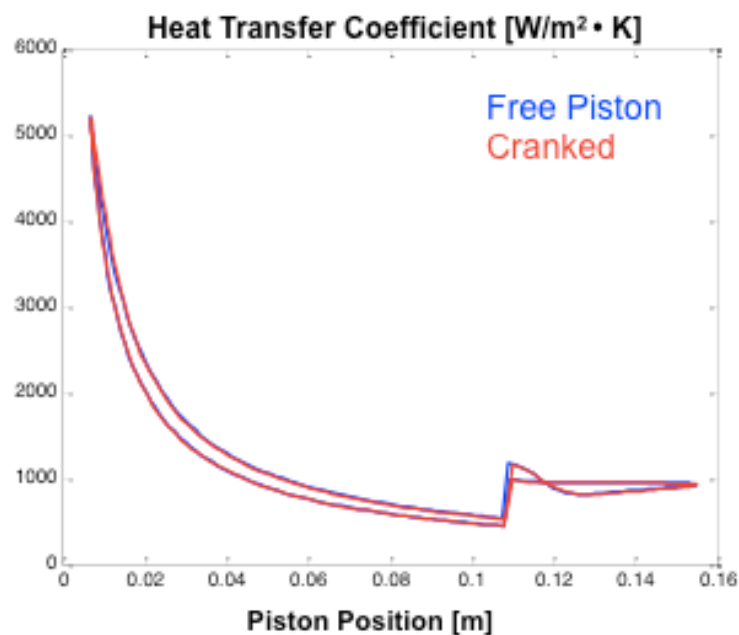
Figure 7-4 In-cylinder heat transfer coefficient as a function of piston position

As one may expected, the heat transfer coefficients for these two cases are almost identical. That is, at any given position, the pressure and temperature inside the cylinder are very close. This is not a surprising result because these two types of engine have same stroke and frequency. That means the amounts of fresh air drawn into the system are close, and thus similar pressure and temperature profiles occur. Therefore, the lower heat loss in the free-piston does not come from the lower heat transfer coefficient. One should not conclude that the free-piston has similar heat transfer coefficient as the crank-driven engine. This statement is only valid in this specific comparison whose stroke and frequency are set to be the same.

As the free-piston has higher acceleration near the combustion top dead center, the volume expands faster. This faster expansion brings the pressure down more rapidly and therefore reduces the heat transfer coefficient. The plot below shows how much time the piston spends near top dead center where the heat transfer is high.
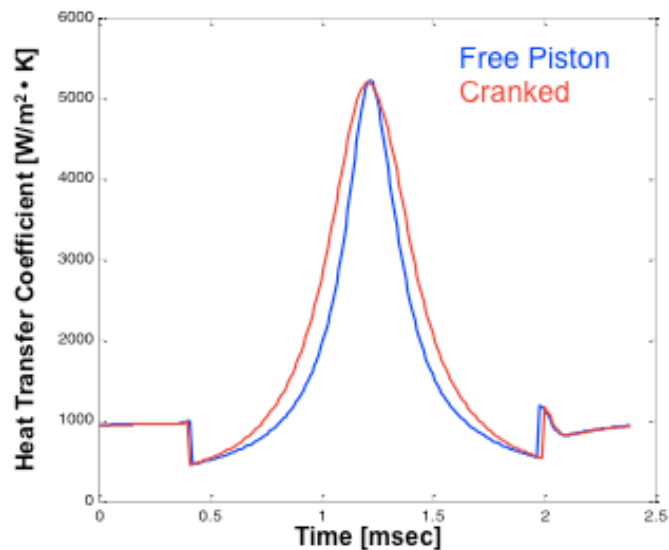
Figure 7-5 Heat transfer coefficient profile within a cycle

As a result, although the heat transfer coefficients for both cases are almost identical as a function of position, they are quite different in time during the closed cycle. Figure 7-5 shows that right after the ports close, the heat transfer coefficient increases in a faster rate, because the faster cranked piston leads to higher pressure and temperature. Near the inward dead center, the coefficients become very similar. However, the free-piston leaves the inward dead center, where the pressure and temperature are both very high, sooner than the cranked piston. Even though the cranked piston reaches higher speed after certain point of expansion, it overall spends more time during the closed cycle. Therefore, it is the velocity profiles that make these two position-wise similar heat transfer coefficient offset in time.

7.3 Applying Heat recovery

It makes sense to take the advantage of the heat recovery on the crank-driven opposed-piston gas turbine, as the structure is identical with the combustion chamber surrounded by the air box. Based on last section, more heat is transferred out of combustion chamber, but now all the heat is recovered by the air box. Even though the Second Law in Chapter 6 says not all of the heat is useful energy, it is interesting to see how this affects the performance.

Piston Type	Free	Cranked	
Fueling / M_{bnc}	80 / 11	80 / NA	[mg / g]
Inj. Position	0.0255	0.0175	[m from center]
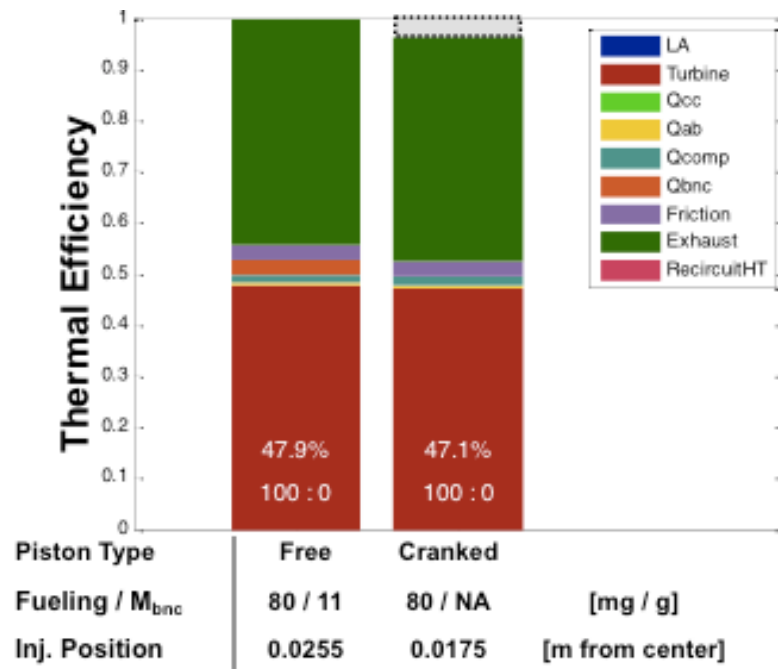
Figure 7-6 Thermal efficiency of free-piston and cranked piston with heat recovery

A similar thermal efficiency plot to Figure 7-3 can be seen above as Figure 7-6. With heat recovery, the light green bar as the combustion heat transfer no more exists. Comparing this with Figure 7-3, the heat loss through air box (yellow bar) becomes larger, even though it is still a small portion. The free-piston and cranked piston gain brake efficiency by 2.8% and 3.6%, respectively. Apparently, the cranked engine benefits from the heat recovery more, as more energy is saved in the system. In addition, due to the heat transfer coefficient in the air box is not highly affected by the piston

dynamics, the significant difference on heat losses is almost eliminated. The turbine then produces similar power output for these two configurations.

The potential disadvantage of the free-piston is the bounce chamber heat loss. As seen in Figure 7-3, the orange bar does not exist in the cranked piston and this part of energy somehow transfer to the gray bar, which is the extra boundary work. If the extra boundary work can be output, the crank-driven opposed-piston gas turbine shows higher potential to produce useful work (efficiency).

Analysis on the energy flow for these two configurations is discussed next. The energy balance equation for the crank-driven engine can be presented as below.

$$\oint \dot{W}_{cylinder} \, dt = \oint (\dot{W}_{compressor} + \dot{W}_{alternator} + \dot{W}_{friction} + \dot{W}_{crank}) dt \qquad (Eq\ 7.2)$$

The bounce chamber work in Eq. 7.1 is replaced by the crank work, namely the work produced by the crankshaft. The crank work can be positive or negative, depending on the cylinder work and compressor work. If the compressor work is smaller than the cylinder work, the crank work is positive and can be useful. On the other hand, negative crank work means the work has to be added on the crank to drive the engine.

The crank-driven engine has fixed stroke and compression ratio, which limit its feasibility for the gas turbine. Considering the comparison in Figure 7-6, the free-piston engine maximizes the compressor work for overall higher pressure in the system to produce maximum turbine work. On the other hand, the cranked engine cannot maximize the compressor work because it is constrained by the constant stroke. The extra work, which is gained from the elimination of bounce chamber, has to be output by the crank as the gray bar.

However, a crucial problem occurs in the crank-driven engine configuration at lower load. In the crank-driven engine configuration, the compressor work is almost a constant at any speed if the small variation of intake mass caused by engine speed is ignored. Therefore, the indicated work has always to be greater than the compressor work to run the device by combustion alone. Running the cranked engine configuration

with less fuel stalls the engine immediately. However, this can be easily achieved in the free-piston gas turbine because the compressor work varies accordingly to the load.

CHAPTER 8

Conclusion on TCFPLA Engine

8.1 Summary

Various designs of free-piston engines were reviewed in Chapter 1. More interests have been raised recently on the free-piston linear alternators (FPLA) for its compact size and high efficiency. The power output of the FPLA is generally small. The previous works reported 7 to 15 kW for the FPLA with 50 mm combustion chamber bore [1] [2]. Sandia FPLA [3] has 80 mm bore with the opposed-pistons structure combining 400 mm of stroke. It generated 30 kW of electric power, realized by delicate control of the bounce chamber mass. Sandia FPLA burned hydrogen in the current experimental work, so it is more likely a concept for the future. German Aerospace Center (DLR) FPLA [4] is the most realized device on automotive application. The target power is 35 kW as the assistant powertrain in an extended-range vehicle and the 80 mm bore and 120 mm stroke make the DLR FPLA more practical and promising.

In this study, the 100-kW TCFPLA engine targets a much higher total power output and integrates both mechanical and electrical power devices in one machine. Although the architecture is the most complicated with many chambers and valves, it has the most advantages regarding efficiency and power-to-volume ratio. The combustion chamber bore is 35 mm, bounce chamber bore 100 mm, and the stroke 250 to 300 mm. This conceptual engine can be further optimized in dimensions to reduce the stroke by decreasing the bounce chamber bore or bounce chamber offset. Note that currently the TCFPLA engine is a single-cylinder device. Further downsizing to 50-kW output and combining two of them in series will make the dimensions more favorable for the vehicle application in any future work.

A free-piston engine model were developed by employing the thermodynamic principles, the Wiebe combustion profile, the Woschini heat transfer correlation, flow calculations, and linear alternator model, as fully described in Chapter 2. In Chapter 3, historical data was used in a comparison to demonstrate the model feasibility. Although the experimental data was very limited for a full validation, the fitted pressure-volume curves verify that the model returns reasonable outcomes. Furthermore, the new model calculated the piston dynamics for stroke and frequency with the assumption of long burn duration confirms that the new model predicts realistic results. Sensitivity tests on heat release profile, heat transfer rate, amount of friction force, and the shape of friction force profile eliminate the possibility that these variables are likely change the system response dramatically. With these being low sensitivity, the possible errors from the experimental measurement are also eliminated. This further confirms the prediction from this new model is trustable. Furthermore, the system energy equation, Eq. 5.2, is automatically satisfied without explicit implement. The Second Law analysis in Chapter 6 additionally concluded reasonable results. These thermodynamic studies combined with the data comparison in Chapter 3 make the model rational and logical for the system level analysis.

Due to the lack of complete geometric information for the GM Hyprex [5], parametric studies on dimensions were performed in Chapter 4. Bounce chamber offset, compressor offset, piston mass, and the combustion-to-compressor area ratio were selected based on the feasible results. A more realistic linear alternator model with electric components was also introduced and integrated in Chapter 4. Fewer coil and magnet numbers were proven to reduce the alternator power takeout. The simplified model introduced in Chapter 2 showed a great agreement with the detailed model. Less computational cost made it more suitable for the current free-piston engine model. To expand the low load operation, the strategy called "recirculation" [5] was introduced. It successfully maintained the low load operation at the cost of efficiency. The size of the recirculation valve becomes an extra parameter in controlling the TCFPLA engine, but

deeper study on this strategy is beyond the current scope. The benefits of the linear alternator are more desired in this research.

Later in Chapter 4, bounce chamber mass and injection position were determined important for both the optimum performance and satisfaction to the restrictions. Engine maps of BSFC and frequency contour were made in the load range from 30 to 100 kW. The TCFPLA engine reached 50% efficiency at mid load with high alternator power takeout. Based on the maps, the linear alternator benefited the efficiency when the load more than 60%. Similar to the conventional engine, the mass flow rate would reduce during high-speed operation, reducing the turbine power output as well as the system thermal efficiency.

In Chapter 5, it is concluded that the linear alternator is a more efficient route for producing the useful work, based on the First Law. Interestingly, based on Second Law efficiency described in Chapter 6, turbine is more efficient with 90% efficiency while the alternator is still 85%. One should not be confused with that the First Law and Second Law reach different conclusions. The efficiency of individual device does not guarantee the overall efficiency, as there are two of them. The linear alternator changes the free-piston engine operating conditions, and this is the reason why the free-piston with linear alternator is more efficient than the one without.

The alternator extracts fuel availability without affecting the exergy gain through combustion, as can been seen in Table 6-3. The increases of exergy from combustion are very close among three cases, but this result ignores the fact that the linear alternator has already extracted power. The free-piston engine with linear alternator in fact obtains more availability through the combustion process. The alternator acts as a resistance for the piston motion, and the reduced speed around the combustion top dead center (IDP) makes the combustion more constant-volume like. This explains why the indicated work is higher for the high alternator case seen in Chapter 5. Furthermore, the compressors obtain more portion of availability from indicated work because of less heat loss in the bounce chamber.

A more theoretical way can be use to describe that the linear alternator makes the system better. Consider a case whose turbine Second Law efficiency is also 85%, same as the alternator. This means the extracted exergy from either device produces the same useful output work. However, the alternator is on the upstream and the turbine has to be the very downstream. Consider two cases with same condition on state 6 and the gained exergy from the fuel are also the same. One of them uses turbine only, and the exhaust waste must contain certain amount of exergy. For the other case, assume the alternator can extract as much exergy as possible to make the final exhaust exergy the same as the turbine only case, meaning that the exhaust flow goes out to ambient right after the combustion chamber with no turbine. Since both devices have 85% Second Law efficiency, the alternator has more potential exergy for use because it is at the upstream position. The turbine inlet exergy, on the other hand, suffers some losses before coming to this stage and therefore has less exergy available. Even though the alternator cannot be operated in such way as to extract all energy otherwise the piston stops moving, this possibility tells the power extracted at the upstream point avoids some losses that is inevitable following the flow downstream. As a result, the alternator can access more exergy and be more efficient than the turbine.

Chapter 7 shows the comparison between the free-piston and cranked piston with almost identical configuration, except the bounce chamber replaced by the crankshaft. The piston motion profiles present a similar comparison as the historical data as below.
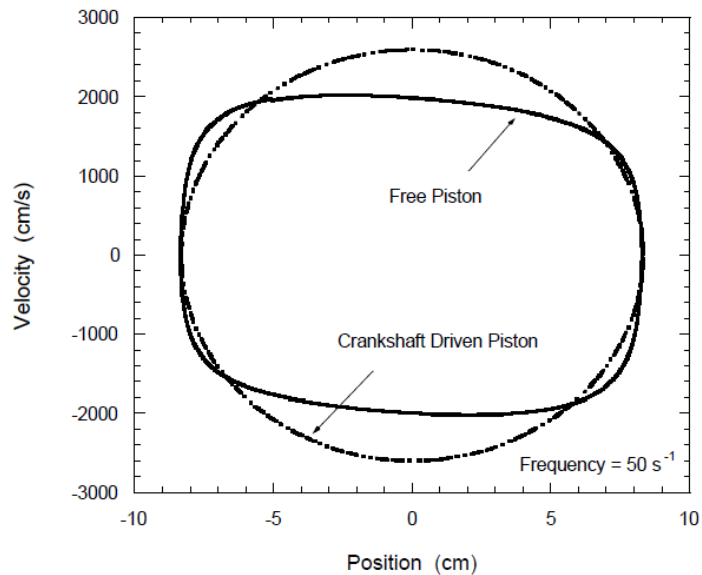
Figure 8-1 Comparison of piston motions between cranked and free-piston

The heat transfers in these two configurations were compared by using the same heat transfer model and wall temperature. The different piston motion profiles distinguish the results of heat transfer regime. As shown in Figure 7-4, the heat transfer coefficient as a function of piston position is almost identical. However, the velocity makes the cranked piston spend more time during the closed cycle where the heat transfer is more intense.

The heat recovery shows the true potential of the cranked-opposed piston configuration, as the elimination of bounce chamber further reduces the loss. In addition, the cranked piston has high controllability compared with the free-piston, as the bounce chamber mass has to be controlled for optimum in the free-piston device. The cranked piston engine simply removes this complexity, including the low load strategy. However, the cost of controllability is the flexibility. The cranked engine has no various compression ratios for alternative fuels. Therefore, the cranked engine may not have a wide efficient range as the free-piston does, because the lack of bounce chamber cannot push the piston to a desired compression ratio. The fixed stroke and compression ratio

155

has no way to effectively compress the in-cylinder mixture as the free-piston. Additionally, the linear alternator was not compared for these two configurations. The linear alternator may fit better on a free-piston engine, as the piston speed is more stable during the middle of the stroke. This stabilizes the electric current and simplified the circuit design. Although the difference between these two configurations is clearly shown, no definite conclusion should be drawn at this point.

The overall efficiency of the TCFPLA engine is about 50%. This number results from 85% turbine isentropic efficiency and 85% of alternator current conversion efficiency. According to the detailed alternator model discussed in Chapter 4, the AC-to-DC conversion efficiency can be as high as 91%, so 85% is a conservative value. Modern diesel engine for automotive application has 40% ~ 45% of thermal efficiency. The conventional gas turbine produces power at 30 ~ 40% of efficiency. More advanced gas turbine with heat recovery system generator (HRSG) can reach higher than 50% efficiency. However, the HRSG is not a small system for automotive use. The TCFPLA engine has comparable efficiency with both diesel engine and gas turbine.

8.2 Future Work

Model improvement could be endless, but several sub-models in the TCFPLA engine model can be updated for improvements in the analysis. The first priority is the combustion model. The current single-zone combustion model results in a uniform condition in the combustion chamber. This ignores the fact that the burned and unburned zones have significant differences. A two-zone model can better predict the in-cylinder conditions. Moreover, the estimation of combustion irreversibility can be more accurate by predicted by a two-zone model [6], as the reactants and the products are at different thermodynamic states. The single-zone model can only calculate the thermodynamic properties for the burned and unburned compositions under the same states (lumped analysis).

Second, the current friction model consists of two parts: kinetic and static. The constants in the friction equation are selected based on the reported data [7]. Friction between piston and cylinder is typically 15% - 20% of the losses in the conventional engine. However, no friction study was made for the free-piston engine. It is generally believed the free-piston engine has less overall friction due to the lack of crankshaft and connecting rods. Instantaneous IMEP method [8] was recently developed based on the force balances on the piston. However, it was claimed to be very sensitive to the force terms. A correlation from experimental work of any free-piston engine is more desired, as the force balance determines the movement of free-piston. Regardless of the linear alternator, all other forces should be able to be measured for the force balance equation as Eq. 2.17, and the friction can be determined.

The bounce chamber is assumed a closed volume. However, in reality the piston cannot be fully sealed. The leakage of mass is inevitable, and the large bore size of the bounce chamber further enhances the loss. In addition, the leakage is a two-way flow as the air in the compressor can enter into the bounce chamber as well. In the Ford version of free-piston engine [9], a pressure regulator is used to fill the mass from the air box into the bounce chambers. This is believed to be similar as the stabilizer in the GS-34 engine [7] that synchronizes the pressure in both bounce chambers. The refilling mechanism was modeled, but dramatically increased the computational time because the mass in and out of the bounce chamber during the expansion and compression stroke requires very fine time steps. Different solvers for the ordinary differential equations or refilling mechanisms may be needed to reduce the cost of such computations.

A control algorithm is definitely needed for the bounce chamber mass and injection timing. Any feedback control with a track of compression ratio can be a way to control the bounce chamber mass. Similarly, the indicated work can be a feedback for the injection timing. With the modern electric sensor and control strategies, the TCFPLA engine could be a next generation hybrid powertrain burning alternative fuels with high efficiency and low cost in the near future.

Bibliography

[1]   L. Li, Y. Luan, Z. Wang, J. Deng and Z. Wu, "Simulations of Key Design Parameters and Performance Optimization for a Free-piston Engine", SAE 2010-01-1105, 2010

[2]   L. Huang, "An Opposed-Piston Free-Piston Linear Generator Development for HEV", SAE 2012-01-1021, 2012

[3]   S. S. Goldsborough, P. Van Blarigan, "A Numerical Study of a Free Piston IC Engine Operating on Homogeneous Charge Compression Ignition Combustion", SAE 1999-01-0619, 1999

[4]   F. Kock, J. Haag, H. E. Friedrich, "The Free Piston Linear Generator - Development of an Innovative, Compact, Highly Efficient Range- Extender Module", SAE 2013-01-1727, 2013

[5]   F. Underwood, "The GMR 4-4 'HYPREX' Engine, A Concept of The Free-Piston Engine for Automotive Use", SAE 570032, 1957

[6]   H. Shapiro and J. van Gerpen, "Two Zone Combustion Models for Second Law Analysis of Internal Combustion Engines," SAE Technical Paper 890823, 1989

[7]   P. Nagar and S. Miers, "Friction between Piston and Cylinder of an IC Engine: a Review," SAE Technical Paper 2011-01-1405, 2011

[8]   D. N. Frey, P. Klotsch, A. Egli, "The Automotive Free-Piston-Turbine Engine", SAE Transaction Vol. 65, p. 628-634, 1957

[9]   A. K. Oppenheim, A. L. London, " The Free-Piston Gas Generator – A Thermodynamic-Dynamic Analysis", Technical Report under Navy Contract N6-ONR-251 Task Order 6, NR-035-104, 1950

APPEXDIX A

Reed Valve

In the GM Hyprex engine, the mechanically operated poppet valve cannot be used because the free-piston has variable stroke and compression ratio. Moreover, there is no reciprocating mechanical connection to a camshaft for valve control. Additional valve control would increase the complexity but not significantly improve the efficiency. Therefore, reed valves are selected for the valve design. The TCFPLA engine follows the GM Hyprex design and has the configuration shown below.
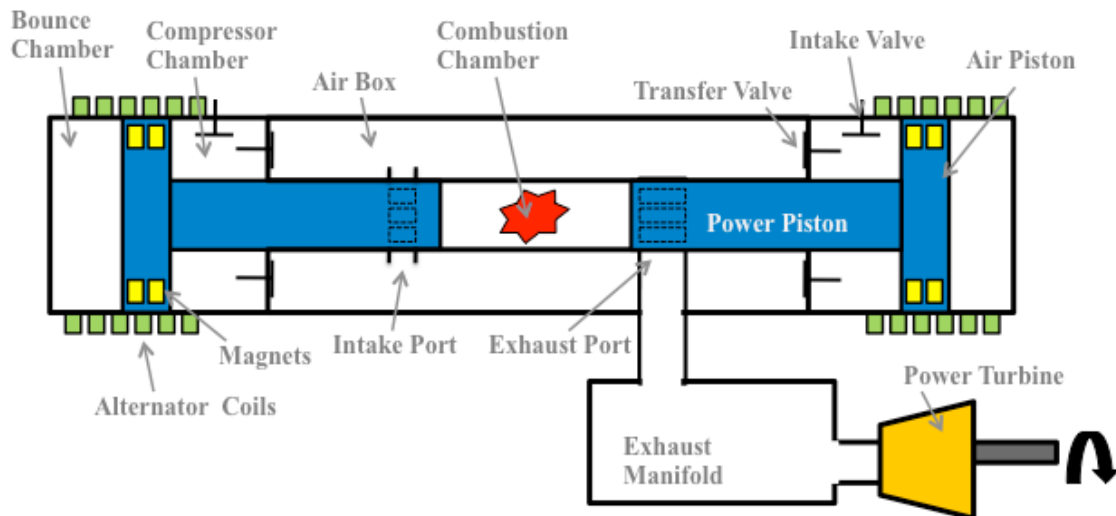

Figure A-1 Configuration of the TCFPLA engine

In Figure A-1, the intake valves and transfer valves are both reed valves. Reed valves are a type of one-way valve, so the blades do not lift if the downstream pressure is higher. The lifted blades uncover the flow area and allow the flow to go through. Larger pressure difference increases the valve lift unless the blades are stopped by stop plates preventing the blades from over bending. The following figure shows the structure of a Reed valve.
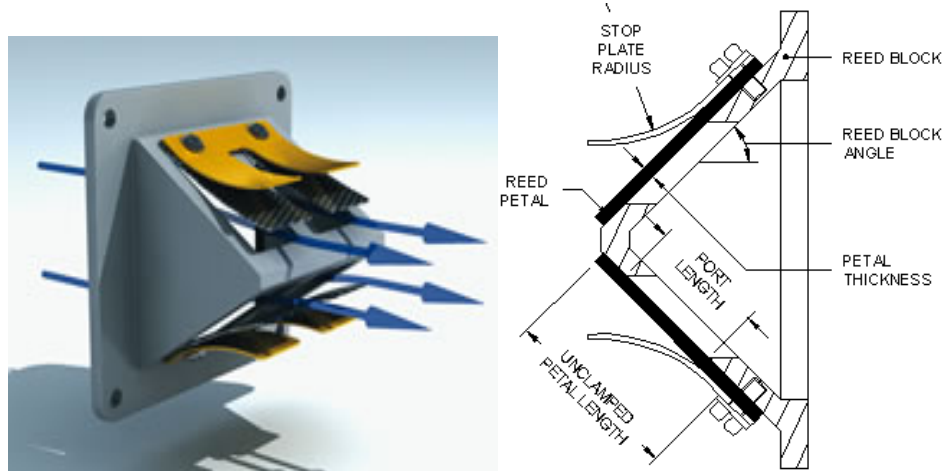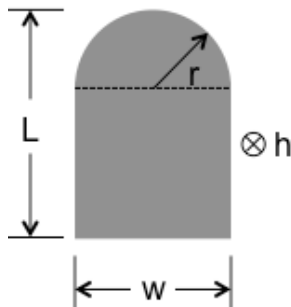
Figure A-2 Reed valve structure

Reed valve are typically modeled as a cantilever beam. The lift of the tip is determined by the pressure force loading on the beam and the material characteristics. Krieger provides an empirical correlation for flow area as a function of reed lift at the tip for a specific reed design. The following table shows the design parameters.

Table A-1 Dimensions of a single reed for Krieger's model

	Variable	Value	Unit
Length	L	1.44	in
Width	w	0.7225	in
Radius	r	0.3613	in
Thickness	h	0.01	in
Density	ρ	0.25	lb_m/in^3
Modulus of elasticity	E	28e6	psi

In the new TCFPLA engine model, the reeds are simplified to rectangular shape, so the radius is not in use. Considering the reed tip behavior, it is devised an equivalent mass-spring system as a second-order ordinary differential equation. Several assumptions were made for the reed. First, the shape of the reed remains in the first

mode of vibration. Second, collision with the stop plate does not change the shape. Third, the load on the reed is uniform. Fourth, the spring force of the reed in bending is linear with the tip displacement. Fifth, the reed stops instantaneously when hitting the stop plate or the reed box. Last, the reed is not damped in its travel. Based on these assumptions, displacement of the reed tip, *x*, can be calculated by Newton's Second Law.

$$\frac{d^2x}{dt^2} = (F_{eq} - kx)/m_{eq}$$

F_{eq} is the equivalent pressure forces, defined as the pressure force multiply by a factor, applied on a reed plate. The factor 0.35 ~ 0.39 is applied because only the tip of reed is calculated but not the whole beam. k is the stiffness of the reed at the tip with the value of 375 N/m and m_{eq} is the equivalent mass of reed tip, which is 25% of the whole reed.

After the modeling and experimental work, the empirical equations, as a function of tip displacement, x, were formed for both the opening position and discharge coefficient as below.

$$Area = -1.07e^{-6} + 1.95x - 8.09x^2 + 28.55x^3 + 759.91x^4 - 5802.9x^5 + 1.07e^{-6}\exp(73.48x)$$

$$C_D = 0.9995 - 7.27x + 94.70x^2 - 842.90x^3 + 4048.23x^4 - 7899.78x^5$$

After the area and discharge coefficient are obtained, the flow equations (Eq. 2.6 and Eq. 2.7) are used to determine the mass flow rate.

In order to obtain a most realistic result, the TCFPLA engine model used the reed valve to predict the valve behavior and corresponding flow. It could be simplified by using a check valve model. Check valve is another type of one-way valve, but the valve opens and closes instantaneously when the upstream pressure is higher than the downstream pressure.   The check valve is modeled as an orifice with discharge coefficient 1.

The following plot shows the total intake mass flow rate with the reed valve or check valve for comparison. Total 50 reed valves are used for the intake, and the check valves have an equivalent area as an orifice of 100 mm in diameter.
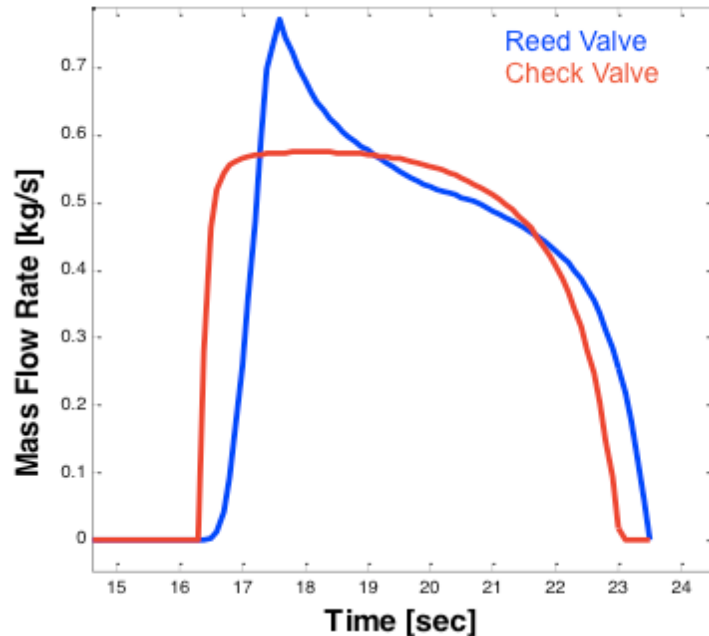

Figure A-3 Intake mass flow rate with reed valve and check valve

As can be seen in Figure A-2, the mass flow rate through the reed valves increase more gradually compared with the flow through the check valve. This is because the reed valve does not open immediately, as the tip displacement follows the governing equation for the motion which includes dynamic effects. The check valve, on the other hand, has the peak mass flow rate right after it opens. The reed valves have maximum mass flow rate because the delay of valve opening increases the vacuum in the compressor. Regarding the flow area, the check valve is about 1.5 times larger than the reed valve, but the total mass flow, or the area under the curves, are not significantly different. This means the reed valves do not restrict the flow due to the complicated behavior.

Observing the total intake mass flow over different loads, the following results show the comparison.
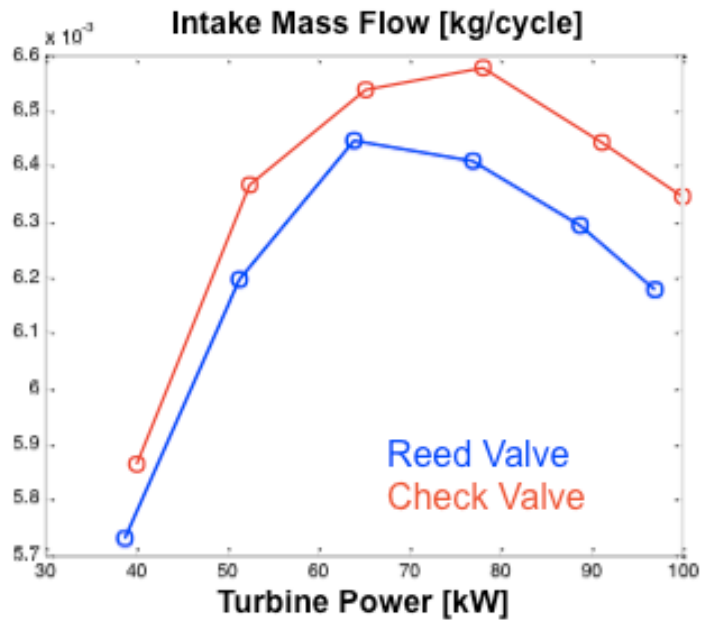
Figure A-4 Intake mass flow rate in a cycle over different load

As seen in Figure A-3, the check valve supplies more intake mass. This result is expected, as the check valve does not have the valve dynamics in the model. Both types of valve show the reduced flow after certain loads, so this is not special for the reed valve. Therefore, regardless of the valve type, high piston speed reduces the intake flow. Less mass flow through the reed valve results in 1% reduction of thermal efficiency.